ÇUKUROVA UNIVERSITY
INSTITUTE OF NATURAL AND APPLIED SCIENCES

MSc THESIS

Servet YOLALAN

INVESTIGATING THE IMPACT OF WIND POWER PLANT ON ELECTRICITY NETWORK

DEPARTMENT OF ELECTRICAL AND ELECTRONICS ENGINEERING

ADANA, 2014

ÇUKUROVA UNIVERSITY
INSTITUTE OF NATURAL AND APPLIED SCIENCES

INVESTIGATING THE IMPACT OF WIND POWER PLANT ON ELECTRICITY NETWORK

Servet YOLALAN

MSc THESIS

DEPARTMENT OF ELECTRICAL AND ELECTRONICS ENGINEERING

We certify that the thesis titled above was reviewed and approved for the award of degree of the Master of Science by the board of jury on 20/02/2014.

Asst. Prof. Dr. Mehmet Uğraş CUMA
SUPERVISOR

Prof. Dr. Mehmet TÜMAY
MEMBER

Asst. Prof. Dr. Lütfü SARIBULUT
MEMBER

This MSc Thesis is written at the Department of Institute of Natural And Applied Sciences of Çukurova University.
Registration Number:

Prof. Dr. Mustafa GÖK
Director
Institute of Natural and Applied Sciences

Not: The usage of the presented specific declerations, tables, figures, and photographs either in this thesis or in any other reference without citiation is subject to "The law of Arts and Intellectual Products" number of 5846 of Turkish Republic.

ABSTRACT

MSc THESIS

INVESTIGATING THE IMPACT OF WIND POWER PLANT ON ELECTRICITY NETWORK

Servet YOLALAN

ÇUKUROVA UNIVERSITY
INSTITUTE OF NATURAL AND APPLIED SCIENCES
DEPARTMENT OF ELECTRICAL AND ELECTRONICS ENGINEERING

Supervisor : : Asst. Prof. Dr. Mehmet Uğraş CUMA
Year: 2014, Pages: 103
Jury : : Prof. Dr. Mehmet TÜMAY
: Asst. Prof. Dr. Lütfü SARIBULUT
: Asst. Prof. Dr. Mehmet Uğraş CUMA

Renewable energy, as a new solution to world's energy needs, is come forward while generating energy with conventional systems are depleting our resources. Since renewable energy is heretofore known the most innocuous power generation method, it is focused on one of the most widely used type of renewable energy generation in this study. In this thesis, a wind farm that includes 16 wind turbines in a sample region is modeled using MATLAB. In case studies, wind turbine low voltage output and medium voltage side faults are investigated.

Key Words: Double Fed Induction Generator, Wind Turbine, Power Quality, Wind Farm Modelling

ÖZ

YÜKSEK LİSANS TEZİ

RÜZGAR SANTRALININ ELEKTRİK ŞEBEKESİNE ETKİSİNİN ARAŞTIRILMASI

Servet YOLALAN

ÇUKUROVA ÜNİVERSİTESİ
FEN BİLİMLERİ ENSTİTÜSÜ
ELEKTRİK ELEKTRONİK MÜHENDİSLİĞİ ANABİLİM DALI

Danışman : : Yrd. Doç. Dr. Mehmet Uğraş CUMA
Yıl :2014, Pages: 103
Jüri : : Prof. Dr. Mehmet TÜMAY
: Yrd. Doç. Dr. Lütfü SARIBULUT
: Yrd. Doç. Dr. Mehmet Uğraş CUMA

Geleneksel yöntemlerle enerji üretimi kaynaklarımızı tüketirken, yenilenebilir enerji dünyanın enerji ihtiyacını karşılamak için yeni bir çözüm olarak ön plana çıkmıştır. Yenilenebilir enerji şu ana kadar bilinen en zararsız enerji üretim şekli olduğundan bu çalışmada yenilenebilir enerji üretim şekillerinden en yaygın olanı üzerine odaklanılmıştır. Bu tezde, örnek bir alanda 16 rüzgâr türbini içeren bir rüzgâr çiftliği MATLAB kullanılarak modellenmiştir. Durum çalışmalarında rüzgâr türbini düşük gerilim çıkışı ve orta gerilim tarafı hataları incelenmiştir.

Anahtar Kelimeler: Çift beslemeli Asenkron Jeneratör, Rüzgar Türbini, Güç Kalitesi, Rüzgar Çiftliği

ACKNOWLEDGEMENTS

The subject of this thesis was suggested by my supervisor, Assist. Prof. Mehmet Ugras CUMA to whom I would like to express my heartfelt thanks for his supervision, guidance, encouragements, extremely useful suggestions and continuous confidence in me throughout this thesis. It has been a great honor to have Asst. Prof. Mehmet Ugras CUMA as supervisor.

I am also grateful to Prof. Dr. Mehmet TUMAY, head of the Department, for his help and support during my study.

I owe special thanks to Tahsin KÖROĞLU for his companionship and cooperation during my study. I also thank to Assist. Prof. Dr. K. Cagatay BAYINDIR for his valuable discussions. I wish to thank M. Mustafa SAVRUN for his technical helps. I am also grateful to the members of the Electrical and Electronics Engineering Department, Çukurova University.

I would like to thank to Dr. Lütfü SARIBULUT for accepting to be the member of examining committee for my thesis.

Finally, I wish to express my deepest gratitude to my parents and extended family for their endless support, encouragement and patience.

CONTENTS **PAGE**

ABSTRACT I
ÖZ II
ACKNOWLEDGEMENTS III
CONTENTS IV
LIST OF TABLE VI
LIST OF FIGURES VIII
LIST OF SYMBOLS XIII
LIST OF ABBREVATIONS XV
1. INTRODUCTION 1
2. WIND ENERGY 7
2.1. Fundamentals of Wind Turbines 7
2.1.1. Capacity factor 9
2.1.2. Number of Blades 9
2.1.3. Operating Region of the Wind Turbine 10
2.2. Classification of Wind Turbines 11
2.3. Wind Turbine Concepts 11
2.3.1. Fixed Speed Wind Turbines 12
2.3.2. Partial Variable Speed Wind Turbine with Variable Rotor Resistance 13
2.3.3. Variable Speed WT with Partial-scale Frequency Converter 14
2.3.4. Variable Speed Wind Turbine with Full-scale Power Converter 15
2.4. Wind Farms 16
2.4.1. AC Connection Topologies 17
2.4.2. DC Connection Topologies 19
3. MODELING OF WIND FARM 21
2.5. Wind Turbine Modeling 23
3.2. Drive Train Modeling 25
2.6. Induction Generator Modeling 30
2.7. AC-DC-AC Converter and DC Link Modeling 32
2.8. Controller Modeling 34
3.5.1. Rotor Side Controller Modeling 34

3.5.2. Grid Side Controller Modeling 35
3.5.3. Pitch Controller Modeling 36
4. MODELING OF WIND FARM IN MATLAB 39
5. SIMULATION RESULTS AND CASE STUDIES 53
5.1. Case 1: Normal Operation (No Fault Condition) 53
5.1.1. Normal Operation at Fixed Speed 53
5.1.2. Normal Operation at Variable Speed 56
5.2. Case 2: Faults in Group A Wind Turbines 63
5.2.1. Phase-B-to-Phase-C Fault 63
5.2.2. Phase-A-to-Ground Fault 67
5.2.3. Three Phase (A-B-C) Fault 71
5.3. Case 3: Faults in Group B Wind Turbines 74
5.3.1. Phase-A-to-Phase-B Fault 74
5.3.2. Phase-C-to-Ground Fault 78
5.3.3. Three Phase (A-B-C) Fault 81
5.4. Case 4: Faults in Medium Voltage Line 85
5.4.1. Phase-A-to-Phase-C Fault 85
5.4.2. Phase-B-to-Ground Fault 89
5.4.3. Three Phase (A-B-C) Fault 92
6. CONCLUSION 97
REFERENCES 99
BIOGRAPHY 103

LIST OF TABLE **PAGE**

Table 1.1. Reliable Energy Production (GWh) – Scenario 2
Table 1.2. Development of Installed Power Among Years (MW) – Scenario 3
Table 3.1. Electrical parameters of Substations: 21
Table 3.2. Existing power cables and their specifications in Wind Farm 23
Table 4.1. Line impedance and Cable Block parameters 45
Table 5.1. FFT Analysis of Substation 1 and 2 55

LIST OF FIGURES **PAGE**

Figure 1.1. Energy Generation by Generation Types in 2012 2
Figure 1.2. Installed Energy Capacity by Resource Types 3
Figure 2.1. Components of WECS connected to grid (Hyonk et al., 2010)..... 7
Figure 2.2. Components of a wind turbine system (Bijaya, 2011)..... 8
Figure 2.3. Wind turbine three blades , two blades and one blade..... 10
Figure 2.4. Power curve of a variable speed wind turbine (Bijaya, 2011)..... 10
Figure 2.5. Fixed speed wind turbine with directly grid connected squirrel-cage induction generator (Molina and Mercado, 2011) 13
Figure 2.6. Partial variable speed wind turbine with variable rotor resistance (Molina and Mercado, 2011) 14
Figure 2.7. Variable speed wind turbine with partial scale power converter (Molina and Mercado, 2011) 15
Figure 2.8. Variable speed wind turbine with full-scale power converter (Molina and Mercado, 2011) 16
Figure 2.9. Radial Connection for AC Topologies (Bahirat et al. 2012) 17
Figure 2.10. Radial Loop Connection for AC Topologies (Bahitar et al. 2012)..... 18
Figure 2.11. AC Star/Cluster Connection (Bahirat et al. 2012) 18
Figure 2.12. DC Transmission System Topologies for Connecting Wind Farms/Parks to the grid: a) park coupled, b) cluster coupled and c) cluster coupled with common DC Bus (Iov et al. 2005) 19
Figure 3.1. General scheme of wind farm model 21
Figure 3.2. Internal Connection of the Wind Farm 22
Figure 3.3. Power coefficient versus λ and β 25
Figure 3.4. Rotational system with a disk (Singh et al., 2011) 26
Figure 3.5. Rotational system incorporating a gear train (Singh et al., 2011) 26
Figure 3.6. Wind turbine drivetrain model (Singh et al., 2011) 29
Figure 3.7. Wind turbine drivetrain model (Gangon et al., 2005)..... 30
Figure 3.8. Equivalent circuit of the DFIG (Gupta et al., 2013) 31
Figure 3.9. Rotor-side converter control (Singh et al., 2011) 35
Figure 3.10. Grid-side converter control (Singh et al., 2011) 36

Figure 3.11. Pitch controller scheme 37
Figure 4.1. Simulation model of the wind farm 39
Figure 4.2. Subsystem model of Group A Wind Turbines 41
Figure 4.3. Subsystem model of Group B Wind Turbines 42
Figure 4.4. Three Phase Source block and parameters 43
Figure 4.5. Block used to model of line impedances 44
Figure 4.6. MV to HV transformer and LV to MV transformer parameters 46
Figure 4.7. Simulink block of double fed induction generator wind turbine 46
Figure 4.8. DFIG Wind Turbine generator data parameter page 47
Figure 4.9. DFIG Wind Turbine converter data parameter page 48
Figure 4.10. DFIG Wind Turbine turbine data parameter page 48
Figure 4.11. DFIG Wind Turbine drive train data parameter page 49
Figure 4.12. DFIG Wind Turbine control parameter page 50
Figure 4.13. Three Phase fault block 51
Figure 4.14. Three phase Fault block parameters 51
Figure 5.1. Phase voltages of High Voltage Line side for 5.1.1 case 53
Figure 5.2. Phase currents of High Voltage Line side for 5.1.1 case 54
Figure 5.3. Active and reactive powers of MV Line side for 5.1.1 case 54
Figure 5.4. Frequency change of MV Line side for 5.1.1 case 55
Figure 5.5. Wind Speeds for Wind Turbine 1 to 4 for case 5.1.2 56
Figure 5.6. Wind Speeds for Wind Turbine 5 to 8 for case 5.1.2 57
Figure 5.7. Wind Speeds for Wind Turbine 9 to 12 for case 5.1.2 58
Figure 5.8. Wind Speeds for Wind Turbine 13 to 16 for case 5.1.2 59
Figure 5.9. Rotor Speeds for Wind Turbine 1 to 4 for case 5.1.2 57
Figure 5.10. Rotor Speeds for Wind Turbine 5 to 8 for case 5.1.2 58
Figure 5.11. Rotor Speeds for Wind Turbine 9 to 12 for case 5.1.2 59
Figure 5.12. Rotor Speeds for Wind Turbine 13 to 16 for case 5.1.2 60
Figure 5.13. Phase voltages of High Voltage Line side for 5.1.2 case 61
Figure 5.14. Phase currents of High Voltage Line side for 5.1.2 case 61
Figure 5.15. Active and reactive powers of MV Line side for 5.1.2 case 62
Figure 5.16. Frequency change of MV Line side for 5.1.2 case 63

Figure 5.17. Phase voltages of High Voltage Line side during 5.2.1 case 64
Figure 5.18. RMS voltages of High Voltage Line side during 5.2.1 case 64
Figure 5.19. Phase currents of High Voltage Line side during 5.2.1 case 65
Figure 5.20. RMS currents of High Voltage Line side during 5.2.1 case 65
Figure 5.21. Active and reactive powers of MV Line side during 5.2.1 case 66
Figure 5.22. Frequency change of MV Line side during 5.2.1 case 67
Figure 5.23. Phase voltages of High Voltage Line side during 5.2.2 case 68
Figure 5.24. RMS voltages of High Voltage Line side during 5.2.2 case 68
Figure 5.25. Phase currents of High Voltage Line side during 5.2.2 case 69
Figure 5.26. RMS currents of High Voltage Line side during 5.2.2 case 69
Figure 5.27. Active and reactive powers of MV Line side during 5.2.2 case 70
Figure 5.28. Frequency change of MV Line side during 5.2.2 case 70
Figure 5.29. Phase voltages of High Voltage Line of the system during 5.2.3 case 71
Figure 5.30. RMS voltages of High Voltage Line side of the system during 5.2.3 case 72
Figure 5.31. Phase currents of High Voltage Line of the system during 5.2.3 case 72
Figure 5.32. RMS currents of High Voltage Line side of the system during 5.2.3 case 73
Figure 5.33. Active and reactive powers of MV Line side during 5.2.3 case 73
Figure 5.34. Frequency change of MV Line side during 5.2.3 case 74
Figure 5.35. Phase voltages of High Voltage Line of the system during 5.3.1 case 75
Figure 5.36. RMS voltages of High Voltage Line side of the system during 5.3.1 case 75
Figure 5.37. Phase currents of High Voltage Line of the system during 5.3.1 case 76
Figure 5.38. RMS currents of High Voltage Line side of the system during 5.3.1 case 76
Figure 5.39. Active and reactive powers of MV Line side during 5.3.1 case 77
Figure 5.40. Frequency change of MV Line side during 5.3.1 case 77

Figure 5.41. Phase voltages of High Voltage Line side during 5.3.2 case 78
Figure 5.42. RMS voltages of High Voltage Line side of the system during 5.3.2 case 79
Figure 5.43. Phase currents of High Voltage Line side during 5.3.2 case 79
Figure 5.44. RMS currents of High Voltage Line side of the system during 5.3.2 case 80
Figure 5.45. Active and reactive powers of MV Line side during 5.3.2 case 80
Figure 5.46. Frequency change of MV Line side during 5.3.2 case 81
Figure 5.47. Phase voltages of High Voltage Line of the system during 5.3.3 case 82
Figure 5.48. RMS voltages of High Voltage Line side of the system during 5.3.3 case 82
Figure 5.49. Phase currents of High Voltage Line of the system during 5.3.3 case 83
Figure 5.50. RMS currents of High Voltage Line side of the system during 5.3.3 case 83
Figure 5.51. Active and reactive powers of MV Line side during 5.3.3 case 84
Figure 5.52. Frequency change of MV Line side during 5.3.3 case 85
Figure 5.53. Phase voltages of High Voltage Line side during 5.4.1 case 86
Figure 5.54. RMS voltages of High Voltage Line side of the system during 5.4.1 case 86
Figure 5.55. Phase currents of High Voltage Line side during 5.4.1 case 87
Figure 5.56. RMS currents of High Voltage Line side of the system during 5.4.1 case 87
Figure 5.57. Active and reactive powers of MV Line side during 5.4.1 case 88
Figure 5.58. Frequency change of MV Line side during 5.4.1 case 88
Figure 5.59. Phase voltages of High Voltage Line side during 5.4.2 case 89
Figure 5.60. RMS voltages of High Voltage Line side of the system during 5.4.2 case 90
Figure 5.61. RMS voltages of High Voltage Line side of the system during 5.4.2 case 90

Figure 5.62. RMS currents of High Voltage Line side of the system during 5.4.2 case..... 91
Figure 5.63 Active and reactive powers of MV Line side during 5.4.2 case..... 91
Figure 5.64. Frequency change of MV Line side during 5.4.2 case 92
Figure 5.65. Phase voltages of High Voltage Line of the system during 5.4.3 case..... 93
Figure 5.66. RMS voltages of High Voltage Line side of the system during 5.4.3 case..... 93
Figure 5.67. Phase currents of High Voltage Line of the system during 5.4.3 case..... 94
Figure 5.68. RMS currents of High Voltage Line side of the system during 5.4.3 case..... 94
Figure 5.69. Active and reactive powers of MV Line side during 5.4.3 case..... 95
Figure 5.70. Frequency change of MV Line side during 5.4.3 case 95

LIST OF SYMBOLS

A_r	: Area Swept By The Rotor Blades
C_{dc}	: Dc Bus Capacitance
C_p	: Performance Coefficient of The Turbine
D	: Damping of System
I_r	: Stator Current
I_{Rm}	: Magnetizing Resistance Current
J	: Moments of inertia
K	: Stiffness of System
L_f	: Inductance of the Filter
L_m	: Magnetizing Inductance
$L_{r\lambda}$	: Rotor Leakage Inductance
$L_{s\lambda}$	: Stator Leakage Inductance
M_{df}	: Modulation Indices of the GSC
M_{dr}	: Modulation Indices of RSC
M_{qf}	: Modulation Indices of the GSC
M_{qr}	: Modulation Indices of RSC
N	: Numbers of Teeth of Gear
P_g	: Active Power at the AC Terminal of the GSC
P_m	: Mechanical Power Extracted From The Wind Turbine
P_r	: Active Power at the AC Terminal of the RSC
R	: Blade Radius
r_f	: Resistance of the Filter
R_m	: Magnetizing Resistance
R_r	: Rotor Resistance
R_s	: Stator Resistance
s	: Slip
v	: Wind Velocity
V_{dc}	: Dc Bus Voltage
V_{df}	: Voltage at the Output of the GSC

V_{dg}	: Represent the Grid Voltage
V_{qf}	: Voltage at the Output of the GSC
V_{qg}	: Represent the Grid Voltage
V_r	: Rotor Voltage
V_s	: Stator Voltage
V_w	: Wind Speed
w_1	: Stator Frequency
w_G	: Wind Turbine Generator Speed
w_T	: Wind Turbine Rotor Speed
β	: Blade Pitch Angle in Degrees
Γ	: Transmitted Torque
λ	: Tip Speed Ratio of The Rotor Blade
ρ	: Air Density
Ω	: Speed of Turbine

LIST OF ABBREVATIONS

AC	: Alternative Current
CF	: Capacity Factor
DC	: Direct Current
DFIG	: Doubly-Fed Induction Generator
GSC	: Grid Side Converter
HZ	: Hertz
IEEE	: Institute of Electrical and Electronics Engineers
IGBT	: Insulated Gate Bipolar Transistor
kV	: Kilovolt
PI	: Proportional Integral
PMSG	: Permanent Magnet Synchronous Generator
PWM	: Pulse Width Modulation
RMS	: Root Mean Square
RSC	: Rotor Side Converter
SCIG	: Squiralle Cage Induction Generator
THD	: Total Harmonic Distortion
TR	: Transformer
WECS	: Wind Energy Conversion System
WRIG	: Wound Rotor Induction Generator
WT	: Wind Turbine

1. INTRODUCTION

Energy, today, has been one of the leading main issues in the development of societies and strengthening their economies. Especially electrical energy is one of the most widely used raw materials in trade and industrial areas. In our world, infrastructure of electricity in general is based on fossil fuels, but this fossil fuel reserves is predicted to run out towards the end of 21st century. Moreover, steadily rising prices of fossil fuels while reserves of fossil fuels are depleting and wastes of fossil fuels after obtaining energy from fossil fuels (CO_2, etc.) and their impacts on our environment are the main results of the usage of fossil fuels.

Conventional electric power generation is generally based on fossil fuels and the mainly these plants are thermal power plants, gas turbines, hydro plants and combined cycle power plants etc. All countries and governments having this type of production in world have been forced to limit their energy policies with environmental policies while getting energy from these sources. As a result of these restrictions, renewable energy sources and production of energy from them came into the agenda. Therefore, countries around the world are showing great interest to renewable energy sources to meet their growing energy demand. As a result of this increased interest in renewable energy resources companies have been invested in this area, so some new terms, which we are not aware of them already, was attended to our lives; wind energy, solar energy, bio-fuel energy, etc. In our country, the interest of renewable energy is increasing in time. Considering that our country's potential of resources, installed capacity in energy production and future energy consumption scenarios it seems that we proceed step by step in renewable energy.

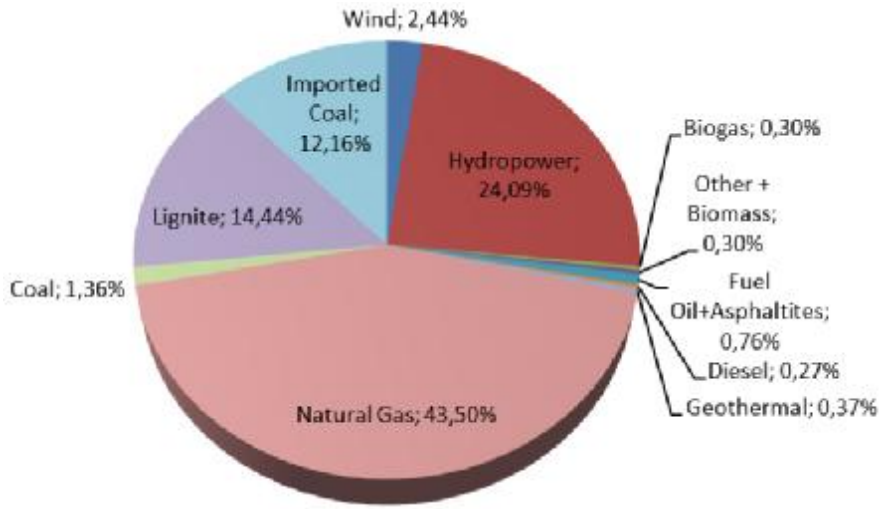


Figure 1.1. Energy Generation by Generation Types in 2012 (Energy Institute)

Table 1.1. Reliable Energy Production (GWh) – Scenario (Energy Institute)

Years	**2014**	**2015**	**2016**	**2017**	**2018**	**2019**	**2020**	**2021**
Lignite	48600	52676	56651	56748	57260	57260	57260	57260
Coal + Asphaltites	3857	4829	5801	5801	5801	5801	5801	5801
Imported Coal	25002	29474	36481	38272	38311	38311	38311	38311
Naturel Gas	150184	162289	167216	167848	168184	168184	168184	168184
Geothermal	1212	1402	1402	1402	1402	1402	1402	1402
Fuel Oil	9034	9034	9034	9034	9034	9034	9034	9034
Diesel	148	148	148	148	148	148	148	148
Nuclear	0	0	0	0	0	4200	12600	21000
Other	1408	1408	1408	1408	1408	1408	1408	1408
Thermal Total	239443	261259	278139	280659	281547	285747	294147	302547
Biogas+Bio mass	1166	1196	1196	1196	1196	1196	1196	1196
Hydropower	48717	54932	62536	67210	689466	69385	69386	69386
Wind	6907	7644	7644	7644	7644	7644	7644	7644
Total	**296233**	**325031**	**349515**	**356709**	**979853**	**363972**	**372373**	**380773**

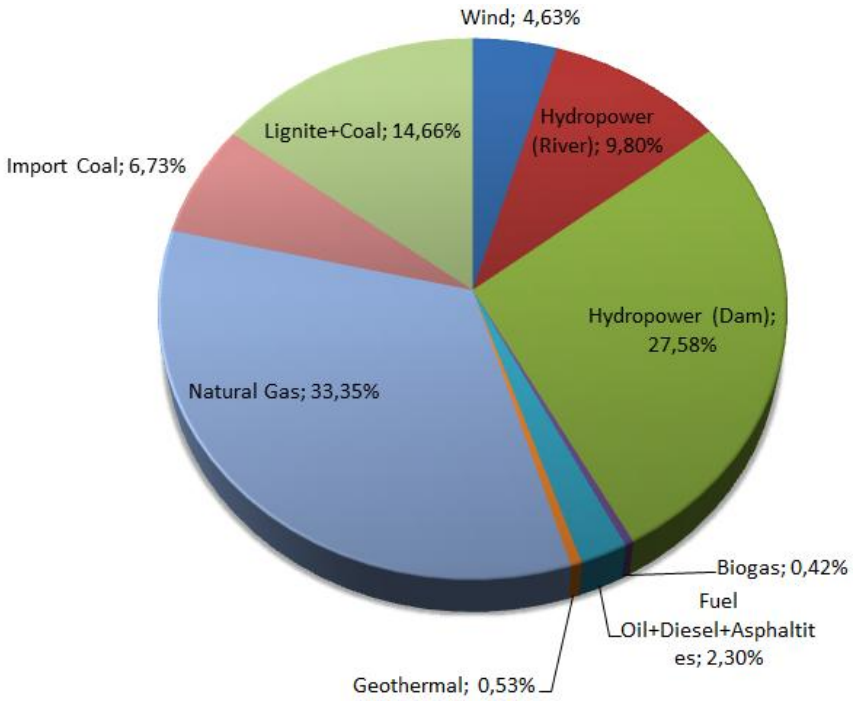


Figure 1.2. Installed Energy Capacity by Resource Types (Energy Institute)

Table 1.2. Development of Installed Power Among Years (MW) – Scenario (Energy Institute)

Years	2014	2015	2016	2017	2018	2019	2020	2021
Lignite	8375	9857	9857	9857	9857	9857	9857	9857
Coal + Asphaltites	690	960	960	960	960	960	960	960
Imported Coal	3881	5081	5681	5681	5681	5681	5681	5681
Naturel Gas	22376	23417	24042	24042	24042	24042	24042	24042
Geothermal	197	197	197	197	197	197	197	197
Fuel Oil	1406	1406	1406	1406	1406	1406	1406	1406
Diesel	26	26	26	26	26	26	26	26
Nuclear	0	0	0	0	0	1200	2400	3600
Other	215	215	215	215	215	215	215	215
Thermal Total	37166	41159	42384	42384	42384	43584	44784	45984
Biogas+Biomass	185	185	185	185	185	185	185	185
Hydropower	24291	28003	31606	33394	33815	33815	33815	33815
Wind	2646	2646	2646	2646	2646	2646	2646	2646
Total	**64288**	**71993**	**76821**	**78609**	**79030**	**80230**	**81430**	**82630**

Integration of this new energy sources into the conventional (grid) system has led some new problems in power quality. In order to handle these problems some new control methods and power electronic equipments are used. New developments

like reconstruction in energy systems and competition in electricity market has made power quality an emerging issue in energy systems. Today, power quality of provided energy is more important than the provided energy. Based on the above, it can be easily said that the main elements of the power system to be concerned about is the quality of the provided energy.

The term “Power Quality” is defined as “Set of parameters defining the properties of power quality as delivered to the user in normal operating conditions in terms of continuity of supply and characteristics of voltage (symmetry, frequency, magnitude, waveform) in IEC (Villalva et al., 2009). In IEEE standard, “power quality” defined as “The concept of powering and grounding electronic equipment in a manner that is suitable to the operation of that equipment and compatible with the premise wiring system and other connected equipment” (Yang et al., 2010). The integration of wind energy into existing power system presents technical challenges and that requires consideration of voltage regulation, stability, power quality problems. The power quality is an essential customer-focused measure and is greatly affected by the operation of a distribution and transmission network. In terms of power quality several aspects on this topic can be classified as;

- Voltage Stability
  - Under-voltage & Over-voltage
  - Voltage Sag
  - Voltage Swell
  - Phase Shift
  - Flicker
  - Frequency
- Continuity of Supplying Power
  - Momentary Interruption
  - Temporary Interruption
  - Sustained Interruption

- Voltage Waveform
  - Transient
  - Three Phase Voltage Unbalance
  - Harmonic Voltage, Current
  - Notch (Chen et al., 2009)

The thesis is organized as follows:

In Chapter 2, the fundamentals of wind energy are described. Classification of wind turbines, wind turbine concepts and wind farms topologies are investigated.

In Chapter 3, the modeling of wind farm is discussed. Wind turbine model, drive train model, doubly fed induction generator model and AC-DC-AC converter model are given. Corresponding controller strategies are presented.

Chapter 4 summarizes the MATLAB/Simulink modeling of wind farm. First, the simulation model is introduced. Secondly, the model blocks used in the simulation are explained.

In Chapter 5, the simulation results are given. The results cover fixed wind speed operation, variable wind speed operation, and several short circuit fault conditions. The active power, reactive power, current, voltage and frequency waveforms are given for each case.

Chapter 6 , the important conclusions of the study are given.

2. WIND ENERGY

In recent years, the environmental pollution has become a major concern in people daily life and a possible energy crisis has led people to develop new technologies for generating clean and renewable energy. Wind energy along with solar, hydropower and tidal energy are possible solutions for an environmentally-friendly energy production. In the past decades, wind power generation has experienced a very fast development and installed wind power capacity has been growing exponentially (Singh et al., 2011).

Wind Energy Conversion System (WECS) is the overall system for converting wind energy into useful mechanical energy that can be used to power an electrical generator for generating electricity. The WECS basically consists of three types of components: aerodynamics, mechanical, and electrical as shown in Figure 2.1 (Hyonk et al., 2010).

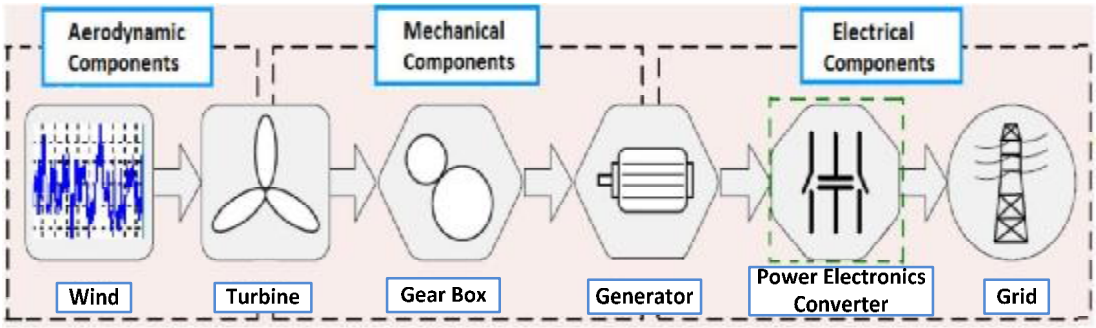


Figure 2.1. Components of WECS connected to grid (Hyonk et al., 2010).

This chapter of the thesis is aimed at presenting a review on the wind turbines and wind farm state of the art technologies.

2.1. Fundamentals of Wind Turbines

The major components of a wind turbine-generator system are shown in Figure 2.2. The wind turbine (WT) is composed of blades, the rotor hub and the

nacelle located immediately behind the rotor hub which houses the gearbox, generator and other components (Jing, 2009).

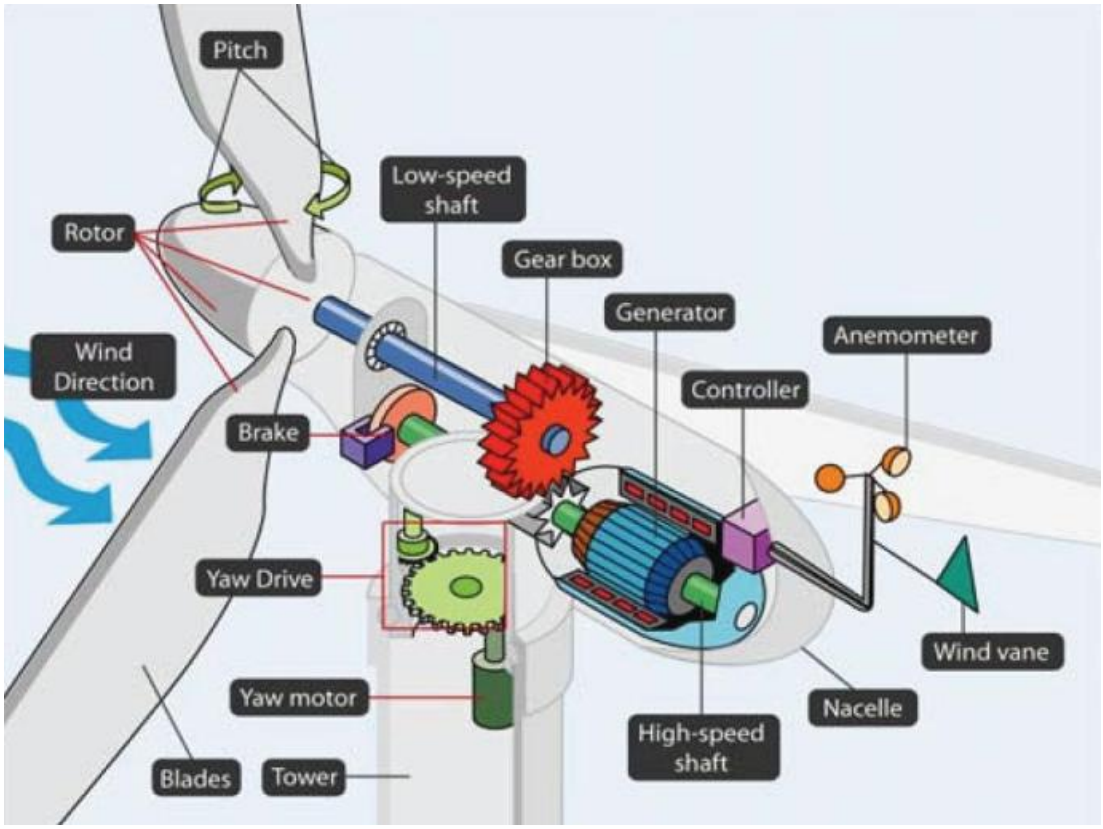


Figure 2.2. Components of a wind turbine system (Bijaya, 2011)

The drive train system consists of turbine rotating mass, low-speed shaft, gearbox, high-speed shaft and generator (Raymond et al., 2009). The drive train system transfers turbine mechanical output power up to the generator rotor where it is converted to electrical power. The wind strikes the rotor on the horizontal-axis turbine, causing it to spin. The low-speed shaft transfers energy to the gear box, which steps up in speed and rotates the high speed shaft. The high speed shaft causes the generator to spin, hence generating electricity. The yaw system is used to turn the nacelle so that the rotor faces into the wind. The low speed shaft contains pipes for the hydraulics system that operates the aerodynamic brake. The high speed shaft is equipped with an emergency mechanical brake which is used in case of failure of the aerodynamic brake (Bijaya, 2011).

The generator usually produces electrical power at low voltage and the transformer steps up the generator output voltage to connected grid voltage. The transformer may be placed at the bottom of the tower or in the nacelle for losses minimization (Bijaya, 2011).

Other components of wind turbine system are the anemometer to measure wind speed and a wind vane which measure the wind direction. Wind speed information is used to determine when the wind speed is sufficient to start up the turbine and when, due to high winds, the turbine must be shut down for safety whereas wind direction measurement is used by the yaw-control mechanism which helps in orienting the rotor to the wind direction (Raymond et al., 2009). Electric fans and oil coolers are used to cool the gearbox and generator (Bijaya, 2011).

2.1.1. Capacity factor

The fraction of the year turbine generator is operating at rated (peak) power. Capacity factor (CF) is equal to the ratio of average output and peak output. It is usually around 30 percent. CF is based on the characteristics. (typically 0.3 or above for good site) (Kalmikov and Dykes, 2010).

2.1.2. Number of Blades

Historically higher speed, lower torque, noisier than three blades but these features are not inherent in two bladed designs. Aerodynamic efficiency 4% lower in two blades than three blades. Statically balanced but not dynamically. Often employs a teeter hinge to reduce cyclic loading. Wind turbine with three blades has dynamically balanced and hence lower cyclic loads with simple rigid hub and more acceptable visual impact (Jamieson, 2005).



Figure 2.3. Wind turbine three blades , two blades and one blade

2.1.3. Operating Region of the Wind Turbine

The operating region of a variable-speed variable-pitch wind turbine can be illustrated by their power curve, which gives the estimated power output as function of wind speed as shown in Figure 2.4.

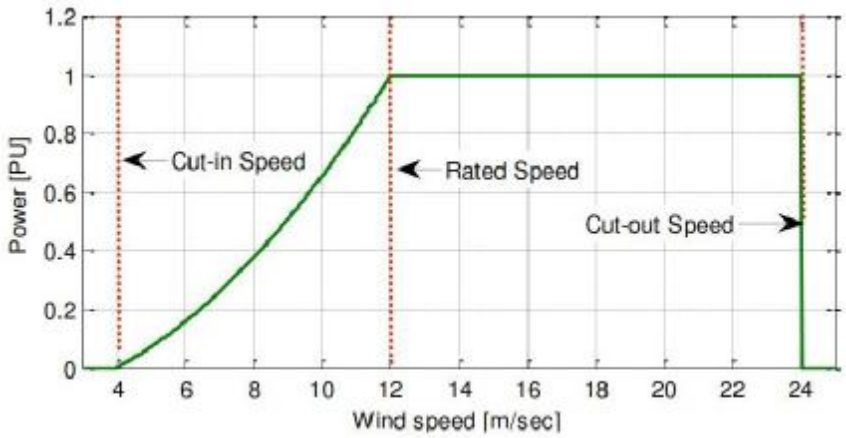


Figure 2.4. Power curve of a variable speed wind turbine (Bijaya, 2011)

Three distinct wind speed points can be noticed in this power curve:

- Cut-in wind speed: The lowest wind speed at which wind turbine starts to generate power.
- Rated wind speed: Wind speed at which the wind turbine generates the rated power, which is usually the maximum power wind turbine can produce.

- Cut-out wind speed: Wind speed at which the turbine ceases power generation and is shut down (with automatic brakes and/or blade pitching) to protect the turbine from mechanical damage (Bijaya, 2011).

2.2. Classification of Wind Turbines

Wind turbines can further be classified into horizontal-axis or vertical-axis. Vertical-axis wind turbines have the advantages that no tower is needed, they operate independently of the wind direction (a yawning mechanism is not needed) and heavy gearboxes and generators can be installed at ground level. However, they have many disadvantages: they are not self-starting, the torque fluctuates with each revolution as the blades move into and away from the wind, and speed regulation in high winds can be difficult (Ackermann, 2000). Wind turbines with horizontal rotor axis have following components; rotor blades, rotor hub, rotor brake and a pitch mechanism, electrical generator and a gearbox, wind measurement system and yaw drive (azimuth tracking), nacelle, tower and foundation control substation and main connection (Dutta, 2006).

2.3. Wind Turbine Concepts

Wind turbines can either be designed to operate at fixed speed (actually within a speed range about 1%) or at variable speed. Many low-power wind turbines built to-date were constructed according to the so-called “Danish concept” that was very popular in the eighties, in which wind energy is transformed into electrical energy using a simple squirrel cage induction machine directly connected to a three-phase power grid (Qiao et al., 2007). The rotor of the wind turbine is coupled to the generator shaft with a fixed-ratio gearbox. At any given operating point, this turbine has to be operated basically at constant speed. On the other hand, modern high-power wind turbines in the 2-10 MW range are mainly based on variable speed operation with blade pitch angle control obtained mainly by means of power electronic equipment, although variable generator rotor resistance can also be used. These wind

turbines can be mostly developed using either a direct-in-line system built with a direct-driven (without gearbox) PMSG grid-connected via a full-scale power converter, or a doubly-fed induction generator (DFIG) system that consists of a DFIG with a partial-scale power converter connected to the rotor windings. Based on these concepts, the most commonly applied wind turbine designs can be classified into four wind turbine concepts, as described below (Molina and Mercado, 2011).

2.3.1. Fixed Speed Wind Turbines

This topology corresponds to the constant or fixed speed controlled wind turbine, with asynchronous squirrel cage induction generator (SCIG) directly connected to the electric grid using a step up power transformer, as depicted in Figure 2.5. Since the squirrel cage induction generator always draws reactive power from the AC network, this concept requires a reactive power compensator, such as a capacitor bank, in order to reduce or even eliminate the reactive power demand from these turbine generators to the grid. It is typically achieved by continuously switching capacitor banks (5-25 steps) according to the active power generated (Molina and Mercado, 2011).

The structure and performance of fixed-speed wind turbines depends on the features of mechanical sub-circuits, e.g., pitch control time constants etc. The reaction time of these mechanical circuits may lie in the range of tens of milliseconds. As a result, each time a burst of wind hits the turbine, a rapid variation of electrical output power can be observed. These variations in electric power generated not only require a firm power grid to enable stable operation, but also require a well-built mechanical design to absorb high mechanical stress, which leads to expensive mechanical structure, especially at high-rated power (Varma and Chakri, 2012).

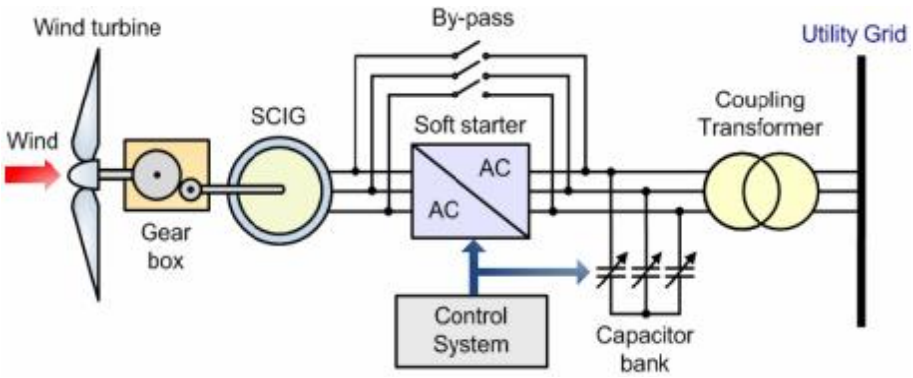


Figure 2.5. Fixed speed wind turbine with directly grid connected squirrel-cage induction generator (Molina and Mercado, 2011)

2.3.2. Partial Variable Speed Wind Turbine with Variable Rotor Resistance

This topology corresponds to the partial variable speed controlled wind turbine with variable generator rotor resistance, aka OptiSlip by the Danish manufacturer Vestas Wind Systems (Krüger and Andresen, 2001), as presented in Figure 2.6. It uses a wound rotor induction generator (WRIG) and has been used since the mid-nineties. In this case, the configuration is analogous to the type A wind turbine concept, with a generator directly connected to the electric grid. However, the rotor windings of the generator are connected in series with a controlled resistance, whose size defines the range of the variable speed (typically 0-10% above the synchronous speed). Capacitor bank performs reactive power compensation and a smoother grid connection is obtained by including a soft starter (Molina and Mercado, 2011).

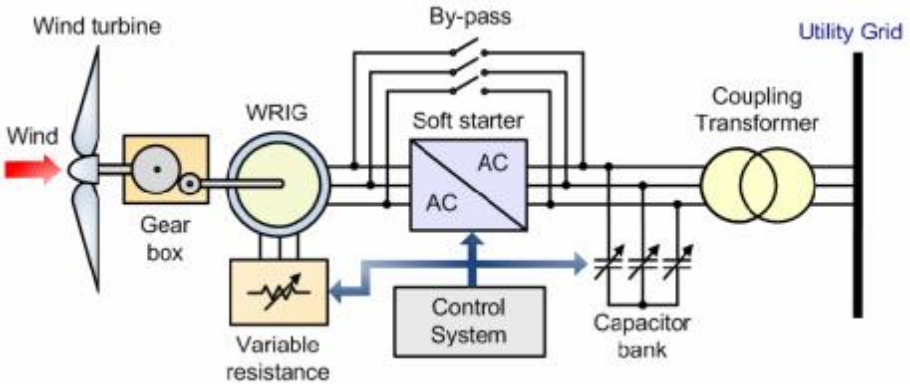


Figure 2.6. Partial variable speed wind turbine with variable rotor resistance (Molina and Mercado, 2011)

2.3.3. Variable Speed WT with Partial-scale Frequency Converter

This concept, aka doubly-fed induction generator (DFIG), corresponds to a variable speed controlled wind turbine with a wound rotor induction generator (WRIG) and a partial-scale power converter (rated approximately at 30% of nominal generated power) on the rotor circuit (Muller et al, 2002). The use of power electronic converters enables wind turbines to operate at variable (or adjustable) speed, and thus permits to provide more effective power capture than the fixed-speed counterparts. In addition, other significant advantages using variable speed systems include a decrease in mechanical loss, which makes possible lighter mechanical designs, and a more controllable power output (less dependent on wind variations), cost-effectiveness, simple pitch control, improved power quality and system efficiency, reduced acoustic noise, and island-operation capability. As shown in Figure 2.7., the rotor stator is directly connected to the electric grid, while a partial-scale power converter controls the rotor frequency and consequently the rotor speed. The partial-scale power converter is composed of a back-to-back four-quadrant AC/DC/AC converter design based on insulated gate bipolar transistors (IGBTs),whose power rating defines the speed range (typically around ±30% of the synchronous speed) (Molina and Mercado, 2011).

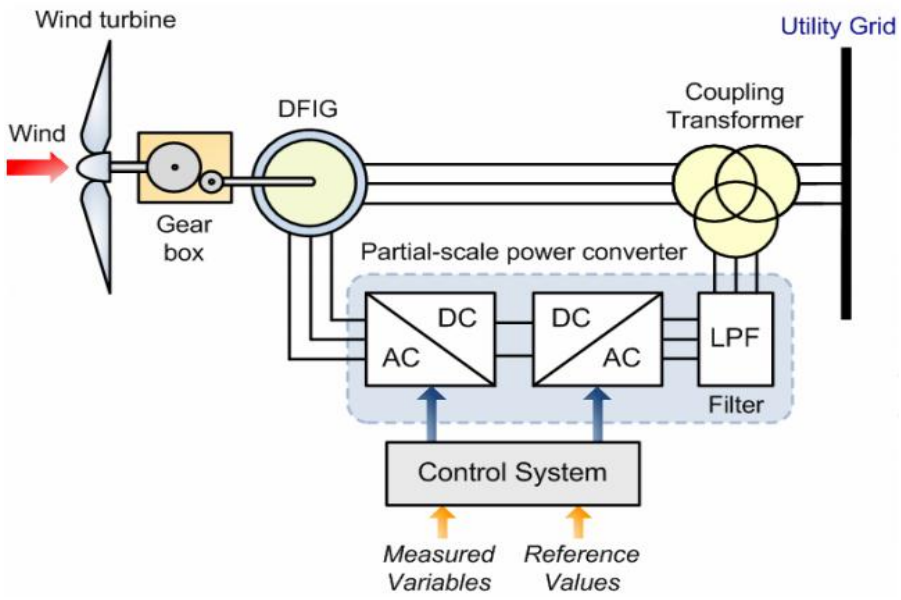


Figure 2.7. Variable speed wind turbine with partial scale power converter (Molina and Mercado, 2011)

2.3.4. Variable Speed Wind Turbine with Full-scale Power Converter

This configuration corresponds to the direct-in-line full variable speed controlled wind turbine, with the generator connected to the electric grid through a full-scale power converter. A synchronous generator is used to produce variable frequency AC power. The power converter connected in series (or in-line) with the wind turbine generator transforms this variable frequency AC power into fixed-frequency AC power. This power converter also allows controlling the reactive power compensation locally generated, and a smooth grid connection for the entire speed range. The generator can be electrically excited (Wound Rotor Synchronous Generator, WRSG) or permanent magnet excited type (Permanent Magnet Synchronous Generator, PMSG). Recently, due to the development in power electronics technology, the Squirrel-Cage induction Generator (SCIG) has also started to be used for this concept. As illustrated in Figure 2.8., the generator stator is connected to the grid through a full scale power converter, which is composed of a back-to-back four-quadrant AC/DC/AC converter design based on insulated gate bipolar transistors (IGBTs). Moreover, using a permanent magnet synchronous generator, the DC excitation system is eliminated and allows reducing weight, losses,

costs, and maintenance requirements (no slip rings are required). Even more, due to the intensified grid codes around the world, direct-driven PMSG wind turbine systems could be favored in the future compared to DFIG wind turbine concepts (Molina and Mercado, 2011; Li et al., 2009).

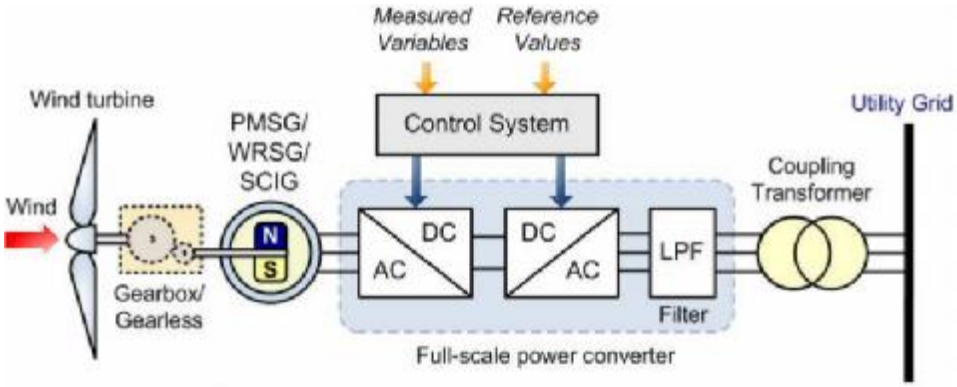


Figure 2.8. Variable speed wind turbine with full-scale power converter (Molina and Mercado, 2011)

2.4. Wind Farms

A wind farm is a collection of wind turbines in the same location and used for the generation of wind power electricity. Installing several turbines in groups at a site leads to large-scale utilisation of wind energy. This has operation, maintenance as well as economic advantages. Any wind energy project will incur fixed costs such as the preparation of the environmental statement, legal fees and project management costs. They are largely independent of the size of the wind farms, so it is desirable tospread them over as large a project as possible (Jenkins et al, 1997). This had led to the construction of large wind farms, some of them having as many as 150 wind turbines and an output of hundreds of megawatts (Martinez, 2007).

The electrical system for a wind farm can be divided into two sections. First, the system within the wind farm connecting all the turbines with each other, this is known as the collection system. The second section is the connection to power system, this is usually at high voltage and referred to as the transmission system. The collection system may collect power either as AC or DC (Bahirat et al. 2012).

2.4.1. AC Connection Topologies

2.4.1.1. Radial Connection

Radially connected wind farm is shown in Figure 2.9. The turbines which are used in the wind farm produce AC power. Several turbines are connected to a common cable depending on the current carrying capacity. Substation is connected to the common connection point of the turbines. Energy collected within the wind farm step-up transformer is transferred to the transmission line (Bahirat et al. 2012).

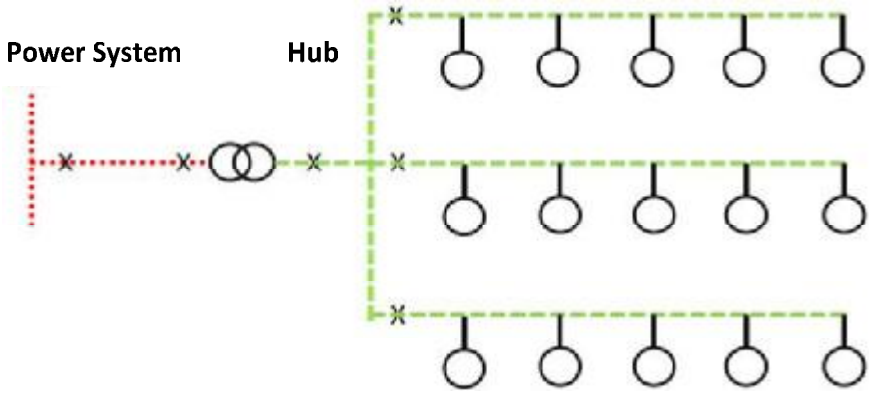


Figure 2.9. Radial Connection for AC Topologies (Bahirat et al. 2012)

2.4.1.2. Radial Loop Connection

Figure 2.10. shows a radial system with loop connections. These looped systems have higher reliability compared to the simple radial system. Phase errors that may occur on the system earthing and short-circuit fault on the supply structure is double alternative energy production has the structure connection. In normal operation mode switches alternative connection structure is the open position. Thus, the possibility of error is reduced within the system (Bahirat et al. 2012).

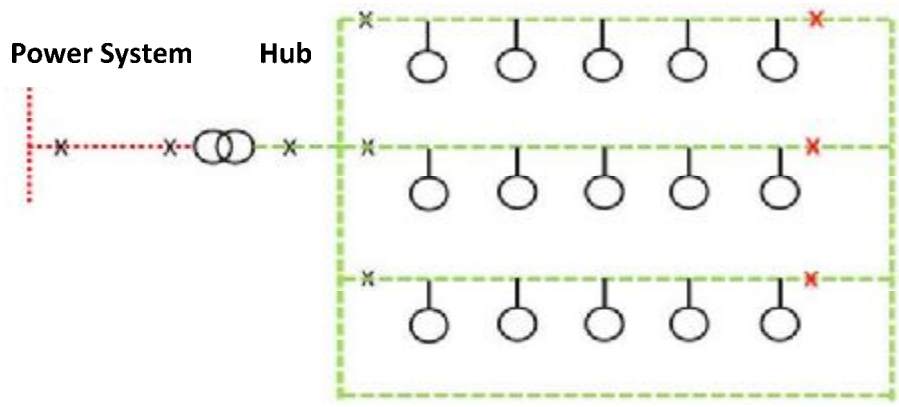


Figure 2.10. Radial Loop Connection for AC Topologies (Bahitar et al. 2012)

2.4.1.3. AC Star/Cluster Connection

Figure 2.11. shows the star or cluster connected AC wind farm topology. In this topology each turbine is connected to a point of interconnection (star/cluster point) by means of its own cable. In this connection the structure of each turbine is connected to the main links of the turbines due to any fault in the system makes the least impact (Bahirat et al. 2012).

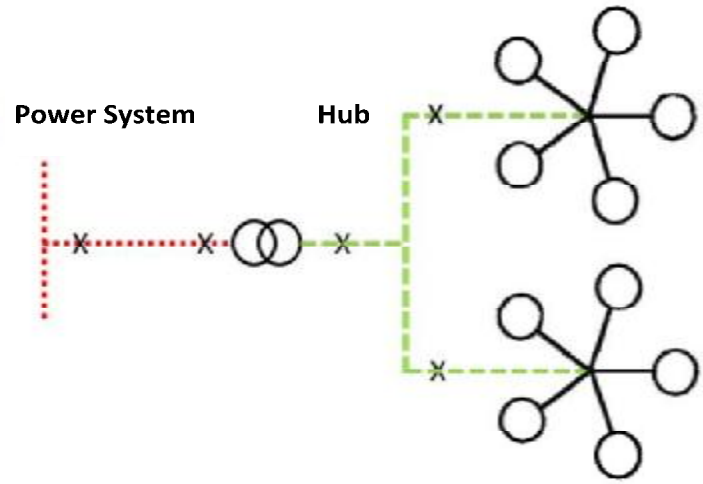


Figure 2.11. AC Star/Cluster Connection (Bahirat et al. 2012)

2.4.2. DC Connection Topologies

There are several DC connection topologies to connect wind farms/parks for DC transmission system. Basically three topologies for a VSC based DC transmission system are of interest in the case of an active stall (fixed speed) wind farm as shown in Figure 2.12.

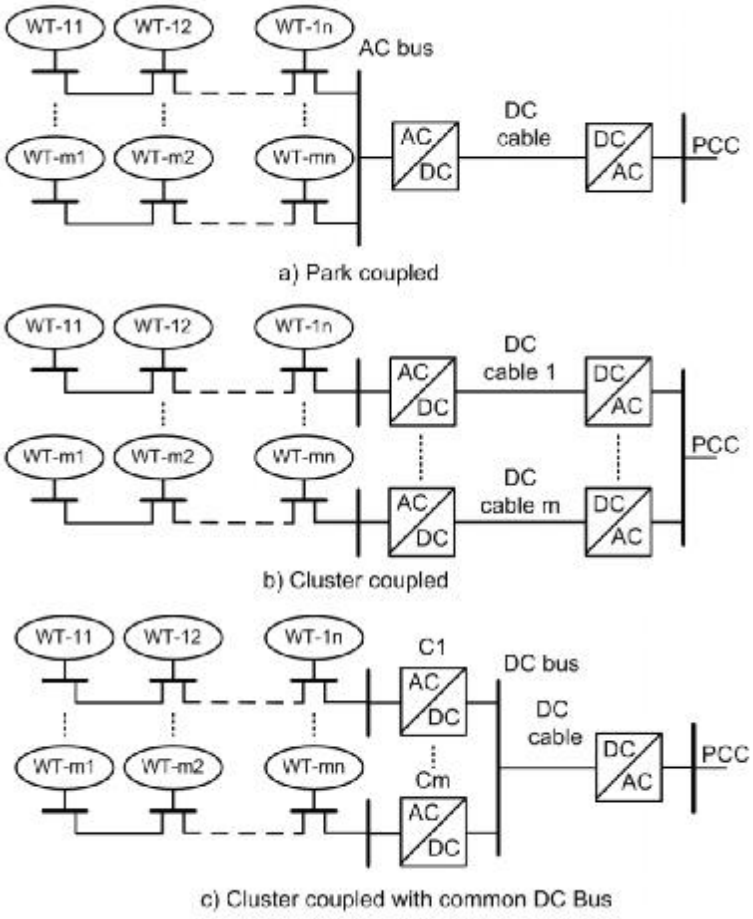


Figure 2.12. DC Transmission System Topologies for Connecting Wind Farms/Parks to the grid: a) park coupled, b) cluster coupled and c) cluster coupled with common DC Bus (Iov et al. 2005)

The park-coupled topology shown in Figure 2.12.a is suitable to connect existing or new wind farms up to a certain power level. This power level depends basically on the DC system topology. In this case the entire park will run at the same speed/frequency. Since the average value of the wind speed inside the wind park

varies considerably a cluster-coupled topology as shown in Figure 2.12.b can improve the total energy capture. In this case the wind park is divided into clusters, which will operate at different speeds/frequencies. Each cluster is connected to the grid by its own DC transmission system. This topology may be a solution for large wind farms. Finally, a common DC-bus can be used for several clusters as shown in Figure 2.12.c. A single DC cable is used to connect the wind farm/park to the grid via a single converter unit. This unit should be dimensioned for the rated power of the wind park (Iov et al. 2005).

3. MODELING OF WIND FARM

In this chapter, the details of a wind farm model are described. Initially, a general scheme of wind farm that is located in a region in Turkey is presented that has totally 48 MVA powered 16 wind turbines in two groups. Then, each component of wind farm model (wind turbine, drive train, converter and controller) are presented in detail and expressed mathematically.

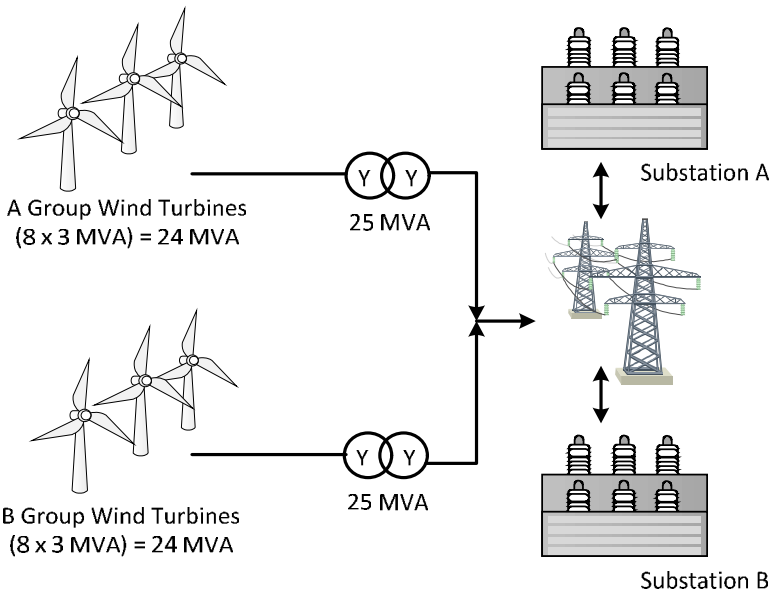


Figure 3.1. General scheme of wind farm model

In Figure 3.1, a wind farm connected to two different substations through two star-star connected transformer is shown. Internal connection of the general scheme of wind farm is also illustrated in Figure 3.2. The parameters of A and B substations are given in Table 3.1.

Table 3.1. Electrical parameters of Substations:

Substation Source	Voltage (Vph-rms)	Frequency (Hz)	Three Phase Short Circuit	Base Voltage (Vrms, ph-ph)	X/R Ratio
Substation A	154 KV	50 Hz	2500 MVA	154 KV	3.27
Substation B	154 KV	50 Hz	2500 MVA	154 KV	3.308

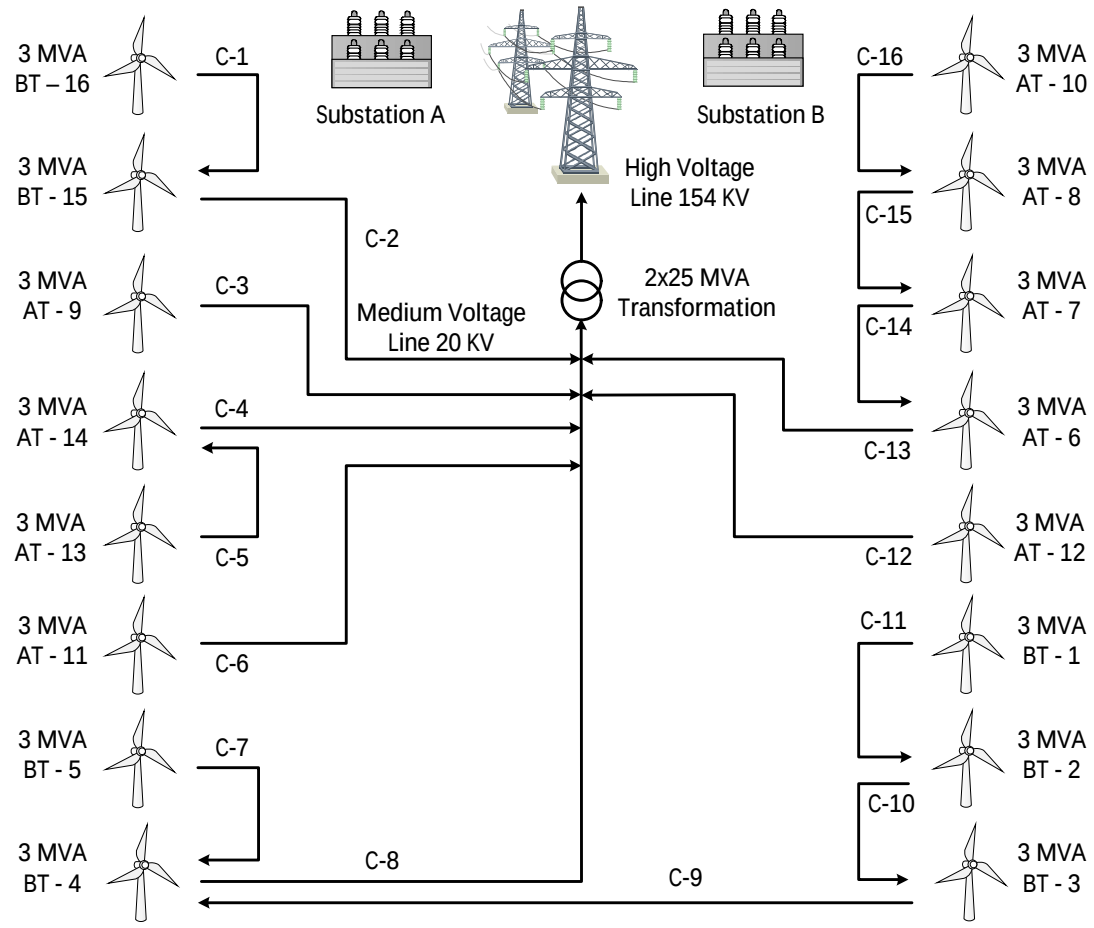


Figure 3.2. Internal Connection of the Wind Farm

Existing power cables and their specifications in the internal connection of the Wind Farm are given in Table 3.2.

Table 3.2. Existing power cables and their specifications in Wind Farm

EXISTING POWER CABLES					
Number	Length (m.)	Cross Section (mm^2)	Characteristic /Type	DC Conductor Resistance at 20 ^oC	Operation Inductance Approx.
C1	391	3*(1*70s/16)	24 kV. XLPE YE3SV	0.268 Ω/km	0.628 mH/km
C2	1009	3*(1*70s/16)	24 kV, XLPE YE3SV	0.268 Ω/km	0.628 mH/km
C3	938	3*(1*70s/16)	24 kV, XLPE YE3SV	0.268 Ω/km	0.628 mH/km
C4	691	3*(1*70s/16)	24 kV, XLPE YE3SV	0.268 Ω/km	0.628 mH/km
C5	580	3*(1*70s/16)	24 kV, XLPE YE3SV	0.268 Ω/km	0.628 mH/km
C6	600	3*(1*70s/16)	24 kV, XLPE YE3SV	0.268 Ω/km	0.628 mH/km
C7	295	3*(1*50s/16)	24 kV, XLPE YE3SV	0.387 Ω/km	0.659 mH/km
C8	270	3*(1*240s/25)	24 kV, XLPE YE3SV	0.075 Ω/km	0.531 mH/km
C9	585	3*(1*120s/16)	24 kV, XLPE YE3SV	0.153 Ω/km	0.585 mH/km
C10	245	3*(1*70s/16)	24 kV, XLPE YE3SV	0.268 Ω/km	0.628 mH/km
C11	285	3*(1*50s/16)	24 kV. XLPE YE3SV	0.387 Ω/km	0.659 mH/km
C12	650	3*(1*70s/16)	24 kV, XLPE YE3SV	0.268 Ω/km	0.628 mH/km
C13	800	3*(1*240s/25)	24 kV, XLPE YE3SV	0.075 Ω/km	0.531 mH/km
C14	360	3*(1*185s/25)	24 kV, XLPE YE3SV	0.099 Ω/km	0.551 mH/km
C15	410	3*(1*120s/16)	24 kV. XLPE YE3SV	0.153 Ω/km	0.585 mH/km
C16	361	3*(1*70s/16)	24 kV. XLPE YE3SV	0.268 Ω/km	0.628 mH/km

2.5. Wind Turbine Modeling

A mathematical model of wind turbine is essential for understanding the behavior over its region of operation because it allows for the development of comprehensive control algorithms. Wind turbine model is developed in this thesis is based on the steady-state power characteristics of the turbine. The output power of the turbine is given by the following equation (Matlab, 2013);

$$P_m = \frac{1}{2}\rho A_r V_w^{\,3} C_p(\lambda, \beta) \tag{3.1}$$

where P_m is the mechanical power extracted from the wind turbine (W), ρ is the air density (kg/m^3), A_r is the area swept by the rotor blades (m^2), V_w is the wind

speed (m/sec) and C_p is the performance coefficient of the turbine, which is a function of λ and β. λ is the tip speed ratio of the rotor blade tip speed to the wind speed (V_{tip}/V_w), β is the blade pitch angle in degrees.

The mechanical power of wind turbine is then normalized and expressed in the p.u. system that is given in Eq. (3.2);

$$P_{m(pu)} = k_p C_{p(pu)} V_{w(pu)}^3 \tag{3.2}$$

$$k_p = \frac{1}{2} \rho A_r \tag{3.3}$$

Performance or power coefficient C_p is the most important parameter in the case of power regulation and depends on wind speed, the speed of the turbine and the pitch of the blades. It is a non-linear function whose value is unique to each turbine type and is a function of wind speed that the turbine is operating in. The power coefficient of the turbine is given by:

$$C_p(\lambda, \beta) = C_1\left(C_2 / \lambda_i - C_3\beta - C_4\right)e^{-C_5/\lambda_i} + C_6\lambda \tag{3.4}$$

$$\frac{1}{\lambda_i} = \frac{1}{\lambda + 0.008\beta} - \frac{0.035}{\beta^3 + 1} \tag{3.5}$$

Fixing the ratio λ and the pitch blades β to their optimum values, the wind system will provide optimum electrical power.

$$\lambda = \frac{\Omega R}{v} \tag{3.6}$$

In Eq (3.6), Ω is the speed of turbine, R is the blade radius and v is the wind velocity. The coefficients from C_1 to C_6 in Eq (3.4) are:

C_1 = 0.5176;

C_2 = 116;

C_3 = 0.4;

C_4 = 5;

C_5 = 21 and

C_6 = 0.0068.

The C_p-λ characteristics, for different values of the pitch angle β, are illustrated in Figure 3.3. The maximum value of C_p (C_{pmax} = 0.48) is achieved for β = 0 degree and for λ = 8.1 (Belmokhtar et al., 2011)

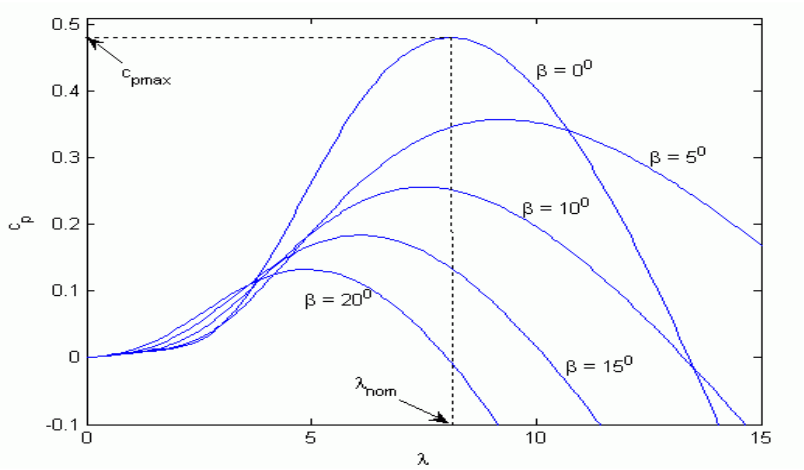


Figure 3.3. Power coefficient versus λ and β

3.2. Drive Train Modeling

The mechanical drive train model consists of the rotor shaft, generator shaft, and a gearbox. Shaft and gearbox in drive train can be modelled using two-mass inertia representation (Kuo, 1995). For a rotational system such as the one shown in Figure 3.4 consisting of a disk with a moment of inertia J mounted on a shaft fixed at one end, let us assume that the viscous friction coefficient (damping) is D and that the shaft torsional spring constant (stiffness) is K (Singh et al., 2011).

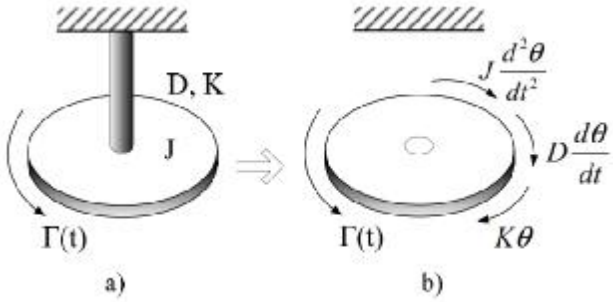


Figure 3.4. Rotational system with a disk (Singh et al., 2011)

The torque acting on the disk can be calculated from the free-body diagram of the disk, shown in Figure 3.4b, as follows;

$$G(t) = J\frac{d^2q(t)}{dt^2} + D\frac{dq(t)}{dt} + Kq(t) \tag{3.7}$$

A more complex rotational system, consisting of two such systems, is shown in Figure 3.5a. The two systems are coupled through a gear train, and Γ is the external torque applied to the disk of System 1. Γ_1 and Γ_2 are transmitted torques. N_1, N_2 are the numbers of teeth of Gear 1 and Gear 2. J_1, J_2, D_1, D_2, K_1, K_2 are the moments of inertia, damping, and stiffness of System 1 and System 2, respectively. The system is still time-dependent, but the notation *t* is dropped for the sake of clarity (Singh et al., 2011).

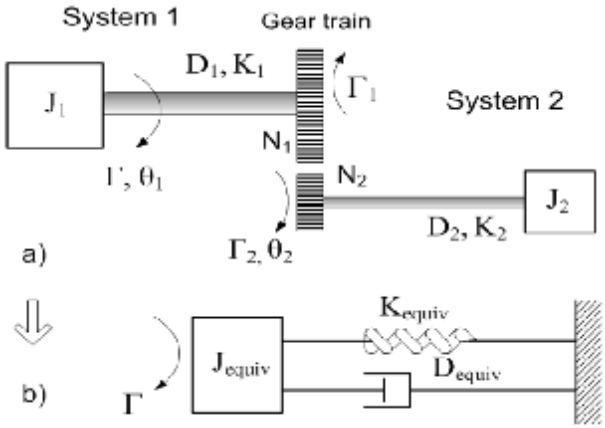


Figure 3.5. Rotational system incorporating a gear train (Singh et al., 2011)

Applying Eq. (3.7) to the system in Figure 3.5a, the torque equation at J_1 is;

$$G(t) = J_1 \frac{d^2 q_1(t)}{dt^2} + D_1 \frac{dq_1(t)}{dt} + K_1 q_1(t) \tag{3.8}$$

The torque equation at J_2 is;

$$G_2(t) = J_2 \frac{d^2 q_2(t)}{dt^2} + D_2 \frac{dq_2(t)}{dt} + K_2 q_2(t) \tag{3.9}$$

Since $\Gamma_1=(N_1/N_2)\,\Gamma_2$ and $\theta_2=(N_1/N_2)\,\theta_1$, the quantities on Gear 2 side can be referred to the Gear 1 side (Kuo, 1995).

$$G_1 = \left(\frac{N_1}{N_2}\right)\left(\frac{N_1}{N_2}\right) J_2 \frac{d^2 q_2}{dt^2} + D_2 \frac{dq_2}{dt} + K_2 q_2 \frac{\ddot{o}}{\div} \tag{3.10}$$

$$G_1 = \left(\frac{N_1}{N_2}\right)\left(\frac{N_1}{N_2}\right) J_2 \left(\frac{N_1}{N2}\right) \frac{d^2 q_1}{dt^2} + D_2 \left(\frac{N_1}{N_2}\right) \frac{dq_1}{dt} + K_2 \left(\frac{N_1}{N_2}\right) q_1 \frac{\ddot{o}}{\div} \tag{3.11}$$

$$G_1 = J_{ref1} \frac{d^2 q_1}{dt^2} + D_{ref1} \frac{dq_1}{dt} + K_{ref1} q_1 \tag{3.12}$$

where J_{refl}, D_{refl}, and K_{ref1} are the quantities reflected on the Gear 1 side. Substituting Eq. (3.12) into Eq. (3.7) and rearranging, we obtain Eq. (3.13) for the applied torque. The system in Figure 3.5a is reduced to the equivalent system in Figure 3.5b with the gear train eliminated.

$$G(t) = J_{equiv} \frac{d^2 q_1(t)}{dt^2} + D_{equiv} \frac{dq_1(t)}{dt} + K_{equiv} q_1(t) \tag{3.13}$$

where;

$$J_{equiv} = J_1 + J_2\left(\frac{N_1}{N_2}\right)^2 = J_1 + J_{ref1} \tag{3.14}$$

$$D_{equiv} = D_1 + D_2\left(\frac{N_1}{N_2}\right)^2 = D_1 + D_{ref1} \tag{3.15}$$

$$K_{equiv} = K_1 + K_2\left(\frac{N_1}{N_2}\right)^2 = K_1 + K_{ref1} \tag{3.16}$$

The simplified wind turbine configuration shown in Figure 3.6a is similar to the system in Figure 3.5a. The wind turbine drivetrain can therefore be modelled as a two-mass system coupled through a gear train. The quantities on the wind turbine rotor side of the gearbox can be reflected to the generator side. This eliminates the gear ratio and results in a two-mass representation of the wind turbine (Figure 3.6b). Neglecting the effects of the gearbox moment of inertia, damping, and stiffness is justifiable since the moment of inertia of the wind turbine rotor is comparatively very high (Singh et al., 2011).

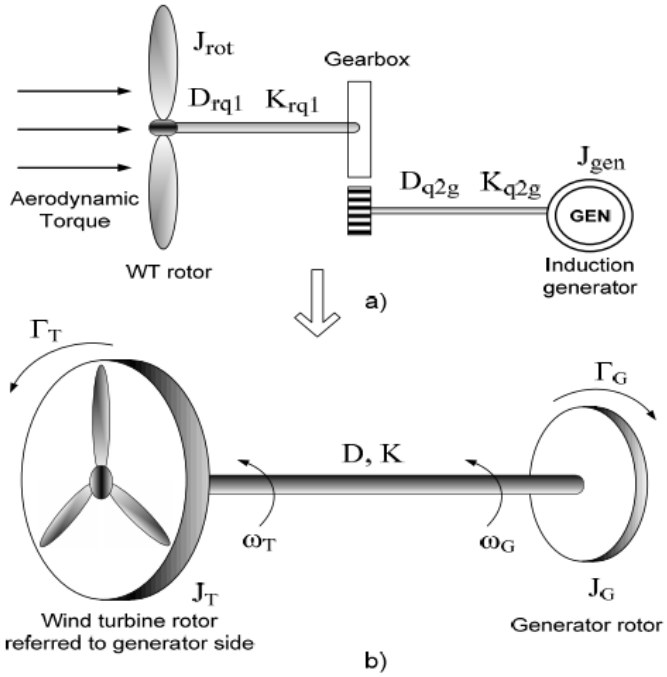


Figure 3.6. Wind turbine drivetrain model (Singh et al., 2011)

Torque equations representing the mechanical behaviour of the wind turbine are derived, based on the two-mass model. The aerodynamic torque from the wind turbine rotor and the electromechanical torque from the directconnect induction generator act in opposition to each other. Torque equations with all quantities referred to the generator side are:

$$J_T \ddot{\theta}_T + D(w_T - w_G) + K(\theta_T - \theta_G) = \Gamma_T \tag{3.17}$$

$$J_G \ddot{\theta}_G + D(w_G - w_T) + K(\theta_G - \theta_T) = -\Gamma_G \tag{3.18}$$

where J_T and J_G are moments of inertia of the wind turbine rotor and the generator (kgmm); Γ_T and Γ_G are wind turbine aerodynamic and generator electromagnetic torques (Nm); w_T and w_G are wind turbine rotor and the generator speeds (rad/s); θ_T and θ_G are angular position of the rotor and the generator (rad); D and K are equivalent damping and stiffness (Nms/rad), (Nm/rad) respectively.

Speeds and torques of the turbine rotor and the generator can be determined for each simulation time step by solving Equations 3.17 and 3.18 using a state-space approach. The state-space equations are (Singh et al., 2011):

$$\frac{d}{dt}(\theta_G - \theta_T) = (\omega_T - \omega_G) \tag{3.18}$$

$$\dot{\omega}_T = \left(\frac{1}{J_T}\right)[T_T - D(\omega_T - \omega_G) - K(\theta_T - \theta_G)] \tag{3.19}$$

$$\dot{\omega}_G = \left(\frac{1}{J_G}\right)[D(\omega_T - \omega_G) + K(\theta_T - \theta_G) - T_G] \tag{3.20}$$

2.6. Induction Generator Modeling

In this thesis, Doubly Fed Induction Generator (DFIG) is used as the generator. The wind turbine and integrated DFIG system is presented in Figure 3.7.

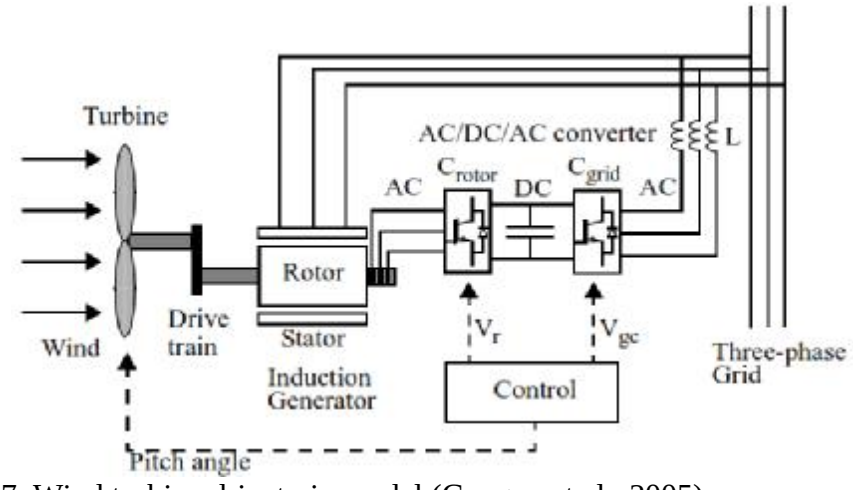


Figure 3.7. Wind turbine drivetrain model (Gangon et al., 2005)

Modeling can be of different type depending upon the type of study but basically modeling consists of the mathematical equations of DFIG which can be

achieved from the equivalent circuit of the DFIG. The equivalent circuit of the DFIG, with inclusion of the magnetizing losses, can be seen in Figure 3.8. This equivalent circuit is valid for one equivalent Y phase and for steady-state with the jω-method for calculations. (Gupta et al., 2013).

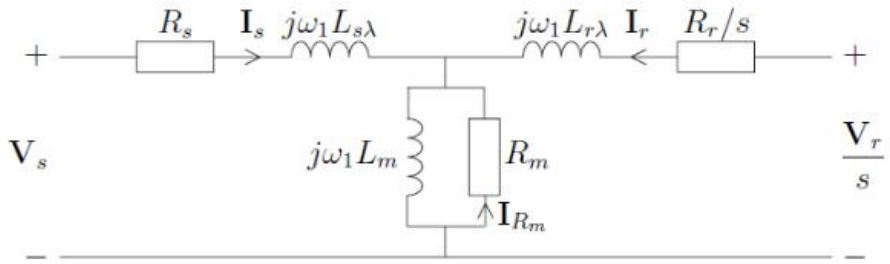


Figure 3.8. Equivalent circuit of the DFIG (Gupta et al., 2013)

Applying Kirchhoff□s voltage law to the circuit in Figure 3.7 yields;

$$V_s = R_s I_s + jw_1 L_{s\lambda} I_s + jw_1 L_m (I_s + I_r + I_{Rm}) \tag{3.21}$$

$$V_{r/s} = (R_r / s) I_r + jw_1 L_{r\lambda} I_r + j_1 L_m (I_s + I_r + I_{Rm}) \tag{3.22}$$

$$0 = R_m I_m + jw_1 L_m (I_s + I_r + I_{Rm}) \tag{3.23}$$

where V_s is stator voltage, R_s is stator resistance, V_r is rotor voltage, R_r is rotor resistance, I_s is stator current, R_m is magnetizing resistance, I_r is stator current, $L_{s\lambda}$ is stator leakage inductance, I_{Rm} is magnetizing resistance current, $L_{r\lambda}$ is rotor leakage inductance, w_1 is stator frequency, L_m is magnetizing inductance and s is slip. The slip s then can be expressed as (Gupta et al., 2013);

$$s(w_1 - w_r)/w_1 = w_2 / w_1 \tag{3.24}$$

where, w_r is the rotor speed and w_2 is the slip frequency. Moreover, if the air gap flux, stator flux and rotor flux and rotor flux are defined as;

$$\psi_m = L_m(I_s + I_r + I_{Rm}) \tag{3.25}$$

$$\psi_s = L_{sl} I_s + L_m(I_s + I_r + I_{Rm}) = L_{sl} I_s + \psi_m \tag{3.26}$$

$$\psi_r = L_{rl} I_r + L_m(I_s + I_r + I_{Rm}) = L_{rl} I_r + \psi_m \tag{3.27}$$

The equations describing the equivalent circuit can be rewritten as:

$$V_s = R_s I_s + j\omega_1 \psi_s \tag{3.28}$$

$$V_{r/s} = (R_r / s) I_r + j\omega_1 \psi_r \tag{3.29}$$

$$0 = R_m I_{Rm} + j\omega_1 \psi_m \tag{3.30}$$

The resistive losses of the induction generator are;

$$P_{loss} = 3\left(R_s |I_s|^2 + R_r |I_r|^2 + R_m |I_{Rm}|^2\right) \tag{3.31}$$

And it is possible to express the electro-mechanical torque, T_e , as;

$$T_e = 3n_p I_m \left|\psi_m I_r^*\right| = 3n_p I_m \left|\psi_r I_r^*\right| \tag{3.32}$$

2.7. AC-DC-AC Converter and DC Link Modeling

The power converter circuit consists of a rotor-side converter (RSC) and a grid-side converter (GSC) connected back-to-back including that of the DC-bus capacitor. According to Kirchhoff's voltage and current laws is governed by the following voltage and current equations (Aganah, 2013):

$$V_{qr} = r_r I_{qr} + p\psi_{qr} + (w - w_r)\psi_{dr} = \frac{M_{qr}}{2} V_{dc} \tag{3.33}$$

$$V_{dr} = r_r I_{dr} + p\psi_{dr} + (w - w_r)\psi_{qr} = \frac{M_{dr}}{2} V_{dc} \tag{3.34}$$

$$C_{dc} p V_{dc} = I_{or} - I_{os} \tag{3.35}$$

$$I_{or} = \frac{3}{4}\left(M_{qr} I_{qr} + M_{dr} I_{dr}\right) \tag{3.36}$$

$$I_{os} = \frac{3}{4}\left(M_{qf} I_{qf} + M_{df} I_{df}\right) \tag{3.37}$$

$$V_{qf} = r_f I_{qf} + L_f p I_{qf} + w L_f I_{df} + V_{qg} = \frac{M_{qf}}{2} V_{dc} \tag{3.38}$$

$$V_{df} = r_f I_{df} + L_f p I_{df} + w L_f I_{qf} + V_{dg} = \frac{M_{df}}{2} V_{dc} \tag{3.39}$$

where M_{qr}, M_{dr} are the modulation indices of RSC; M_{qf}, M_{df} are the modulation indices of the GSC; V_{qf}, V_{df} are the voltages at the output of the GSC and I_{qf}, I_{df} are the corresponding currents injected into the grid; V_{dc} is the DC bus voltage; C_{dc} is the DC bus capacitance; r_f, L_f are the resistance and inductance of the filter at the GSC output; and V_{qg}, V_{dg} represent the grid voltages (Aganah, 2013).

The active power flow through the back-to-back PWM converter is balanced by the dc-link capacitor. The power balance equation can be represented as follow:

$$P_r = P_g + P_{DC} \tag{3.40}$$

where P_r is the active power at the ac terminal of the RSC; P_g is the active power at the ac terminal of the GSC; P_{DC} is the active power of the link capacitor. These are given in the following equations (Tang et al., 2013);

$$P_r = v_{dr} i_{dr} + v_{qr} i_{qr} \tag{3.41}$$

$$P_g = v_{dg} i_{dg} + v_{qg} i_{qg} \tag{3.42}$$

$$P_{DC} = v_{DC} i_{DC} = - C v_{DC} \frac{dv_{DC}}{dt} \tag{3.43}$$

Substituting (3.41) - (3.43) into (3.40), the model of the dc link capacitor can be derived as follows (Tang et al., 2013):

$$C_{V_{DC}} \frac{dv_{DC}}{dt} = v_{dg} i_{dg} + v_{qg} i_{qg} - \left(v_{dr} i_{dr} + v_{qr} i_{qr} \right)$$

2.8. Controller Modeling

3.5.1. Rotor Side Controller Modeling

The rotor-side converter of DFIG is connected to the grid-side converter through a DC link capacitor. Assuming that the grid-side converter maintains a constant DC-link voltage, the role of the rotor side converter is to inject rotor frequency (variable) currents into the rotor circuit in such a manner as to achieve decoupled active and reactive power control. Since the converter operates in a stator-flux *dq0*-reference frame the rotor current is decomposed into an active power (*q-axis*) and a reactive power (*d-axis*) component. With change in wind speed, slip changes and thus the frequency or rotor currents. Actual active power (P_{gen}) is compared with the set point value (P_{ref}) which is determined by the wind speed. A PI controller is used as seen in Figure 3.9, to generate the required value *of q-axis* rotor

I_{qr}, Similarly, for reactive power, another PI controller is used to generate the required d-axis rotor current I_{dr} (Singh et al., 2011).

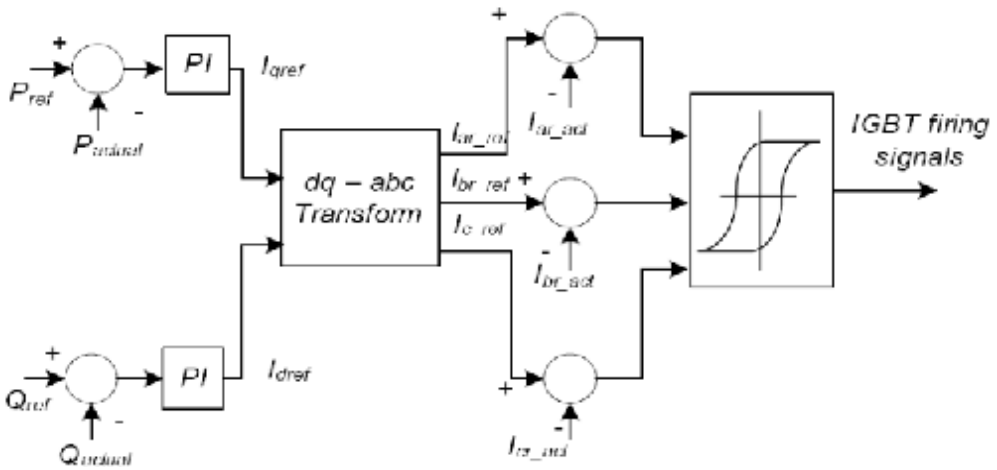


Figure 3.9. Rotor-side converter control (Singh et al., 2011)

3.5.2. Grid Side Controller Modeling

The grid side converter is responsible for balancing power injected into the DC link capacitor versus active power exchanged with the grid. The converter at the grid side is controlled in a manner so to achieve constant link voltage across the DC link capacitor. A relation between the DC link voltage and the *dq0-axis* stator currents and stator voltages is used to model the control and firing circuit for the grid-side converter. Field-oriented control, using Clarke and Park transforms, is used to obtain the actual *dq0-axis* stator currents and stator voltages. The desired *dq0* voltages to keep the DC link voltage constant, are obtained by comparing the actual value of the DC link voltage. PI controller is used to obtain the desired values of the stator voltages in *dq0* frame. The proportional gain (K_p) and integral gain (K_i) constants for the PI controller were determined using the Ziegler-Nichols method. These desired *dq0* voltages are then transformed to *abc* frame by applying the inverse Park-Clarke transforms to fire the IGBTs. Figure 3.10 shows the block diagram for the grid-side converter control circuit and the inverse Park-Clarke transform.

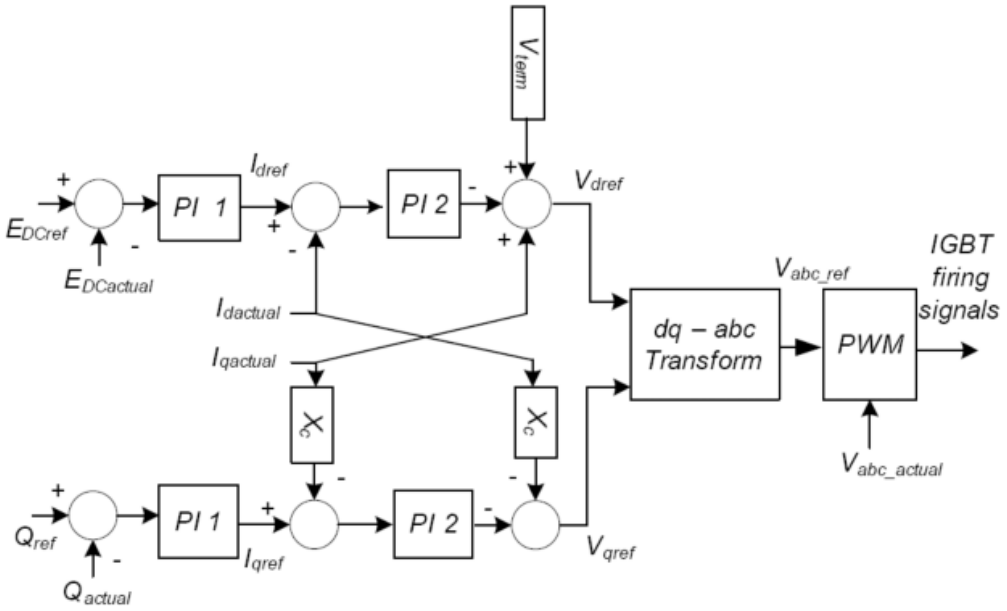


Figure 3.10. Grid-side converter control (Singh et al., 2011)

3.5.3. Pitch Controller Modeling

The pitch control changes blade pitch angle at higher than rated wind speeds to spill excess power. Thus, power output is maintained at rated value even though wind speed exceeds rated wind speed. In this particular implementation, reference power is per unitized and converted to reference speed based on look-up table. A multiplier after look-up table is included to maintain stability.

The pitch angle controller is shown in Figure 3.11. The reference speed and actual speed are compared and error drives the upper PI controller. Reference power and actual power are also compared and error drives the lower PI controller. PI controller outputs are summed and hard limited to generate the pitch angle signal. The pitch angle signal is active only when wind speed is close to rated, and otherwise is fixed at zero (Singh et al., 2011).

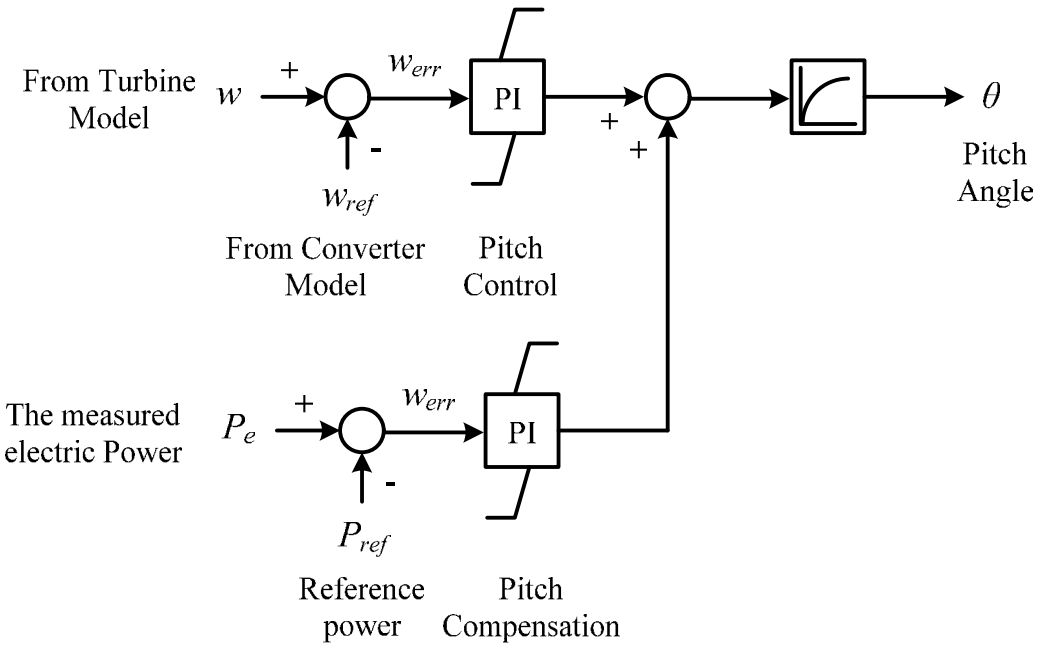


Figure 3.11. Pitch controller scheme

4. MODELING OF WIND FARM IN MATLAB

This chapter covers the MATLAB/Simulink modeling of wind farm given in previous chapter. Noting that Figure 3.2 shows the internal connections of wind farm and Table 3.1 and Table 3.2 give the parameters of the substations, wind turbines and cables used between wind turbines.

The overall simulation model of the wind farm is too big to fit in a page. Therefore, the wind farms are modeled as two subsystems. There are two wind farm groups named as Group A Wind Turbines and Group B Wind Turbines as it is in real. The overall simulation model is given in Figure 4.1 below.

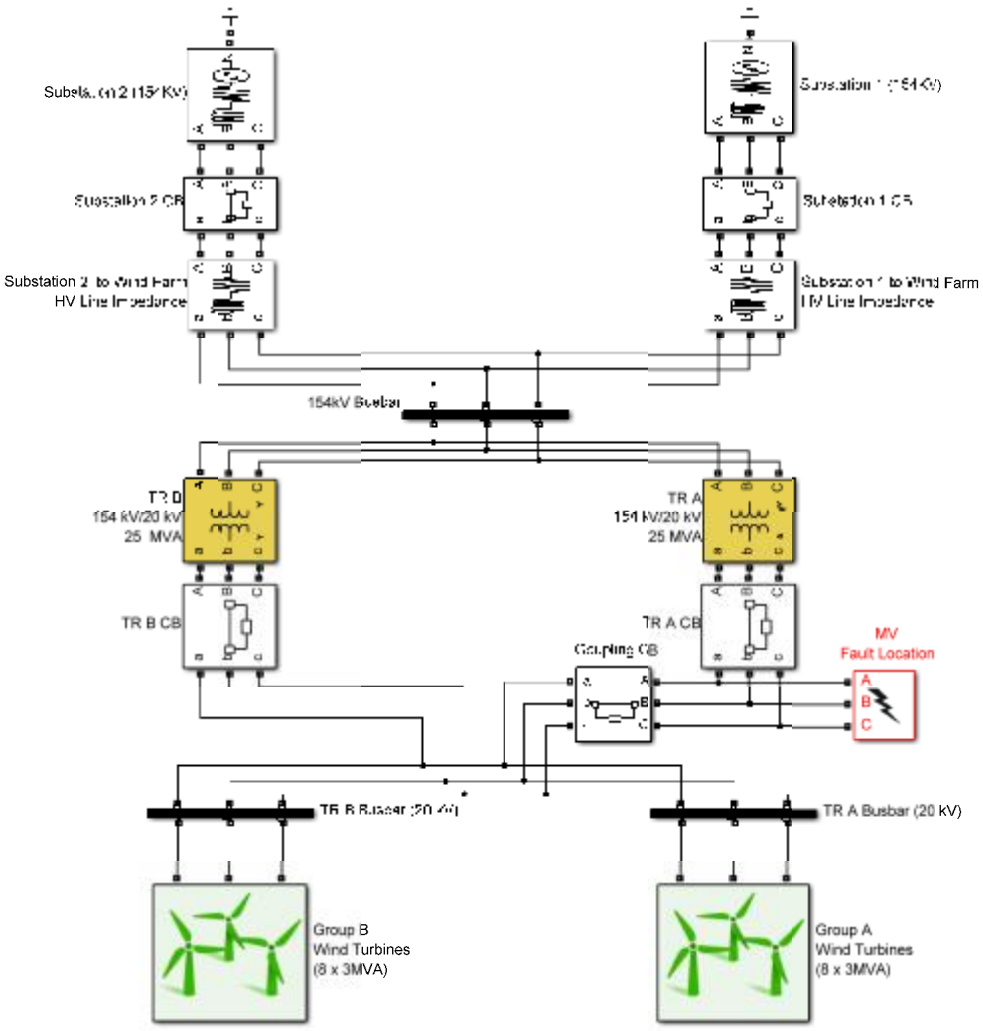


Figure 4.1. Simulation model of the wind farm

There are two large transformer substations connecting the modeled wind farm to the national grid. These substations are named as Substation 1 and Substation 2 in the model. Each substation has a circuit breaker for protection purposes. There are two lines feeding the 154 kV busbar which the wind farm transformers connected. The line fed from the Substation 1 is named as Substation 1 to Wind Farm HV Line. Similary, Substation 2 to Wind Farm HV Line is the second line feeding the 154 kV busbar.

Two 25 MVA, 20 kV/154 kV transformers, transformer A named as “TR A” and transformer B named as “TR B”, are used to connect the wind farm turbines to the 154 kV grid. Wind turbines are grouped into “Group A” and “Group B”. There are 8 wind turbines at each group. Transformer A is used to step up the voltage coming from Group A wind turbines where transformer B is used for Group B wind turbines.

Transformer A and transformer B have their own circuit breakers. A coupling circuit breaker is used to couple the transformer A with transformer B. There are two medium voltage busbars at 20 kV level at the input terminals of transformer A and B. Group A wind turbine transformer secondaries are connected to TR A busbar and Group B wind turbine transformer secondaries are connected to TR B busbar.

The aim of this thesis is to investigate the impact of a real wind farm to the national grid. To achieve this goal, several short circuit faults are created at different locations in the model. One of this short circuit locations is the “MV Fault Location”.

Figure 4.2 shows the inside of the Group A Wind Turbines subsystem. It can be seen from that each wind turbine is connected to 20 kV medium voltage level by means of 1 kV/20 kV three phase transformer. Each turbine has its own circuit breaker for protection functions. The turbines are named by using the convection that the first letter gives the group name of the turbine and “T” stands for the turbine, the number at last is the turbine number. As an instance “AT3” means the wind turbine in the group A with the number of three.

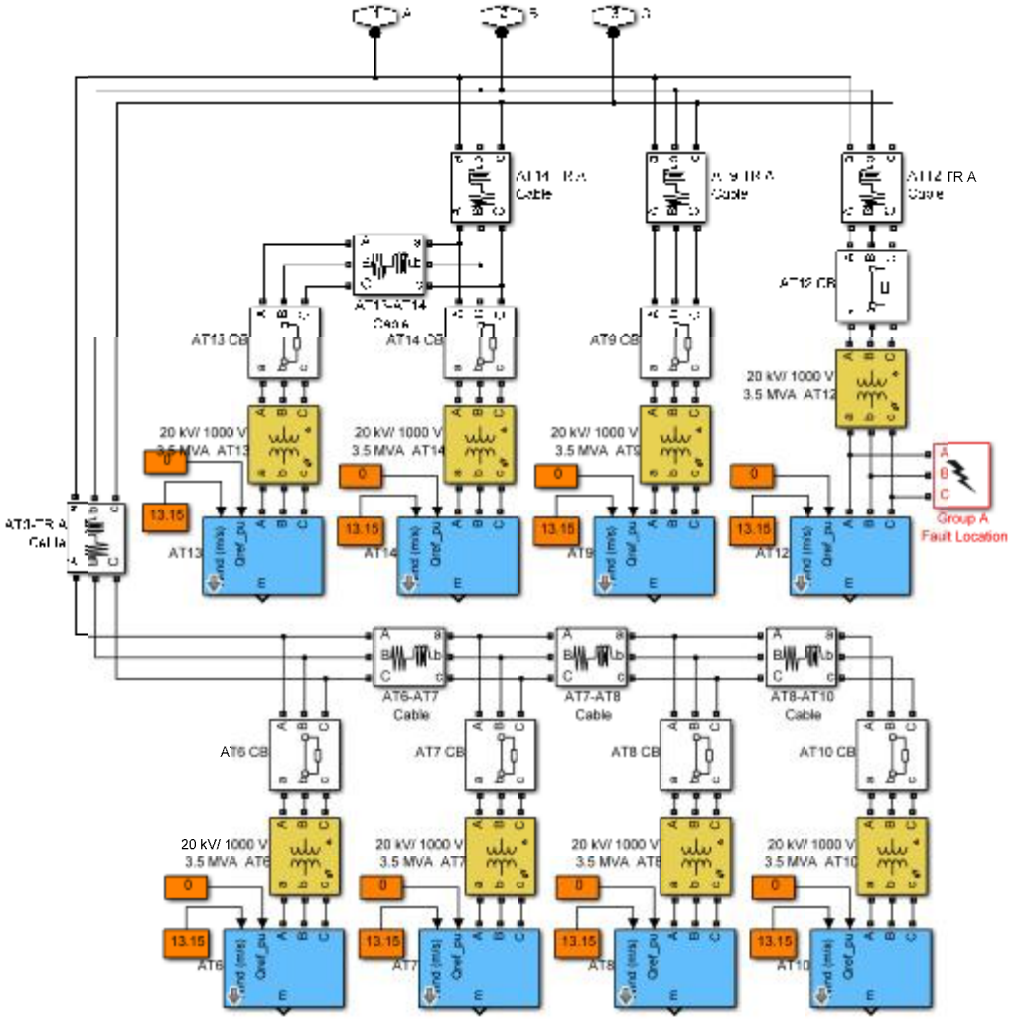


Figure 4.2. Subsystem model of Group A Wind Turbines

AT10 is connected to AT8 by using a cable connection named as AT8-AT10 cable in the model. Similarly, AT8 is connected to AT7 using AT7-AT8 cable. This convection is used throughout the overall model. The last connection in this radial line is the AT7 to AT6 connection. From AT6 turbine, the total power is transferred to TR A over the AT6-TR A Cable.

AT13 is connected to AT14 and from AT14, these two turbines are connected to the MV busbar over AT14-TR A Cable. AT9 and AT12 have their own cables for the connection to MV level.

Each turbine has two inputs. One of these inputs is used for wind speed while the other input is used for reference reactive power. A fixed rate of wind speed is

applied to whole system as only short circuit durations will be dealt. To investigate the impact of a short circuit occurred in the Group A, “Group A Fault Location” is used.

Figure 4.3 is used to illustrate the internal connections of Group B wind turbines. The same convection is used for Group B wind turbines.

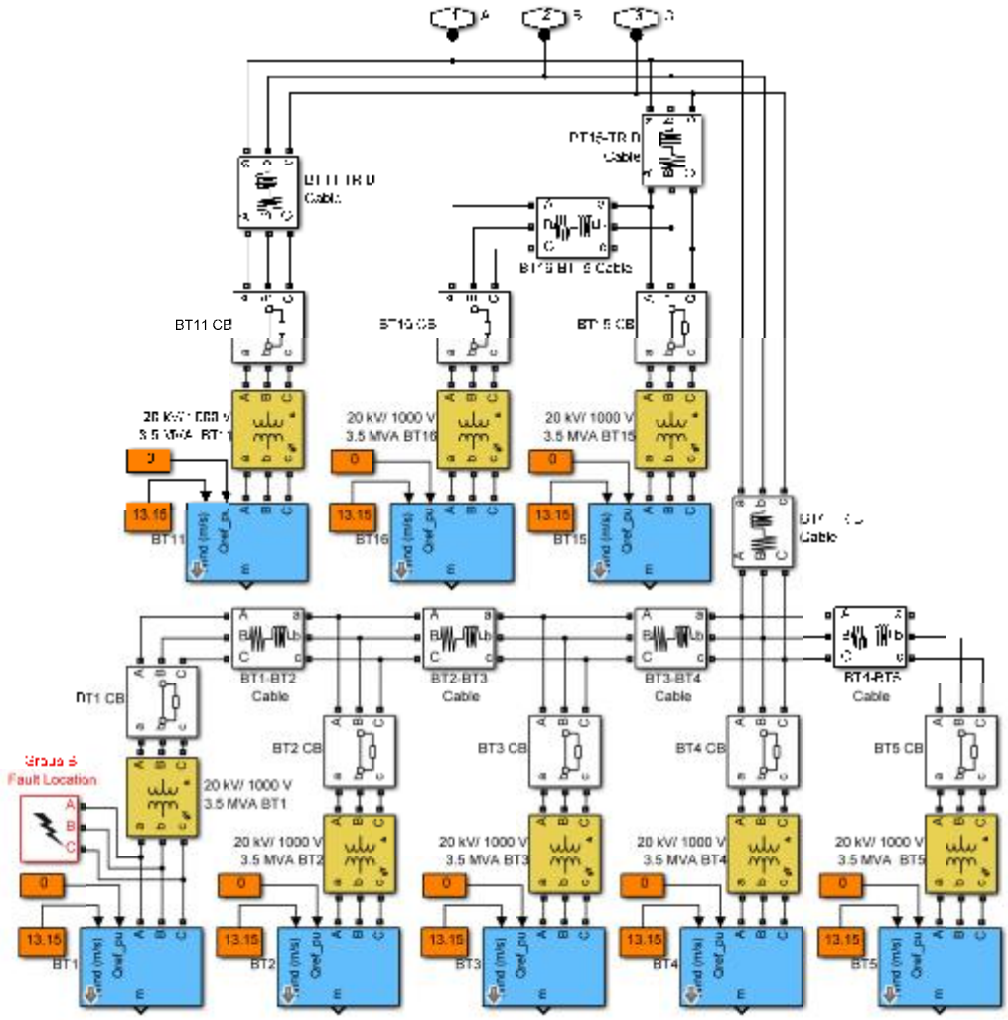


Figure 4.3. Subsystem model of Group B Wind Turbines

From the Figure 4.3, it can be seen that BT1 is connected to BT2, BT2 is connected to BT3 and BT4. And BT5 is also connected to BT4. From BT4, a line used to connected the total power generated by BT1, BT2, BT3, BT4 and BT5 to TR

B. BT11 is connected to 20 kV busbar through it's own line. BT16 is connected to BT15 and a line connects BT15 to medium voltage busbar.

Group B Fault Location block is connected near BT1 output. It will be used to investigate the short circuit effects to the grid caused from Group B wind turbines.

The main blocks used to model the wind farm is explained in the following pages. The first block to consider is Three Phase Source which can be seen in Figure 4.4. The same figure also covers the block parameters. This block is used to model transformer substations in the real world.

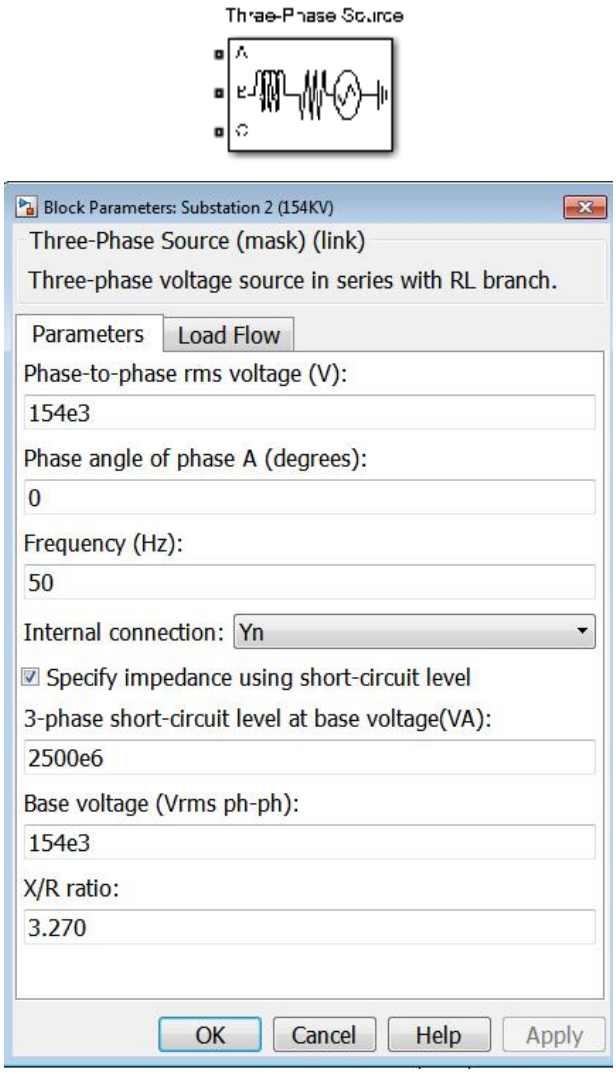


Figure 4.4. Three Phase Source block and parameters

From the block parameters, it is easy to see that the source has a phase-to-phase rms voltage of 154 kV with 0 degree phase angle. The output frequecny of the source is 50 Hz. The impedance of the source is given using short-circuit level. The values are taken from the real world case. The short circuit current level is 2500 MVA. And the X/R ratio of the source is 3.270.

The high voltage line which is not too long is modeled using Three Phase Series RLC Branch with series resistor and inductor. High voltage lines from Substations to transformers and cables between transformers and wind turbines are modeled by this block. Figure 4.5 shows the block and Table 4.1 gives the line or cable names, lengths, R and X parameters used in simulation.

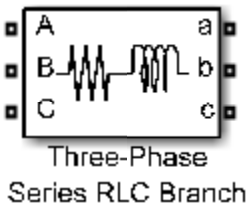


Figure 4.5. Block used to model of line impedances

Table 4.1. Line impedance and Cable Block parameters

Line/Cable Name	Length(km)	R (ohm)	X (ohm)
Substation1 to Wind Farm HV Line Imped.	16,801	2,2546942	0,023000569
Substation2 to Wind Farm HV Line Imped.	10,346	1,3884332	0,014163674
BT1 to BT2 Cable	0,285	0,1102950	0,000187815
BT2 to BT3 Cable	0,245	0,0656600	0,000153860
BT3 to BT4 Cable	0,585	0,0895050	0,000342225
BT4 to BT5 Cable	0,295	0,1141650	0,000194405
BT4 to TR B Cable	0,270	0,0203580	0,000143370
BT16 to BT15 Cable	0,391	0,1047880	0,000245548
BT11 to TR B Cable	0,600	0,1608000	0,000376800
BT15 to TR B Cable	1,009	0,2704120	0,000633652
AT6 to AT7 Cable	0,360	0,0356760	0,000198360
AT7 to AT8 Cable	0,410	0,0627300	0,000239850
AT8 to AT10 Cable	0,822	0,2751550	0,000530507
AT6 to TR A Cable	0,800	0,0603200	0,000424800
AT9 to TR A Cable	0,938	0,2513840	0,000589064
AT12 to TR A Cable	0,650	0,1742000	0,000408200
AT13 to AT14 Cable	0,580	0,1554400	0,000364240
AT14 to TR A Cable	0,691	0,1851880	0,000433948

The wind turbines are connected to the national grid via two medium voltage to high voltage transformer. And low voltage to medium voltage transformers are used to built the medium voltage from the wind turbine outputs. Figure 4.6 shows the Simulink block for the transformer. The same block is used for both types of transformers.

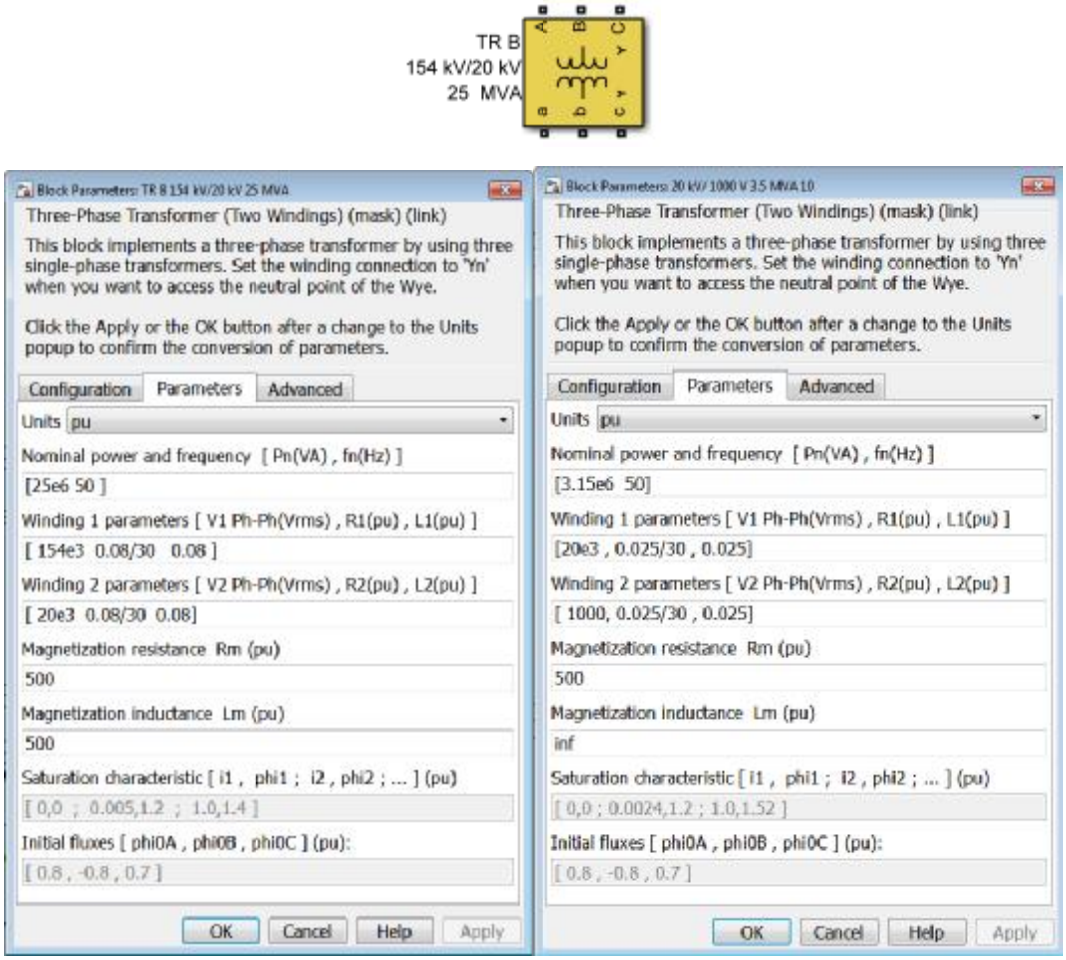


Figure 4.6. MV to HV transformer and LV to MV transformer parameters

The wind turbines are based on Double Fed Induction Generator in real wind farm. The wind turbines of the real farm are modeled using DFIG Wind Turbine block in Simulink which is shown in Figure 4.7. There are five parameter pages for this block.

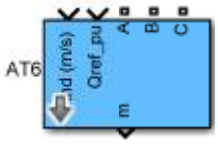


Figure 4.7. Simulink block of double fed induction generator wind turbine

The first parameter page covers the generator data. Nominal power of the generator, line to line stator voltage, rotor voltage and rated frequency are the main parameters. It can be seen from Figure 4.8, the wind turbine is rated at 3 MVA with a

power factor of 0,9. The stator line to line rms voltage is 1000V and rotor line to line rms voltage is 400V. The rated frequency of the generator is 50 Hz.

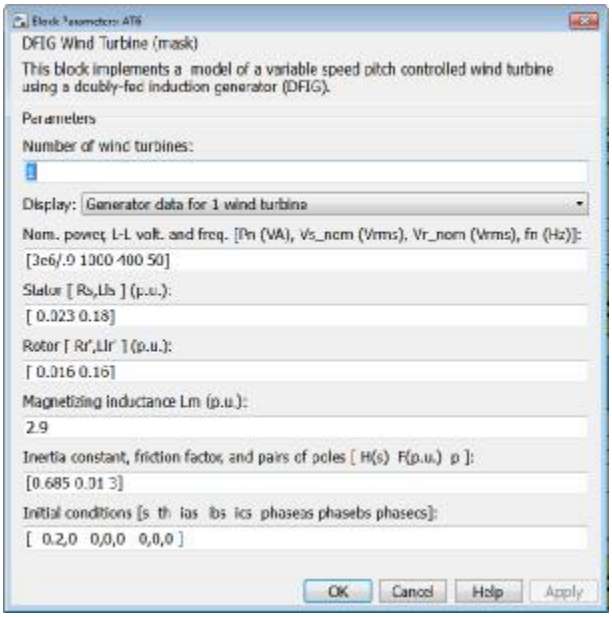


Figure 4.8. DFIG Wind Turbine generator data parameter page

The second parameter page is used to input the converter parameters to the simulation model. This parameters cover grid side converter maximum current, grid side coupling inductor resistance and inductance, nominal DC bus voltage, DC bus capacitor and line filter capacitor. Figure 4.9 shows the parameters used in the simulation.

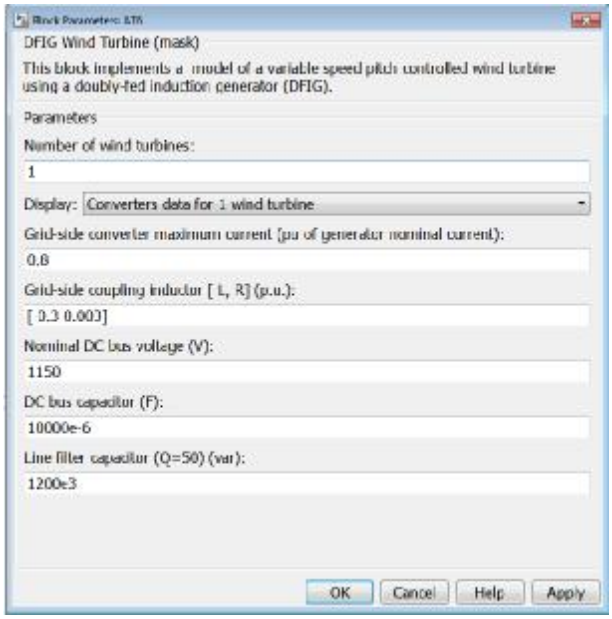


Figure 4.9. DFIG Wind Turbine converter data parameter page

Nominal mechanical output power of the turbine, wind speed at nominal speed and Cp max and initial wind speed are input to the simulation model using the third page of the DFIG Wind Turbine which can be seen in Figure 4.10. From the figure, it is easy to see that the mechanical power of the turbine is 3 MW, and its rated wind speed is 11 m/s. The simulation assumes that the initial wind speed is 11 m/s.

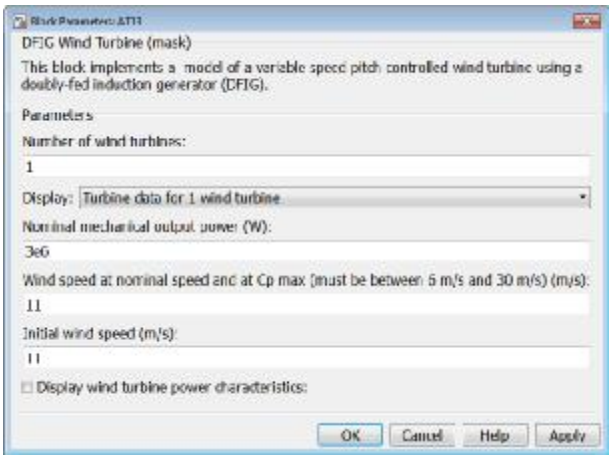


Figure 4.10. DFIG Wind Turbine turbine data parameter page

The fourth page is the drive train data parameter page that can be seen in Figure 4.11. Turbine mechanical parameters are entered to the simulation model using this page. As previous parameters, these parameters are taken from the real wind turbine.

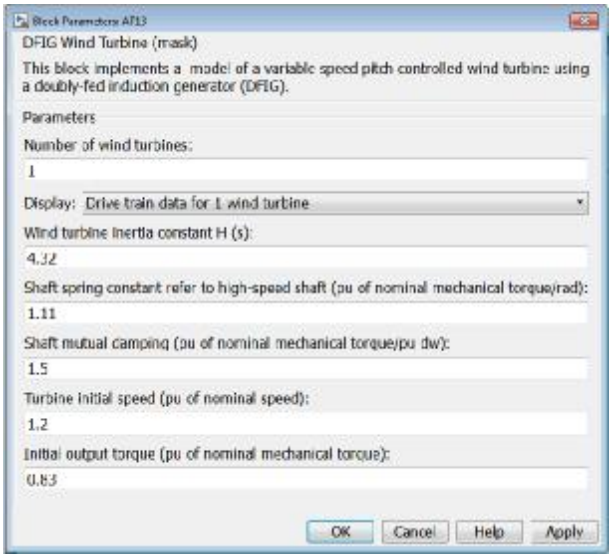


Figure 4.11. DFIG Wind Turbine drive train data parameter page

The last page of DFIG Wind Turbine covers control parameters of the system. In a DFIG turbine, a dc bus voltage regulator, grid side converter current regulator, speed regulator, rotor side converter current regulator, reactive power and voltage regulator and pitch controller are employed. Figure 4.12 shows the control parameters of the wind turbines used in the simulation.

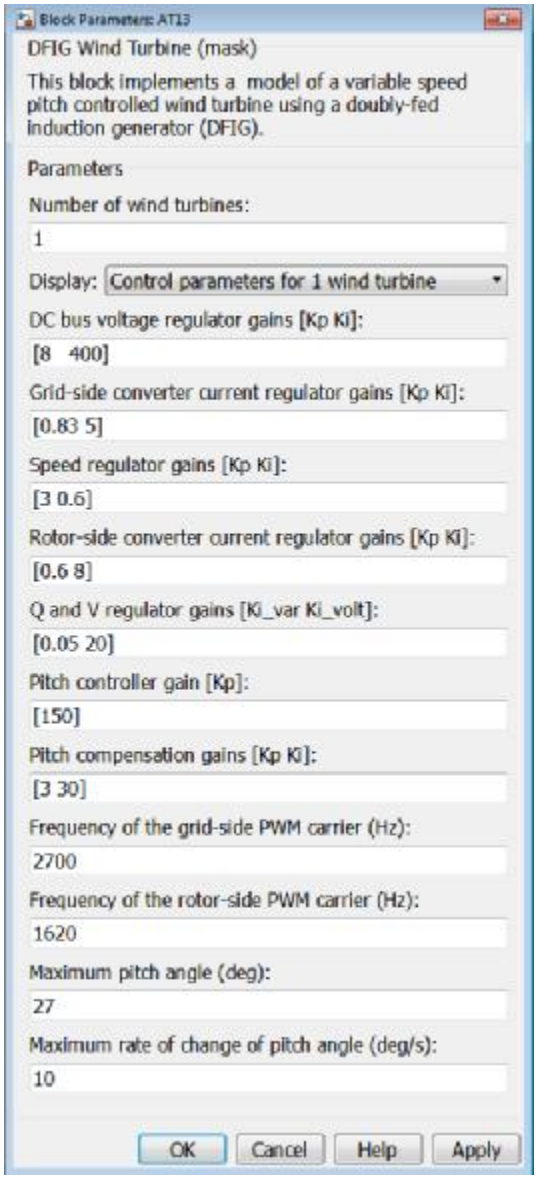


Figure 4.12. DFIG Wind Turbine control parameter page

To regulate the DC bus voltage between back to back converter, a PI controller is employed. PI controllers also used for grid side and rotor side converter current control as well as speed control of wind turbine.

Reactive power and voltage are controller by an integral law. Pitch controller has only a proportional gain, while pitch compensation controller uses a PI structure. The pulse width modulation frequency of both converters are also input to the last page of the DFIG Wind Turbine block.

The last important block used in the simulation is the Three phase Fault which can be seen in Figure 4.13.



Figure 4.13. Three Phase fault block

Figure 4.14 shows the main block parameters of Three Phase Fault. One can select which phase will fault using the checkboxes. The fault times can be adjusted by entering the required start and stop times to the transition times parameter.

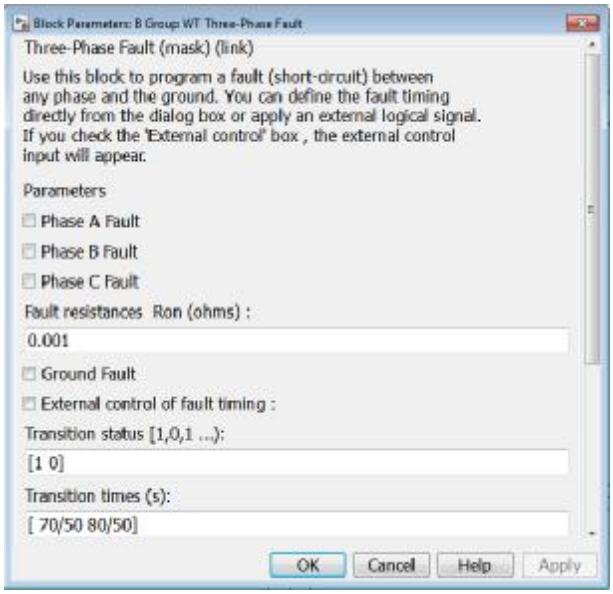


Figure 4.14. Three phase Fault block parameters

In this chapter, the simulation model build in the thesis is introduced . Next chapter covers the simulation results for different case studies.

5. SIMULATION RESULTS AND CASE STUDIES

In this chapter, to investigate the impact of the aforementioned wind farm on the interconnected transmission system, several case studies are carried out. These cases cover harmonic impact of wind power on the system and different short circuit situations. Various short circuit faults are created in cases and the results are investigated. In this context, A group wind turbine, B group wind turbine and medium voltage line faults are examined. Simulation results of normal operation of wind farm system with fixed and variable wind speeds are also analyzed.

5.1. Case 1: Normal Operation (No Fault Condition)

5.1.1. Normal Operation at Fixed Speed

In this case study, same wind speed characteristics (13.15 m/s) is considered for each wind turbine in the wind farm. The system performance is evaluated without any fault condition. Voltage and current waveforms for each phase for this case are shown in Figure 5.1 and Figure 5.2 respectively.

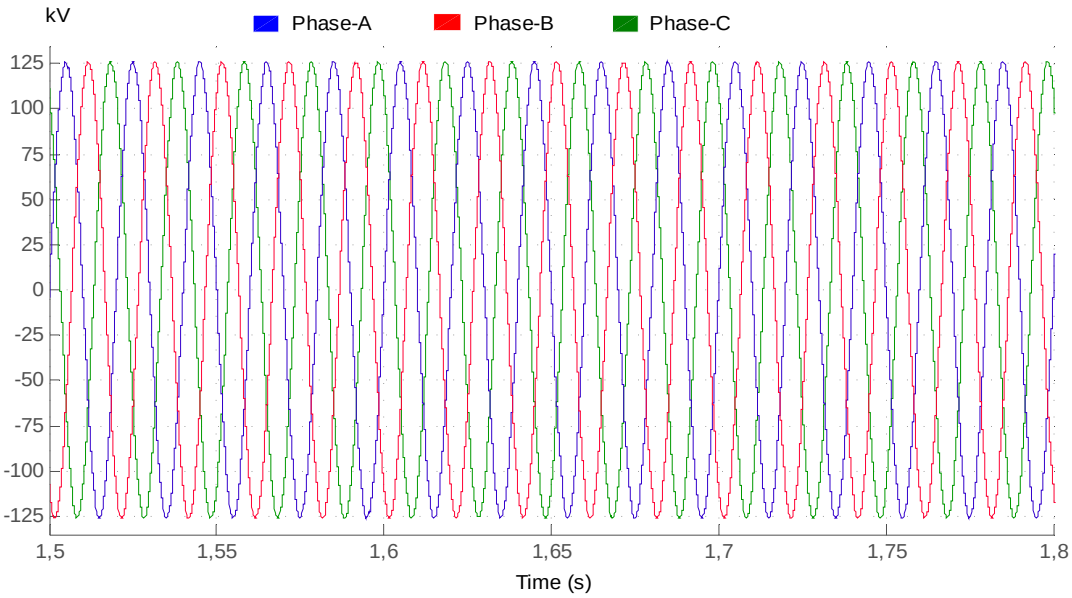


Figure 5.1. Phase voltages of High Voltage Line side for 5.1.1 case

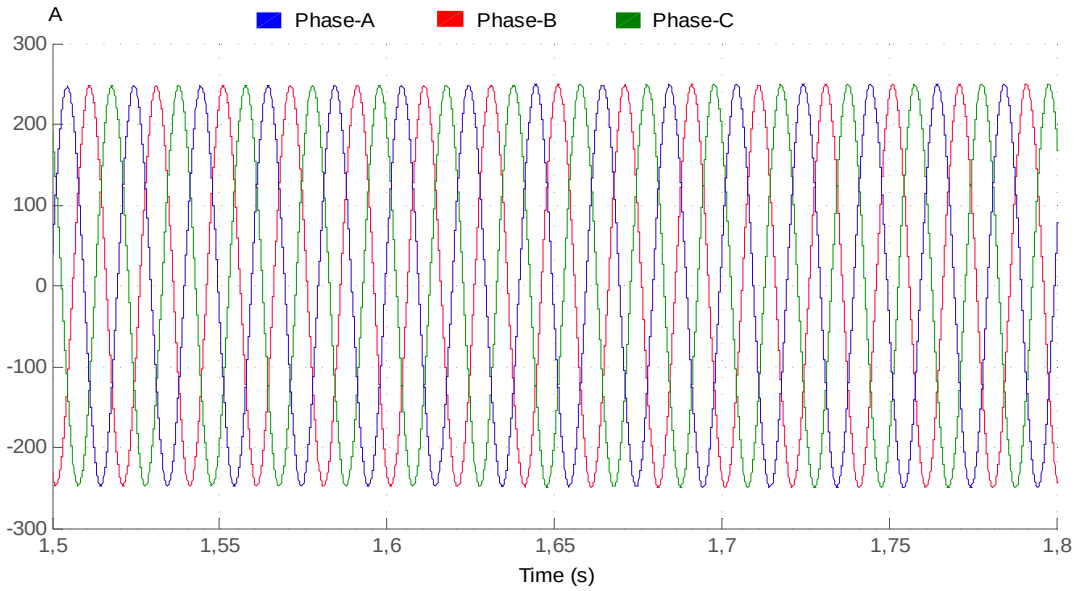


Figure 5.2. Phase currents of High Voltage Line side for 5.1.1 case

Active and reactive power at the point of common coupling that A and B group wind turbines are connected on medium voltage line are measured and showed in Figure 5.3. It is observed that generated active power is constant at 48 MW and no reactive power is absorbed from interconnected transmission system, as there is no fault.

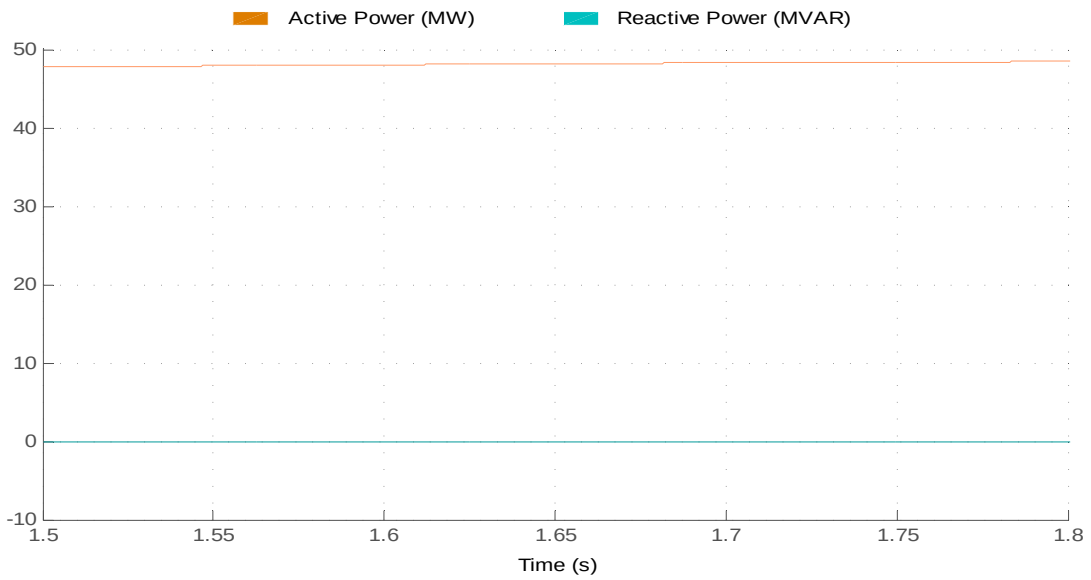


Figure 5.3. Active and reactive powers of MV Line side for 5.1.1 case

Frequency deviation is observed and presented in Figure 5.4, as it is seen from the figure that frequency is not changed during this case.

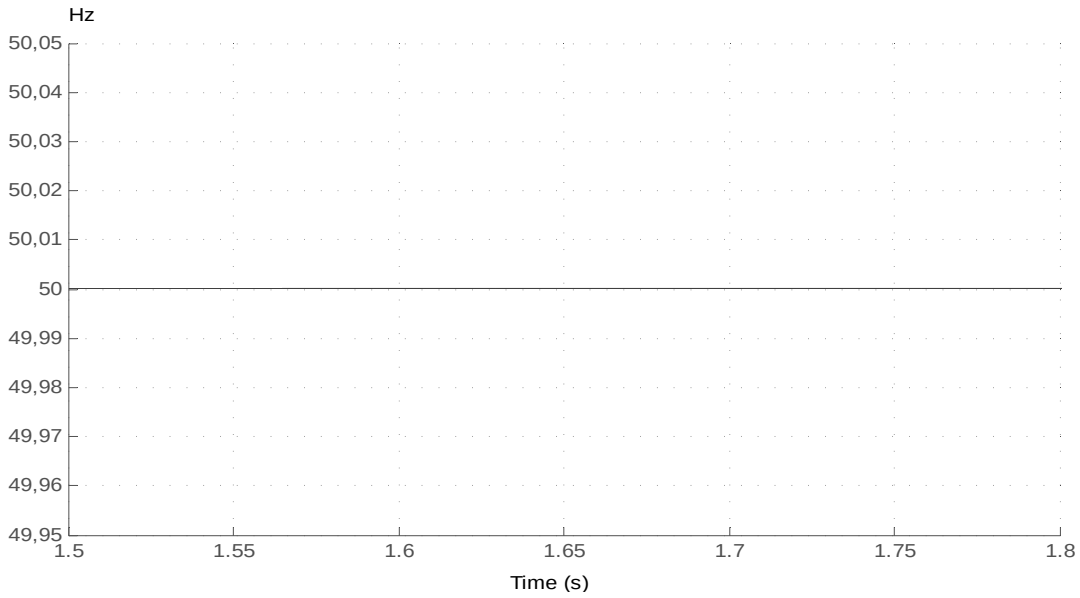


Figure 5.4. Frequency change of MV Line side for 5.1.1 case

For steady state operation, voltage and current total harmonic distortion (THD) values of the system for Substation 1 and 2 are given in Table 5.1. Voltage and current THD are always kept below the harmonic limits during steady state operation which is 3% at high voltage side.

Table 5.1. FFT Analysis of Substation 1 and 2 at normal operation

Substation	Voltage/Current	Phase	THD (%)
Substation 2	Voltage	A	0.12
Substation 2	Voltage	B	0.12
Substation 2	Voltage	C	0.12
Substation 2	Current	A	0.69
Substation 2	Current	B	0.71
Substation 2	Current	C	0.62
Substation 1	Voltage	A	0.15
Substation 1	Voltage	B	0.15
Substation 1	Voltage	C	0.15
Substation 1	Current	A	0.69
Substation 1	Current	B	0.71
Substation 1	Current	C	0.62

5.1.2. Normal Operation at Variable Speed

In this case, Arma Wind Gaussian Noise Generator module is used to generate random wind speeds for each wind turbine in the wind farm. Different wind speeds are created as shown in Figure 5.5, Figure 5.7, Figure 5.9 and Figure 5.11 for 16 different wind turbines in wind farm system.

For comparison purposes, the rotor speeds of corresponding turbines are also given in Figure 5.6, Figure 5.8, Figure 5.10 and Figure 5.12.

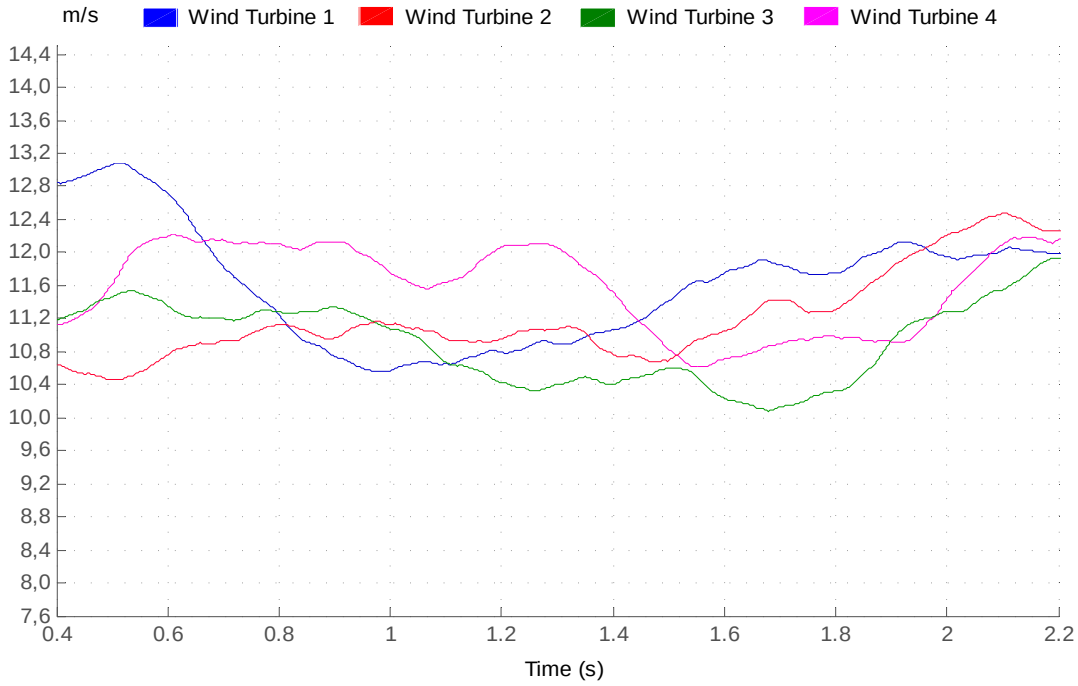


Figure 5.5. Wind Speeds for Wind Turbine 1 to 4 for case 5.1.2

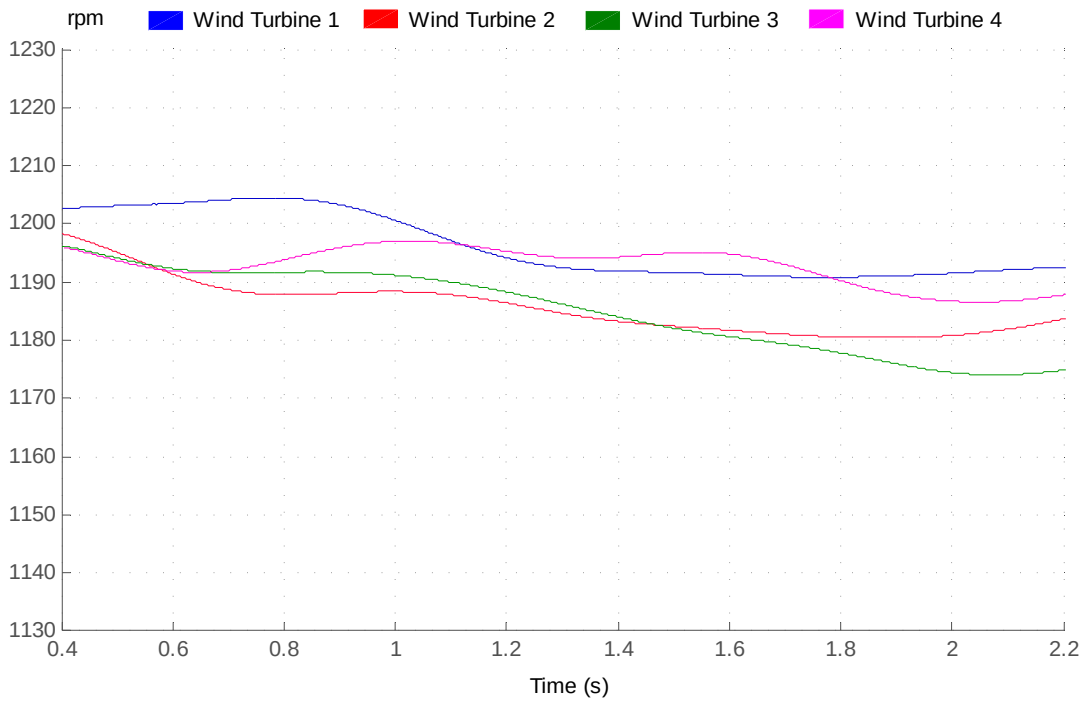


Figure 5.6. Rotor Speeds for Wind Turbine 1 to 4 for case 5.1.2

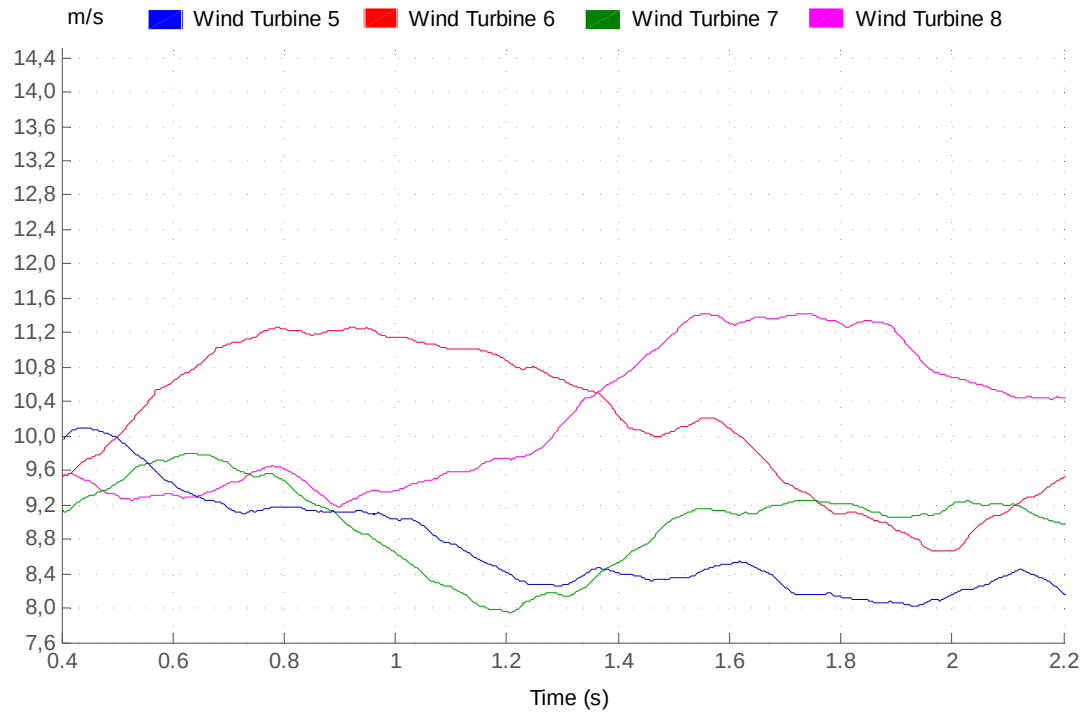


Figure 5.7. Wind Speeds for Wind Turbine 5 to 8 for case 5.1.2

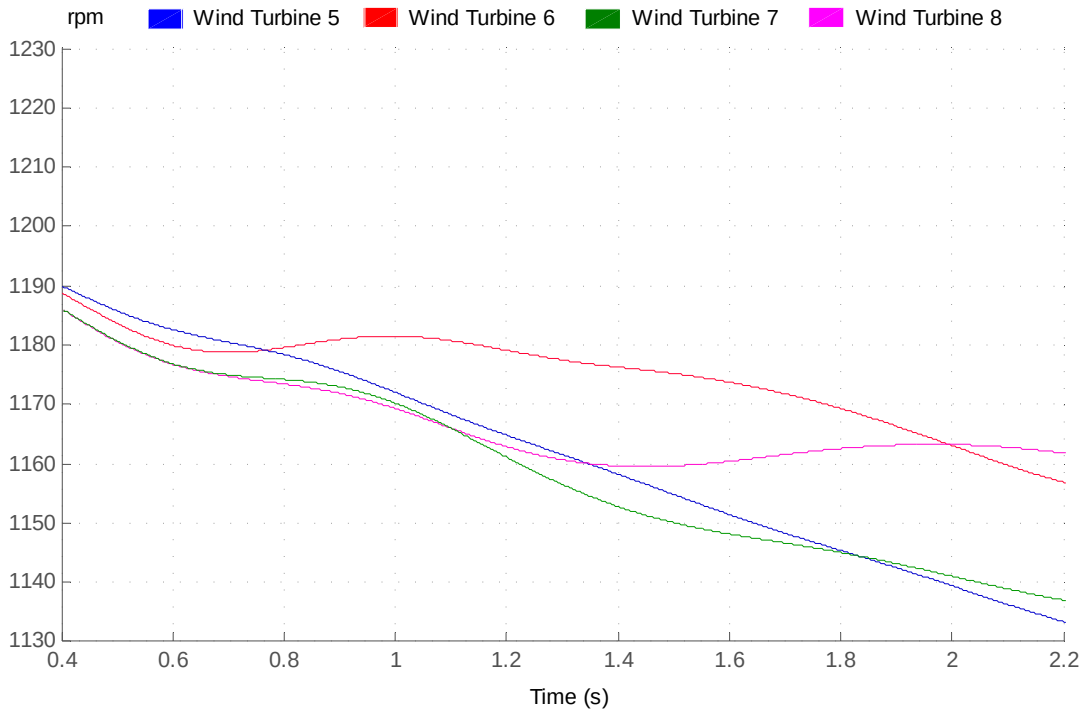


Figure 5.8. Rotor Speeds for Wind Turbine 5 to 8 for case 5.1.2

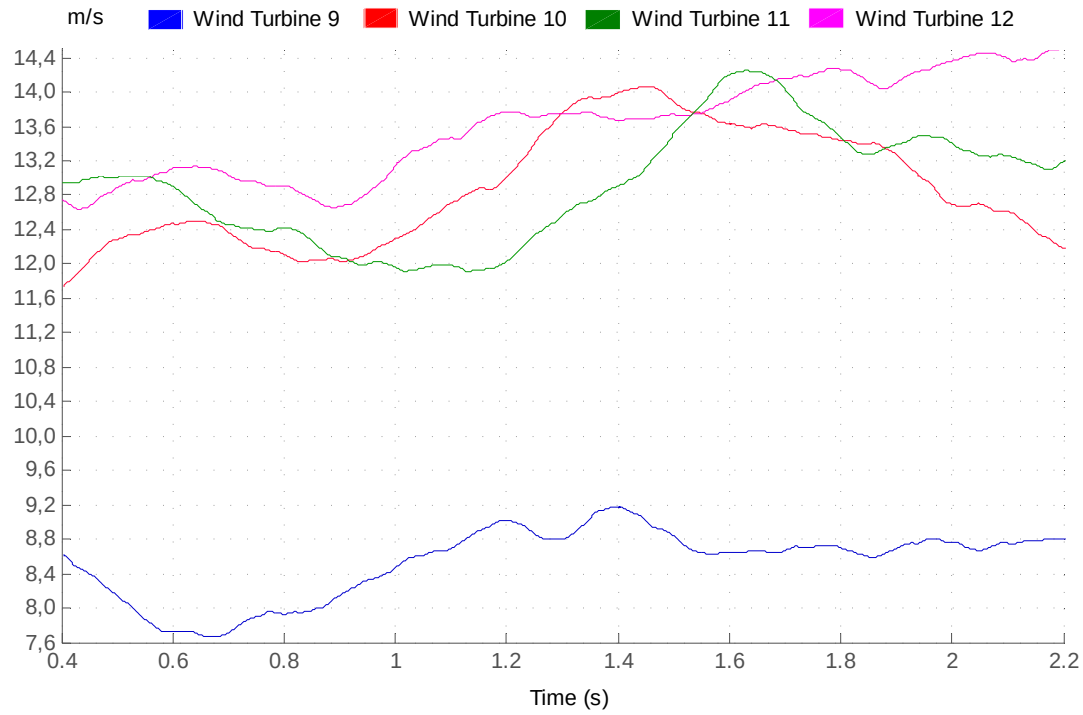


Figure 5.9. Wind Speeds for Wind Turbine 9 to 12 for case 5.1.2

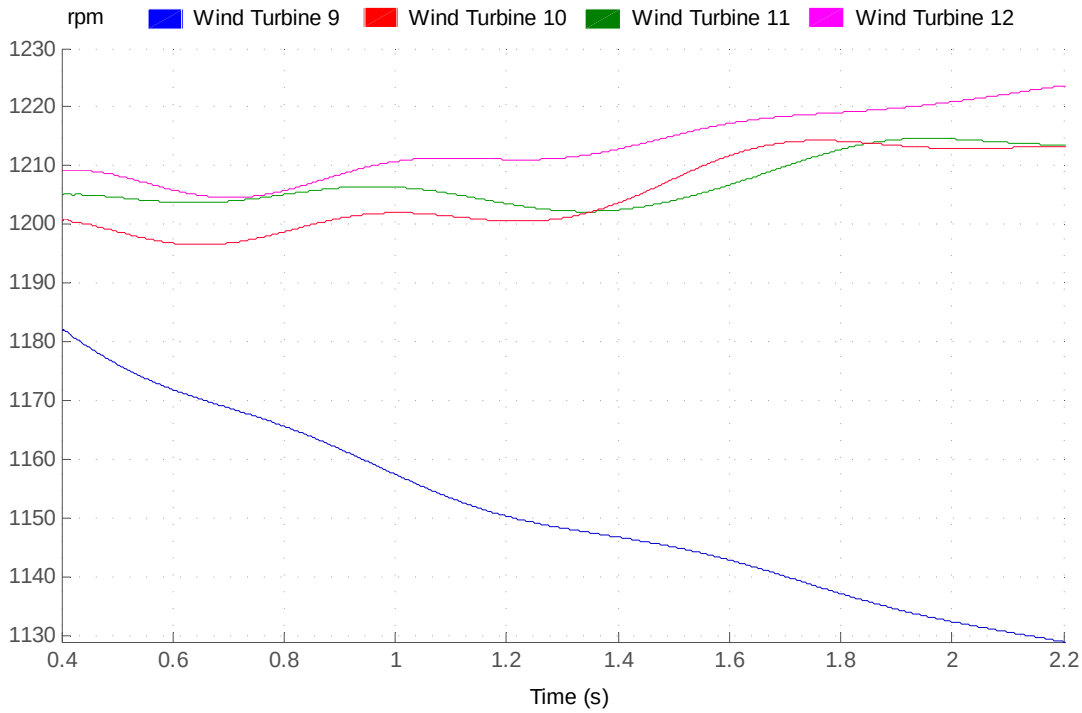


Figure 5.10. Rotor Speeds for Wind Turbine 9 to 12 for case 5.1.2

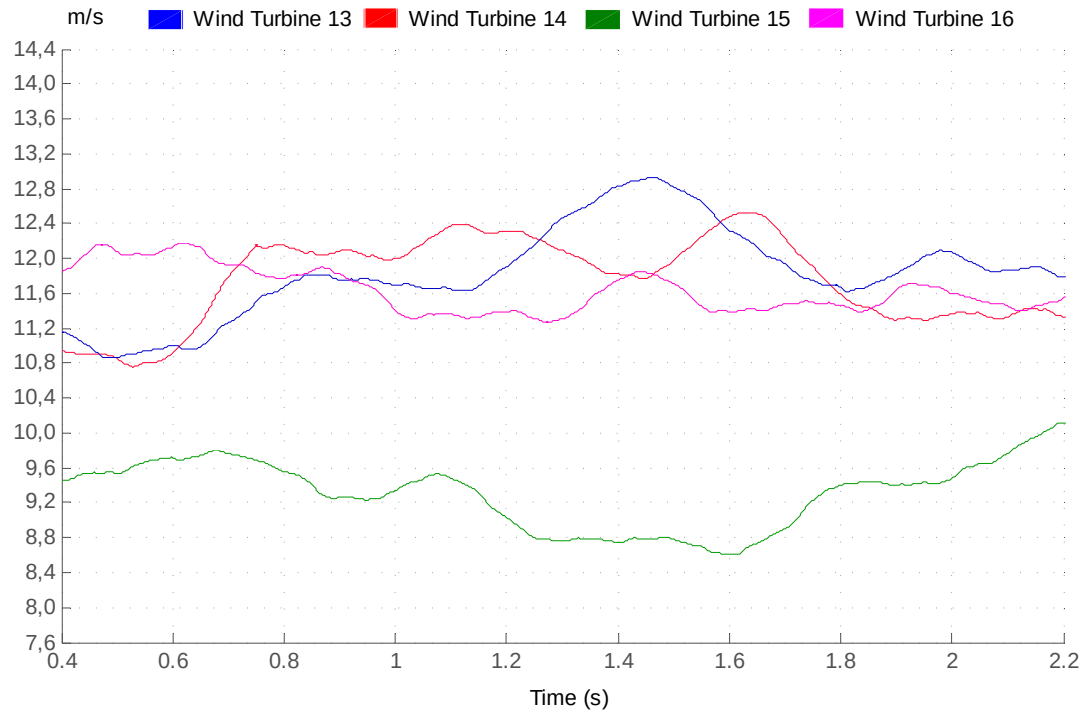


Figure 5.11. Wind Speeds for Wind Turbine 13 to 16 for case 5.1.2

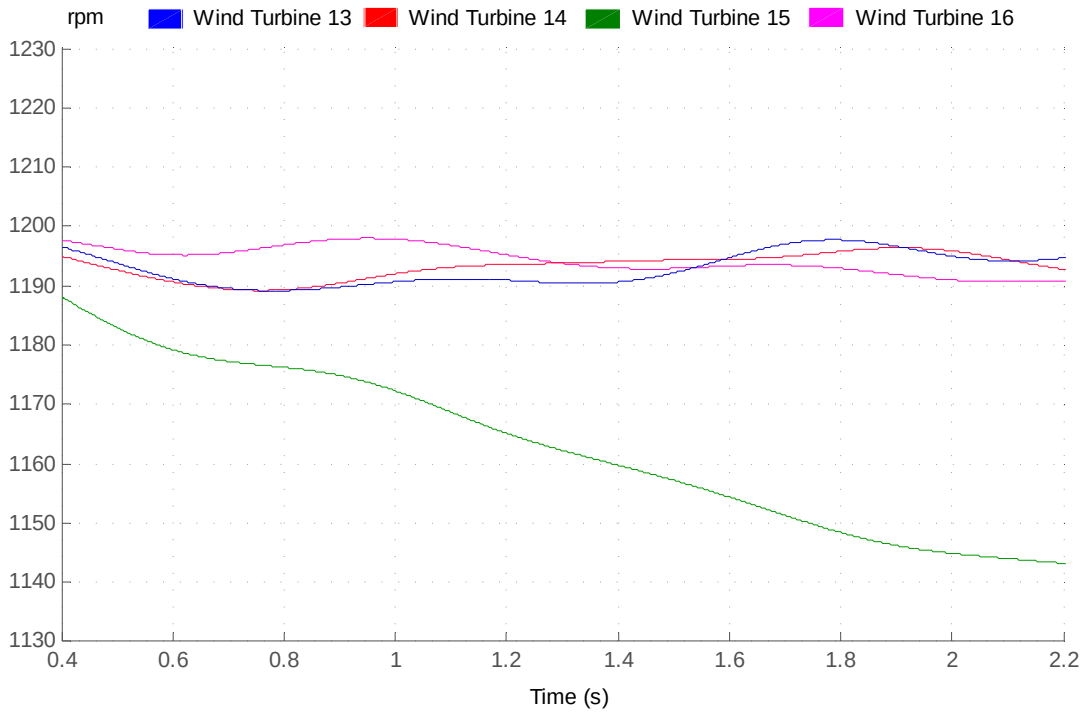


Figure 5.12. Rotor Speeds for Wind Turbine 13 to 16 for case 5.1.2

The system performance with variable wind speed is evaluated under no fault condition. Voltage and current waveforms for each phase for this case are shown in Figure 5.13 and Figure 5.14 respectively.

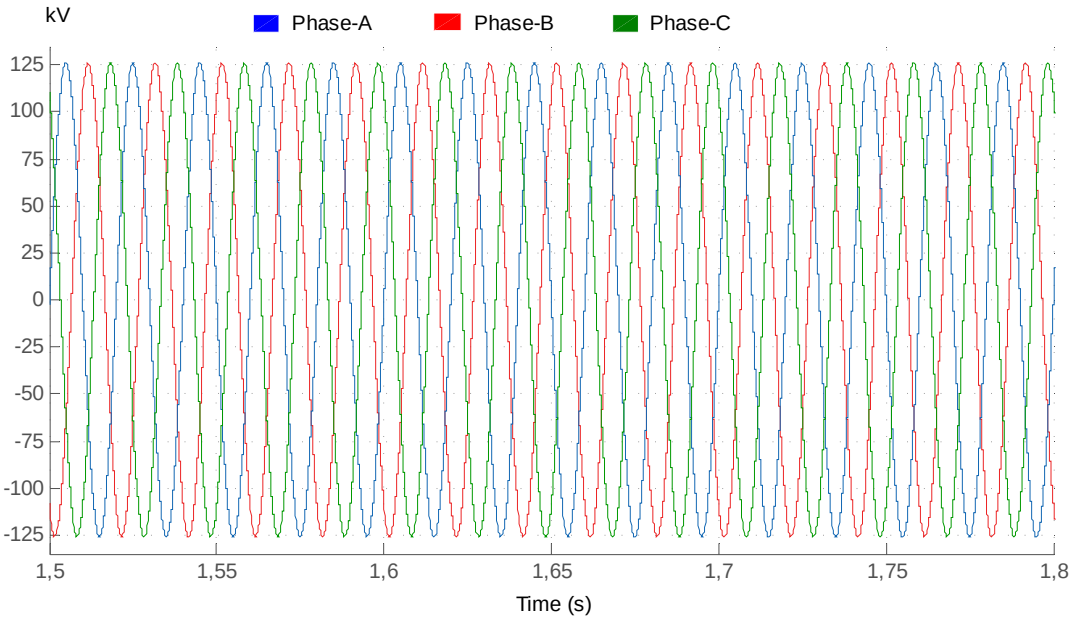


Figure 5.13. Phase voltages of High Voltage Line side for 5.1.2 case

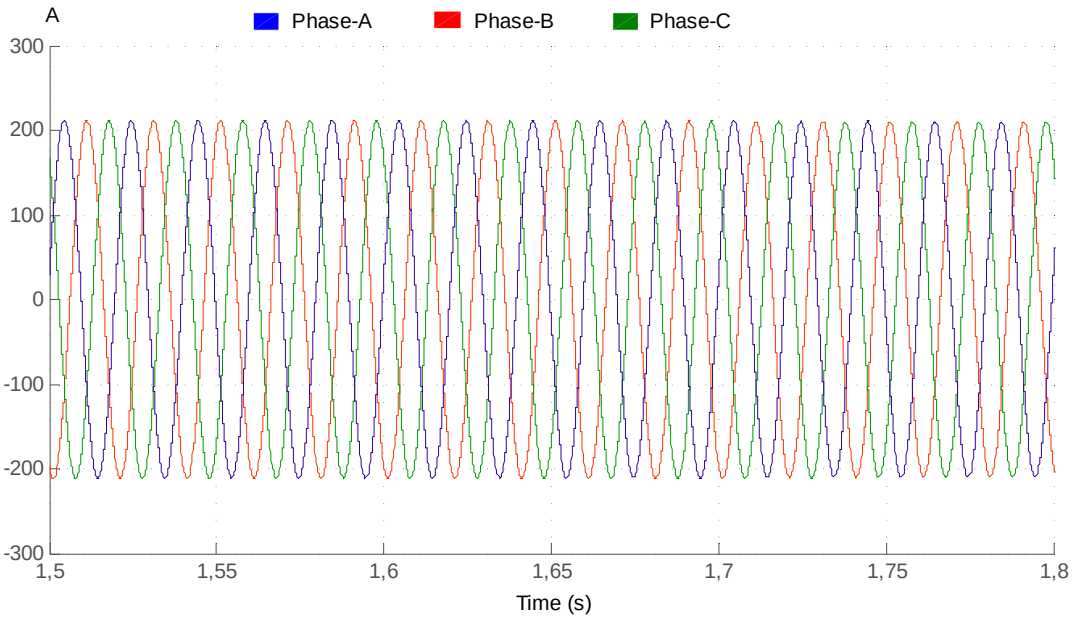


Figure 5.14. Phase currents of High Voltage Line side for 5.1.2 case

Active and reactive power at the point of common coupling are measured and showed in Figure 5.15 for this case. It is observed that generated active power is constant at 39.8 MW and no reactive power is absorbed from interconnected transmission system.

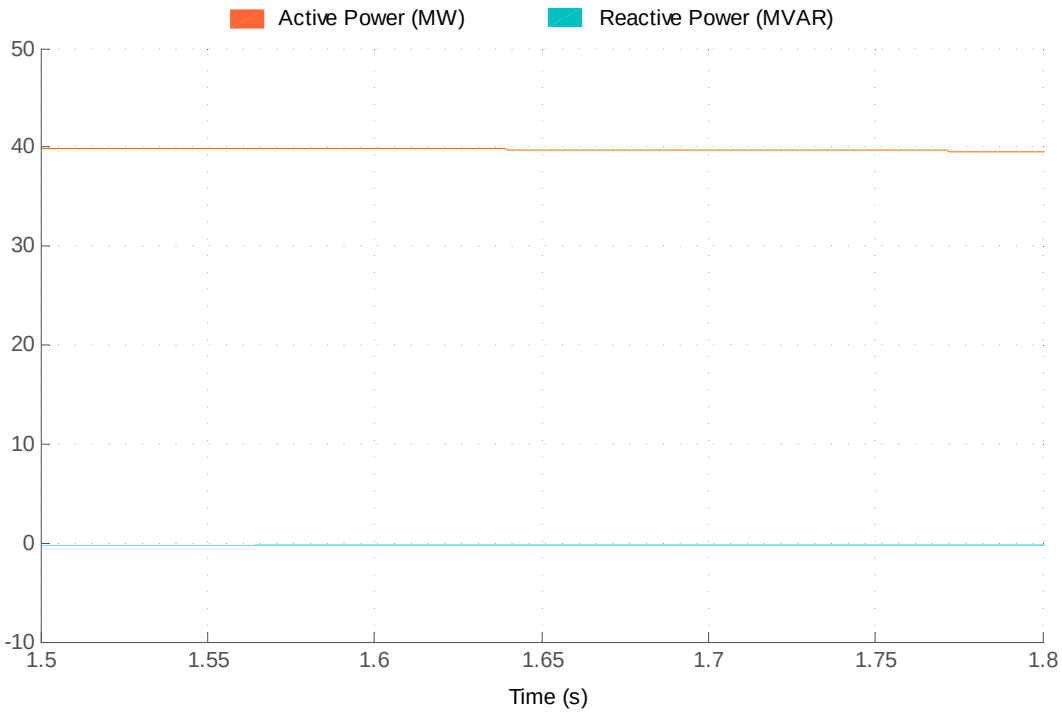


Figure 5.15. Active and reactive powers of MV Line side for 5.1.2 case

Frequency deviation is observed and presented in Figure 5.16 and seen that frequency is not changed during this case as there is no fault.

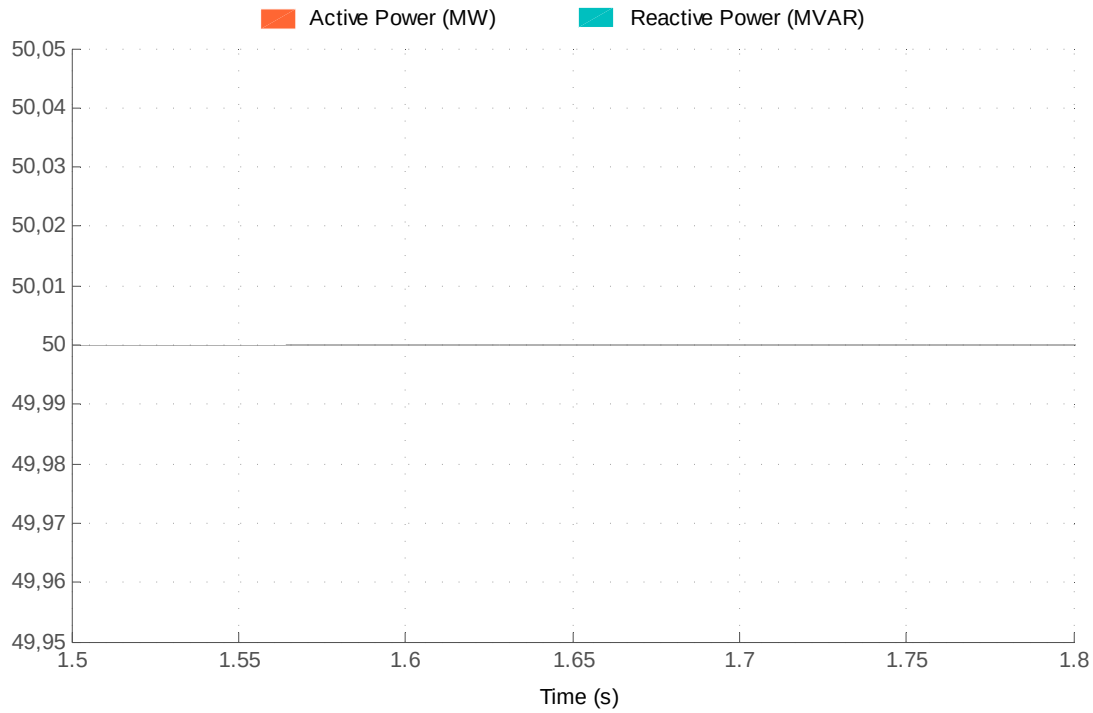


Figure 5.16. Frequency change of MV Line side for 5.1.2 case

5.2. Case 2: Faults in Group A Wind Turbines

5.2.1. Phase-B-to-Phase-C Fault

In the first case, phase-to-phase fault in Group A wind turbines is investigated which occurs on B and C phases between 1.6 s and 1.7 s that fault time is determined as 0.1 seconds. The fault occurs on the Wind Turbine 12 (WT12) low voltage output that can be seen in Figure 4.2 in Chapter 4. This fault condition and its effect on high voltage side is investigated. During the short circuit fault, low voltage sag was observed in phases of high voltage side (interconnected transmission system) of the region. Figure 5.17 shows the voltage waveforms of each phase seen from high voltage side. Figure 5.18 shows the rms values of these voltages and as it can be seen from this figure clearly that, RMS value of Phase-A and Phase-C voltages are decreased from 89.1 kV to 88.6 kV that approximately 0.6% voltage sag occurs in phases of A and C. Phase-B RMS voltage is decreased from 89.1 kV to 87.8 kV, so 1.5 % sag occurs.

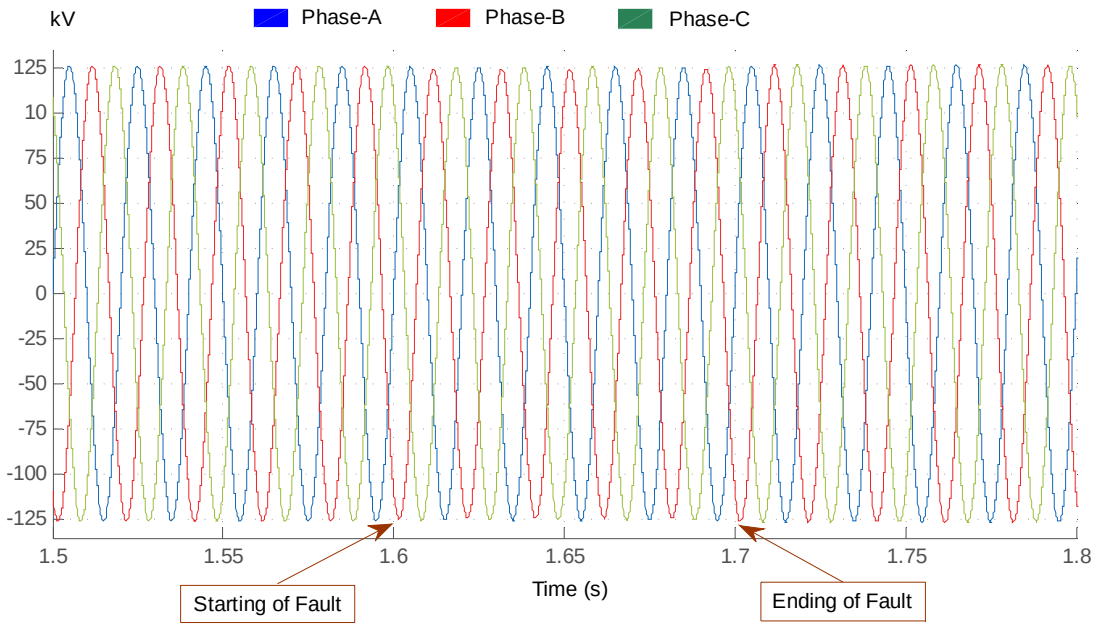


Figure 5.17. Phase voltages of High Voltage Line side during 5.2.1 case

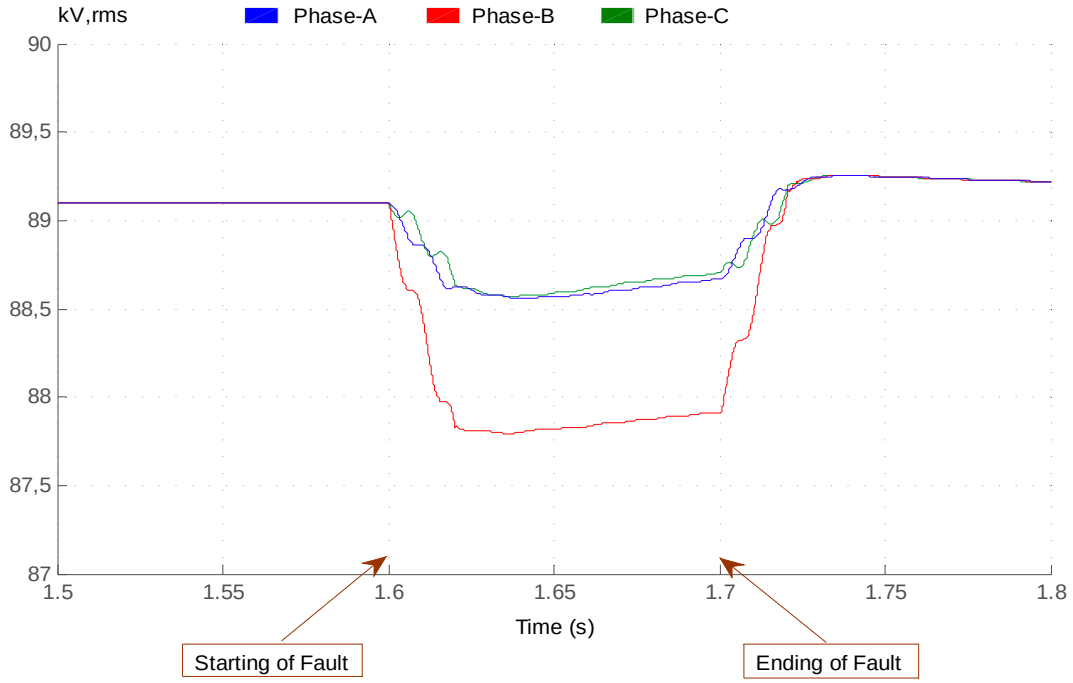


Figure 5.18. RMS voltages of High Voltage Line side during 5.2.1 case

Figure 5.19 shows that the phase current waveforms and Figure 5.20 presents the rms currents. For steady state operation, the nominal rms current is 180 A. However, rms values of short-circuit currents are reached to 145 A at Phase-A, 240

A at Phase-B and 255 A at Phase-C respectively during phase-to-phase fault occurred on Group A wind turbines.

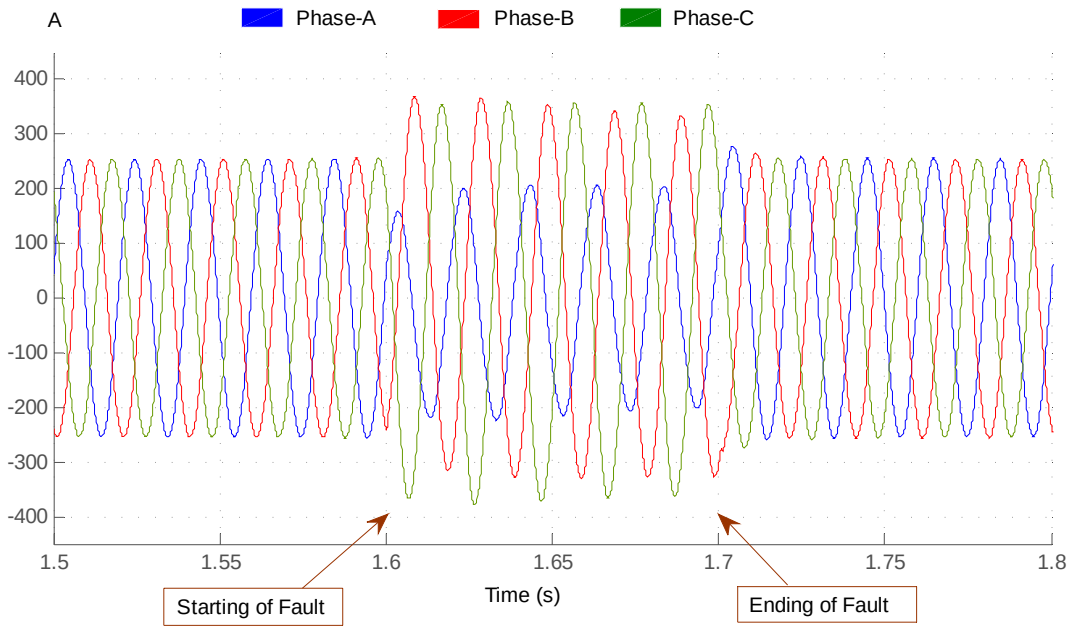


Figure 5.19. Phase currents of High Voltage Line side during 5.2.1 case

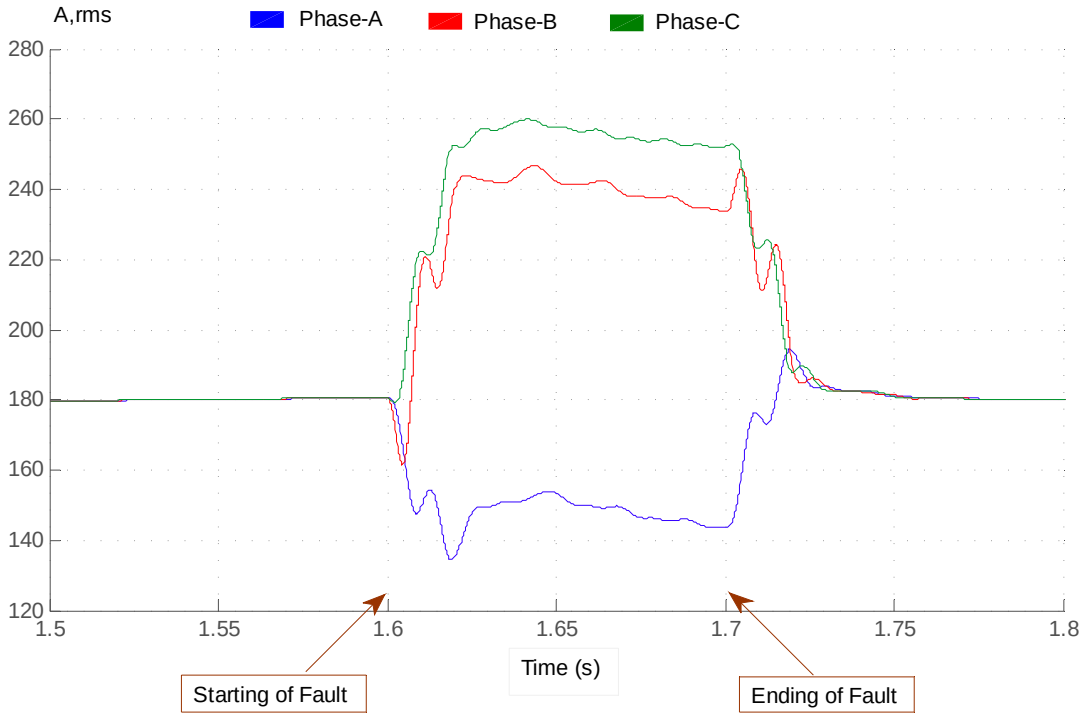


Figure 5.20. RMS currents of High Voltage Line side during 5.2.1 case

Active and reactive power is measured at the point of common coupling. Active and reactive power change at medium voltage line is given in Figure 5.21 during phase-to-phase fault occurred at WT12. It is observed that generated active power is decreased from 48 MW to 46.6 MW and 22 MWAR reactive power is absorbed from interconnected transmission system during phase-to-phase fault. The reactive power drawn is the result of remaining wind turbines in the wind farm. To maintain the power and voltage at set point, each wind turbine draws reactive power.

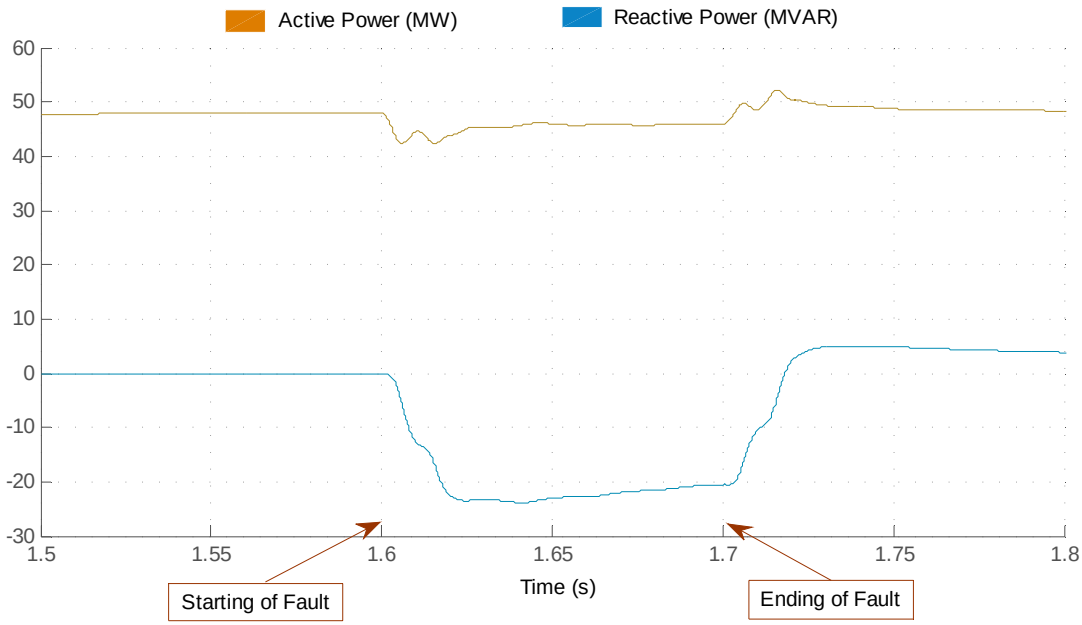


Figure 5.21. Active and reactive powers of MV Line side during 5.2.1 case

Frequency deviation is observed and presented in Figure 5.22 during fault. It is seen that frequency is changed between 49.98 Hz to 50.02 Hz which is an acceptable value.

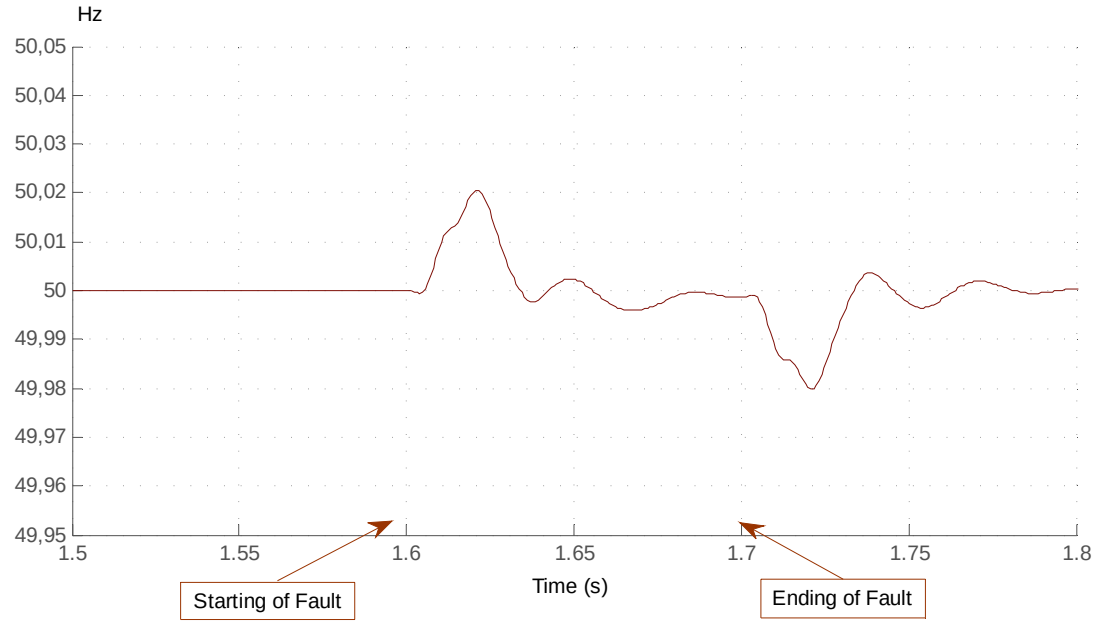


Figure 5.22. Frequency change of MV Line side during 5.2.1 case

5.2.2. Phase-A-to-Ground Fault

In the second case, phase-to-ground fault is considered, since it is the most common type of short circuit faults. Phase-to-ground fault on Phase-A in Group A wind turbine 12 low voltage side is created during 1.6 s < t < 1.7 s. The impact of this fault on high voltage side of system is investigated. During the short circuit fault, low voltage sag in all phases of interconnected transmission system was observed. The voltage waveform of each phase seen from high voltage side is presented in Figure 5.23 and the rms values of phase voltage are shown in Figure 5.24 respectively. It can be seen from Figure 5.24 that, RMS value of Phase-A voltage is decreased from 89.1 kV to 88.4 kV, so 0.8 % sag occurs; RMS values of Phase-B and Phase-C voltages are decreased from 89.1 kV to 88.9 kV that approximately 0.6% voltage sag occurs. The phase current waveforms and the rms currents injected from interconnected transmission system are presented in Figure 5.25 and Figure 5.26 respectively. The nominal rms current is 180 A for steady state operation of wind farm system. During phase-to-ground fault occurred on Group A wind turbines, rms values of short-circuit currents are reached to 234 A at Phase-A, 192 A at Phase-B and 163 A at Phase-C respectively.

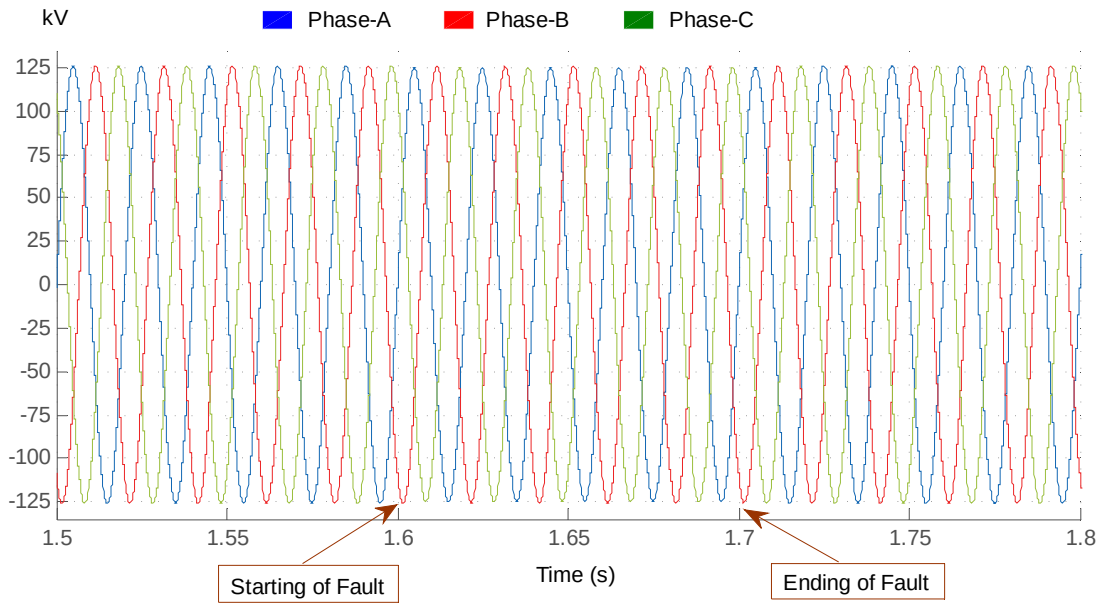


Figure 5.23. Phase voltages of High Voltage Line side during 5.2.2 case

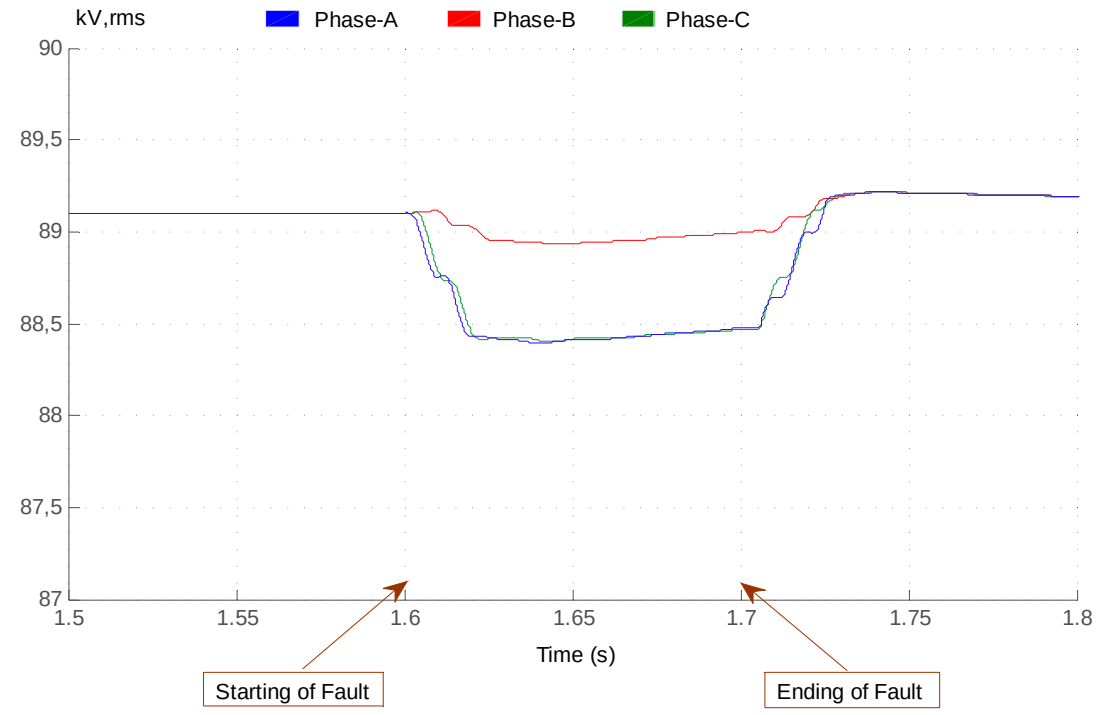


Figure 5.24. RMS voltages of High Voltage Line side during 5.2.2 case

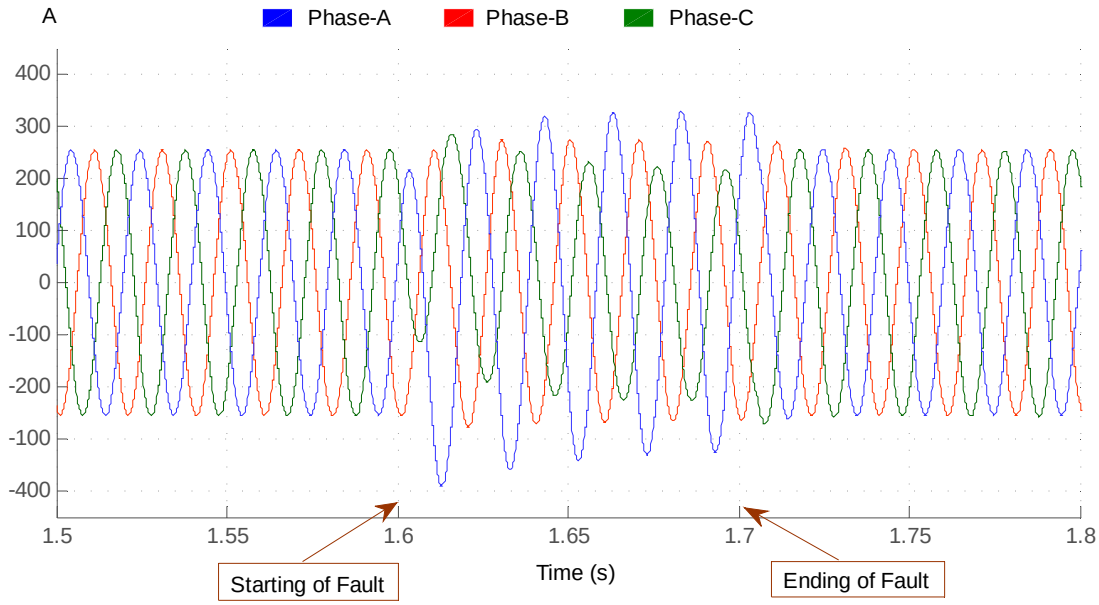


Figure 5.25. Phase currents of High Voltage Line side during 5.2.2 case

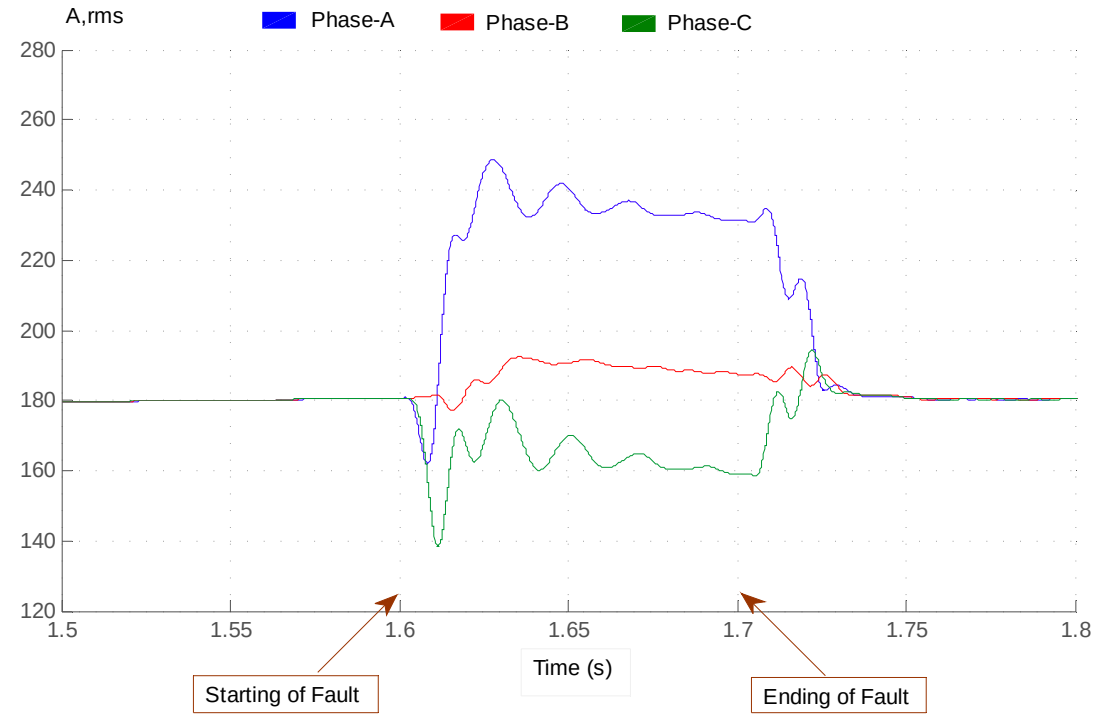


Figure 5.26. RMS currents of High Voltage Line side during 5.2.2 case

Active and reactive power is measured on medium voltage line and the change is showed in Figure 5.27 during phase-to-ground fault occurred in A group wind turbine. It is observed that generated active power is decreased from 48 MW to

45.8 MW and 15.6 MWAR reactive power is absorbed from interconnected transmission system during phase-to-ground fault. The reactive power absorbed is smaller than phase-to-phase fault case as the fault only occurred on single phase.

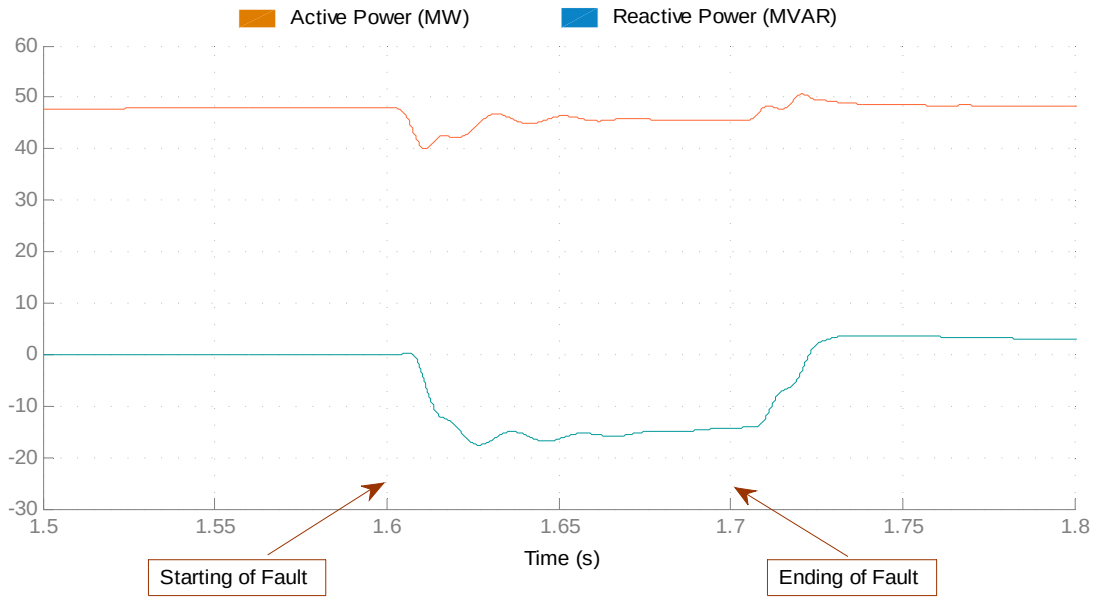


Figure 5.27. Active and reactive powers of MV Line side during 5.2.2 case

Frequency deviation is observed and shown in Figure 5.28 during phase-to-ground fault occurred in WT12 in Group A.

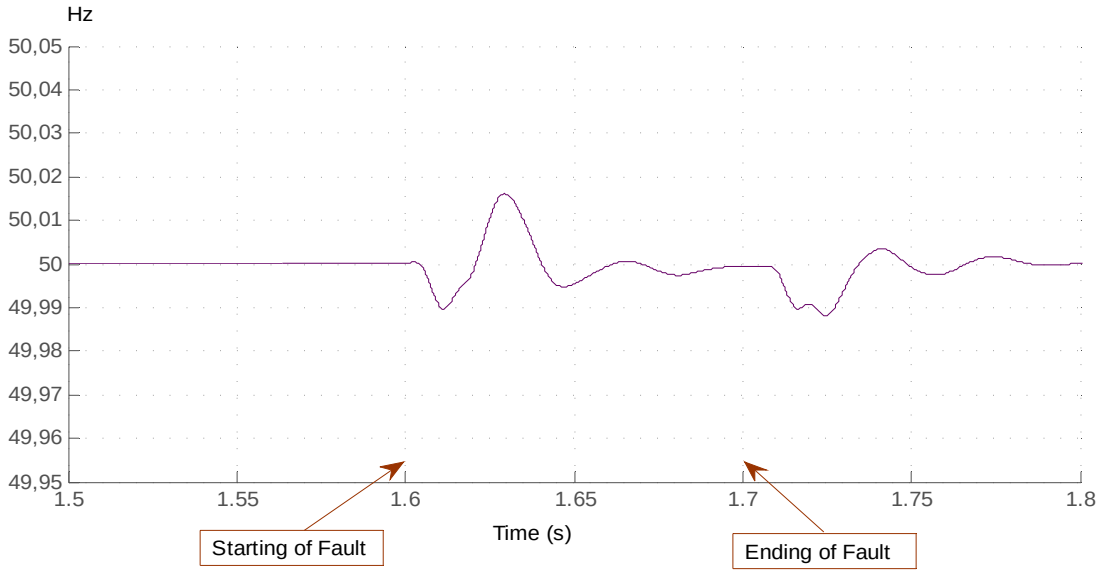


Figure 5.28. Frequency change of MV Line side during 5.2.2 case

5.2.3. Three Phase (A-B-C) Fault

In this case, three phase fault in Group A wind turbines is investigated which occurs on A, B and C phases between 1.6 s and 1.7 s. This fault condition affects high voltage side of system and relatively low voltage sag was observed. Figure 5.29 and Figure 5.30 shows the voltage waveforms of each phase seen from high voltage side and the rms values of these voltages respectively. As it can be seen from this figure, RMS value of all phase voltages are decreased from 89.1 kV to 87.7 kV that approximately 1.6% voltage sag occurs in phases of A, B and C in a balanced manner.

Figure 5.31 shows that the phase current waveforms and Figure 5.32 presents the rms currents injected from interconnected transmission system. For steady state operation, the nominal rms current is 180 A. However, rms values of short-circuit currents are reached to 259 A at Phase-A, 255 A at Phase-B and 258 A at Phase-C respectively during three phase fault occurred on A group wind turbine.

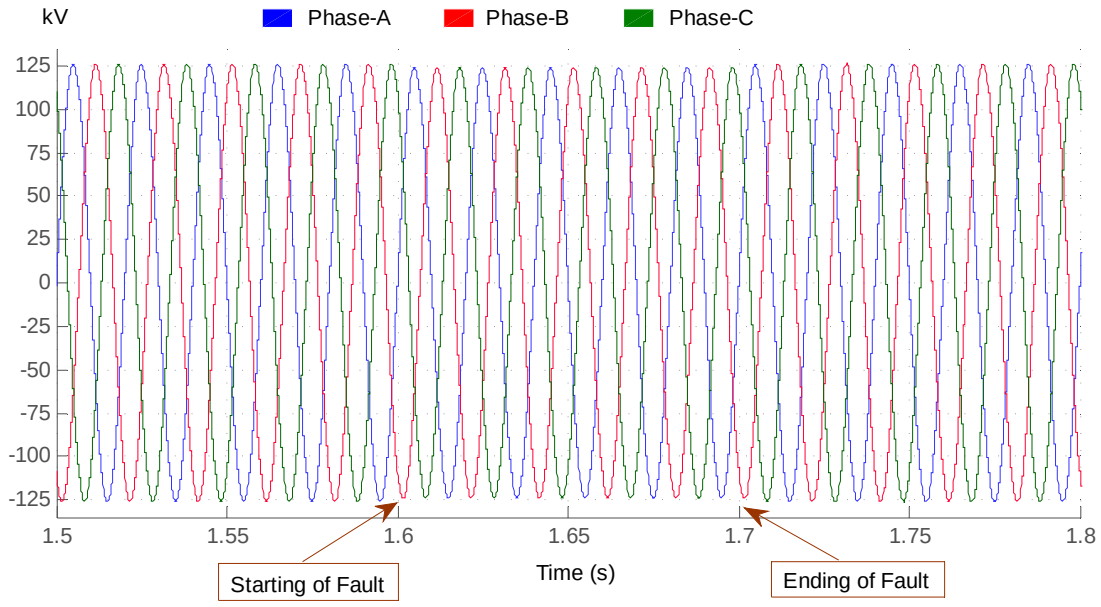


Figure 5.29. Phase voltages of High Voltage Line of the system during 5.2.3 case

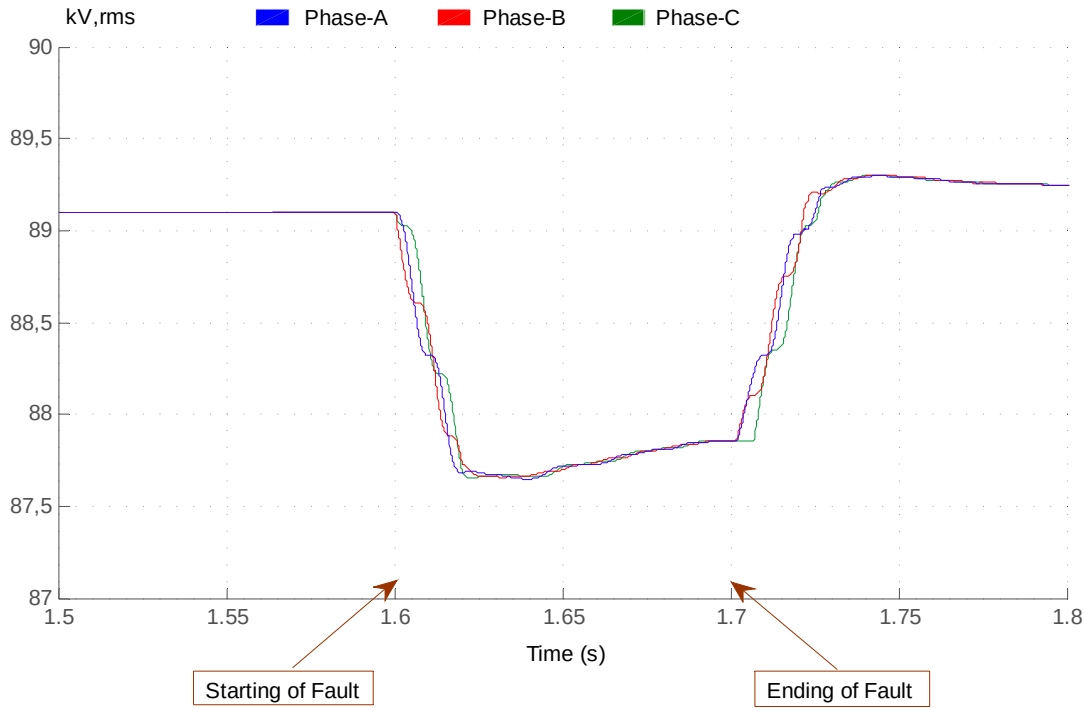


Figure 5.30. RMS voltages of High Voltage Line side of the system during 5.2.3 case

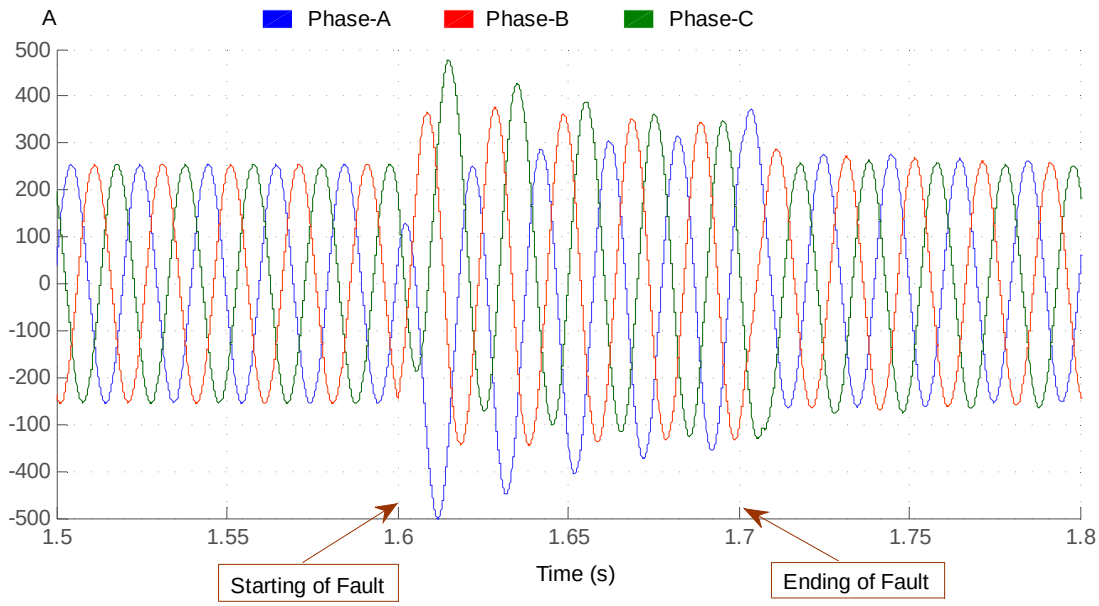


Figure 5.31. Phase currents of High Voltage Line of the system during 5.2.3 case

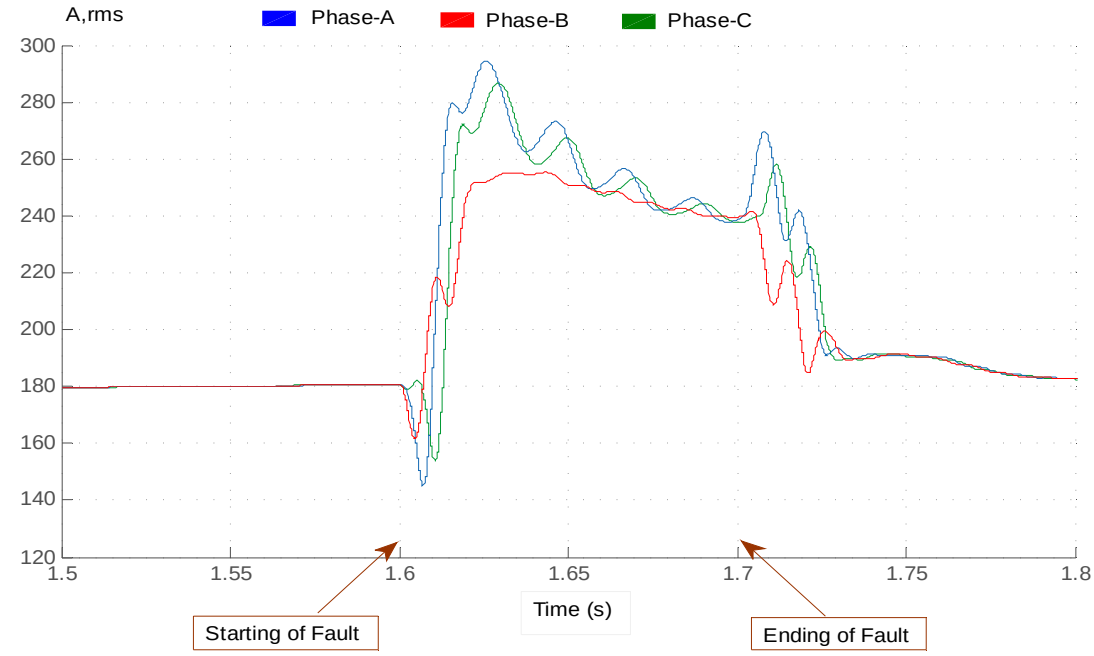


Figure 5.32. RMS currents of High Voltage Line side of the system during 5.2.3 case

Active and reactive power change observed on medium voltage line and is presented in Figure 5.33 during three phase fault at A group wind turbine. Active power is decreased from 48 MW to 40.5 MW and 38 MVAR of reactive power is absorbed from interconnected transmission system during three phase fault.

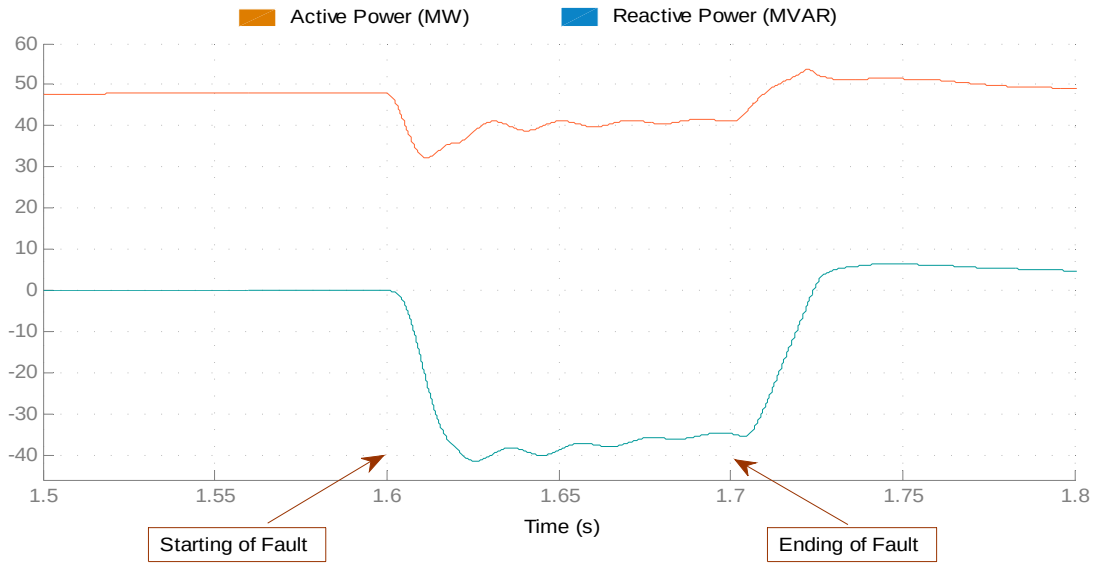


Figure 5.33. Active and reactive powers of MV Line side during 5.2.3 case

Frequency deviation is observed and presented in Figure 5.34 during three phase fault occurred in A group wind turbine. It is seen that frequency is changed between 49.98 Hz to 50.03 Hz.

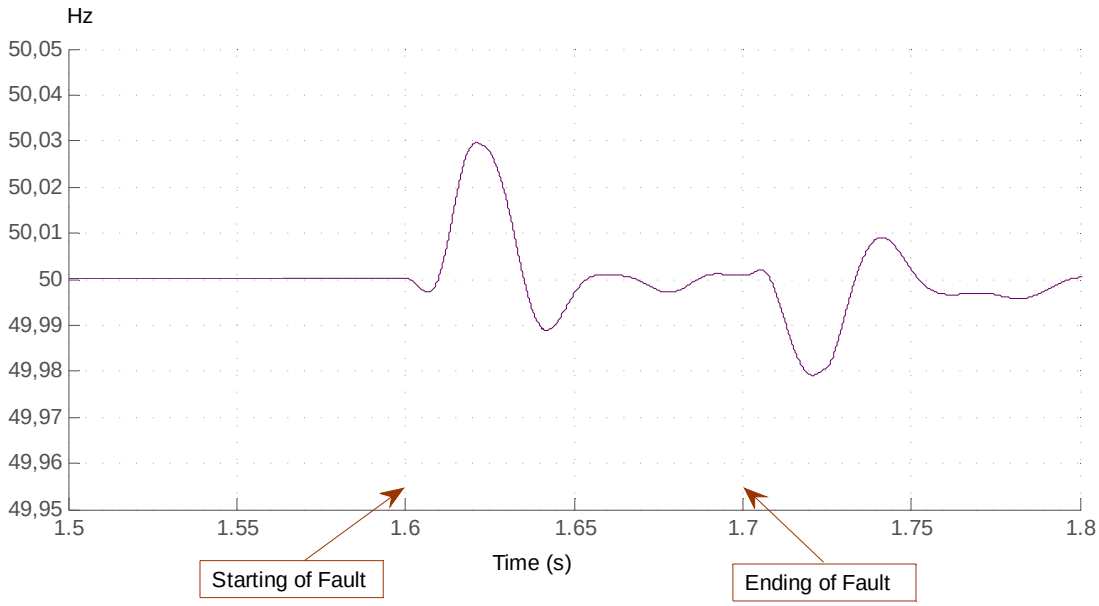


Figure 5.34. Frequency change of MV Line side during 5.2.3 case

5.3. Case 3: Faults in Group B Wind Turbines

5.3.1. Phase-A-to-Phase-B Fault

In this case study, phase-to-phase fault which occurs on B and C phases between 1.8 s and 1.9 s in B group wind turbine is investigated. The fault location is the output of Wind Turbine 1 (WT1) in Group B. This fault condition and its effect on high voltage side of system is analyzed. During the short circuit fault, low voltage sag was observed in phases of interconnected transmission system. Figure 5.35 shows the voltage waveforms of each phase seen from high voltage side. Figure 5.36 shows that the rms value of Phase-A voltage is decreased from 89.1 kV to 87.8 kV corresponds to 1.5 % sag occurs in Phase-A; rms voltages of Phase-B and Phase-C are decreased from 89.1 kV to 88.6 kV that approximately 0.6% voltage sag occurs in phases of B and C.

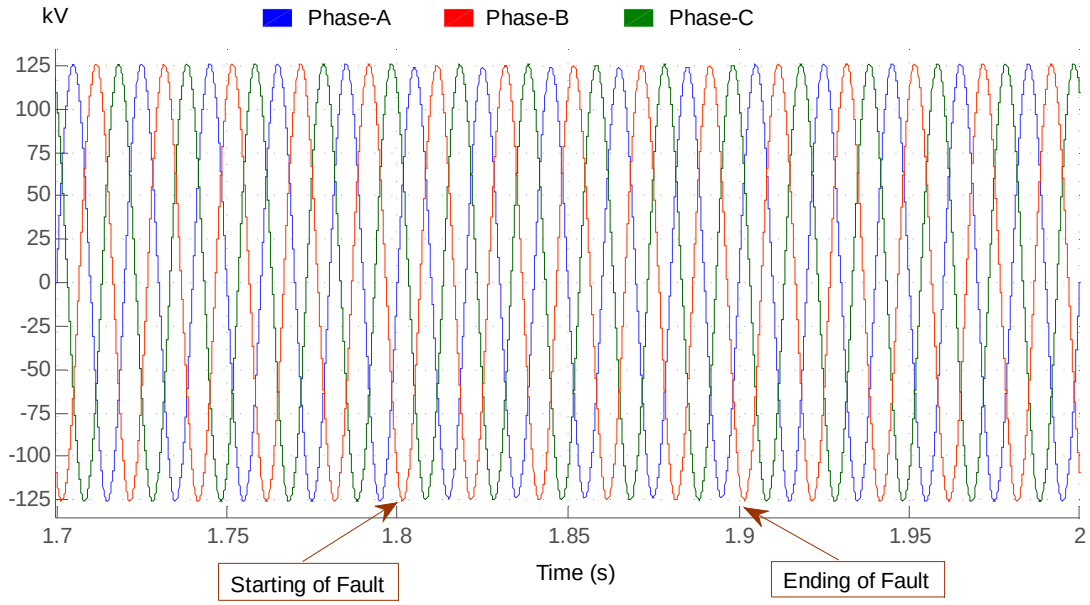


Figure 5.35. Phase voltages of High Voltage Line of the system during 5.3.1 case

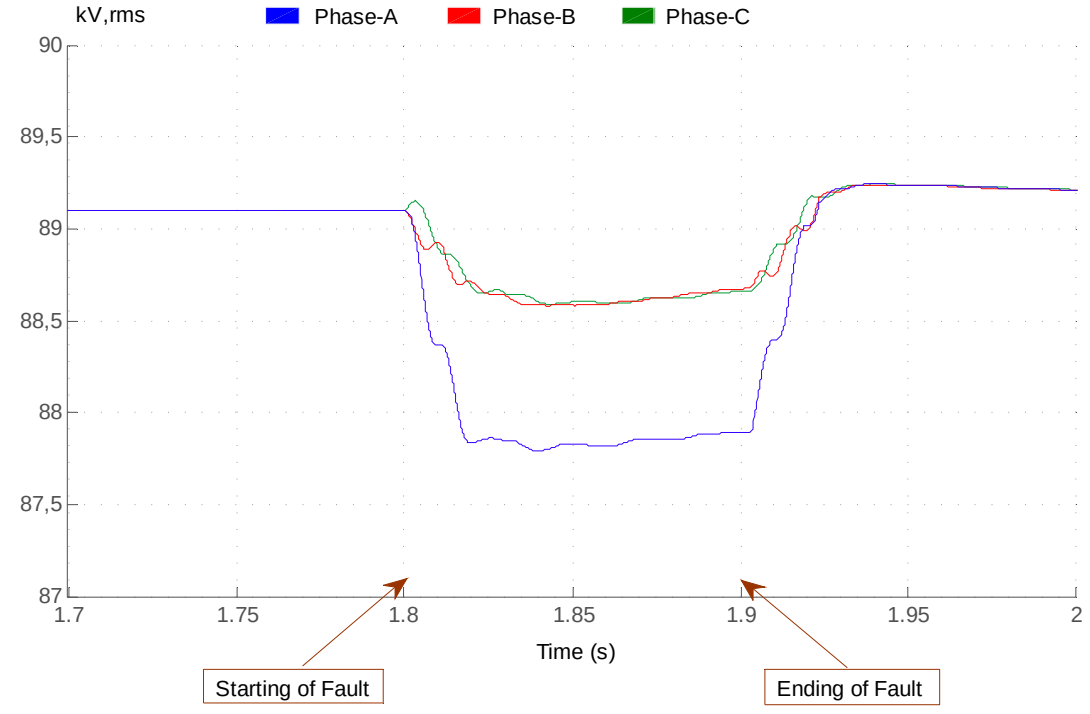


Figure 5.36. RMS voltages of High Voltage Line side of the system during 5.3.1 case

The phase current waveforms and the rms currents are presented in Figure 5.37 and Figure 5.38 respectively. The nominal rms current is 182 A for steady state operation and during phase-to-phase fault occurred on WT1, rms values of short-

circuit currents are 251 A at Phase-A, 265 A at Phase-B and 163 A at Phase-C respectively.

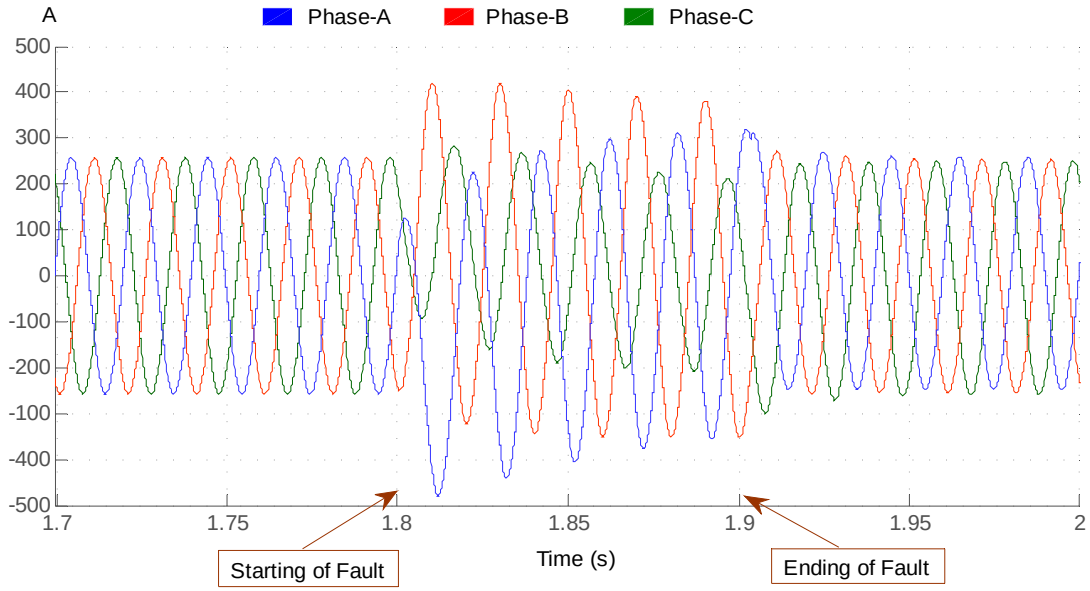


Figure 5.37. Phase currents of High Voltage Line of the system during 5.3.1 case

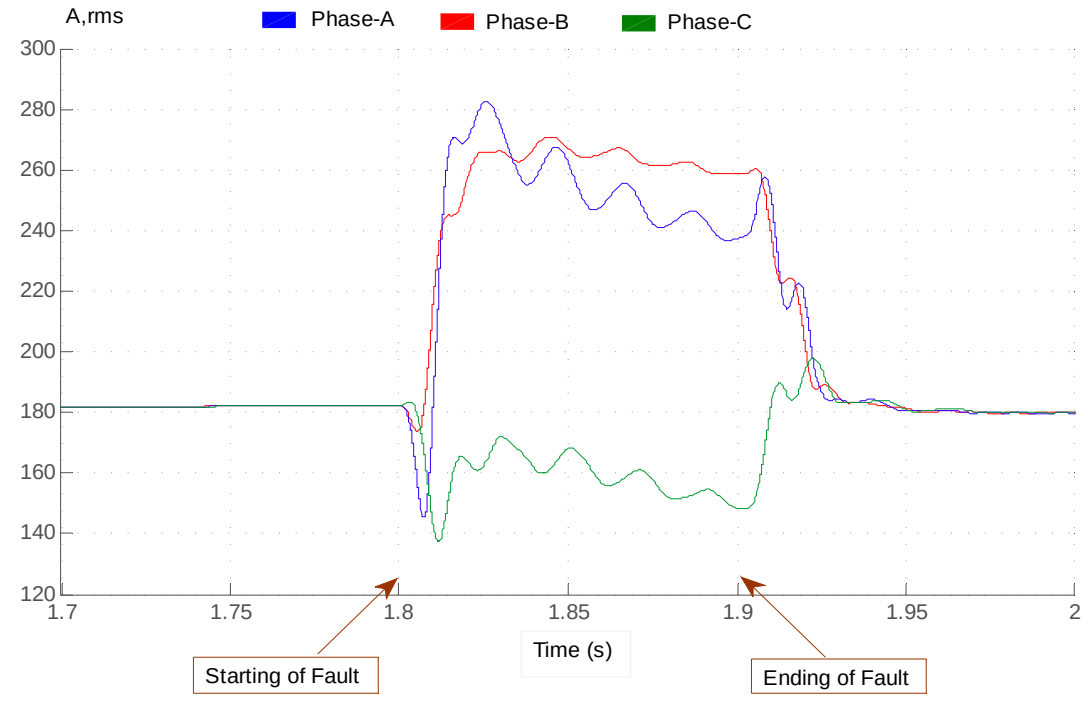


Figure 5.38. RMS currents of High Voltage Line side of the system during 5.3.1 case

Active and reactive power change at medium voltage line is presented in Figure 5.39 during phase-to-phase fault occurred in B group wind turbine. Generated active power is decreased from 48 MW to 47.4 MW and 23 MWAR reactive power is absorbed from interconnected transmission system.

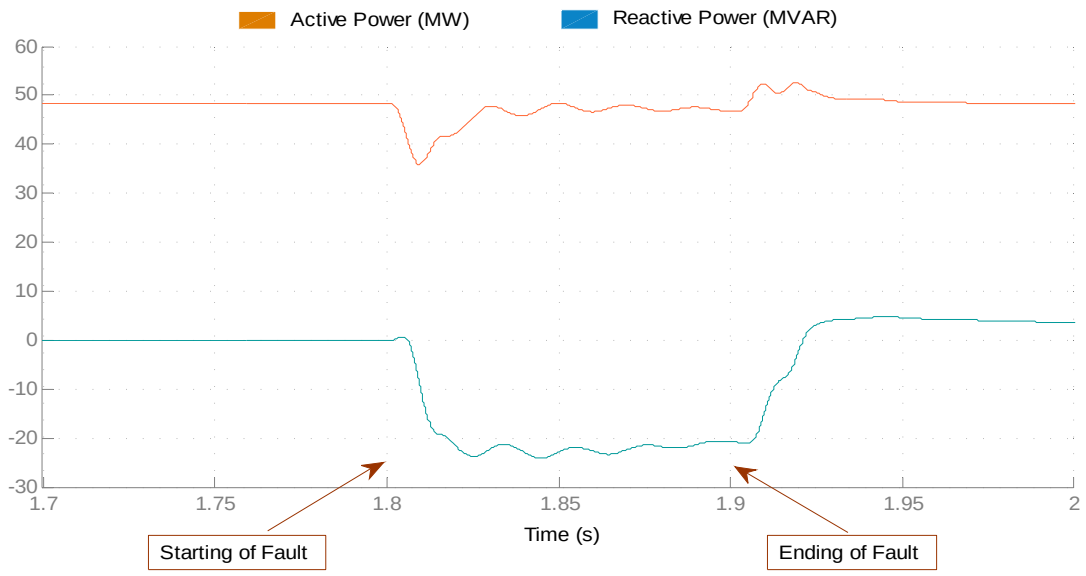


Figure 5.39. Active and reactive powers of MV Line side during 5.3.1 case

Frequency deviation is observed and presented in Figure 5.40 during phase-to-phase fault occurred in B group wind turbine.

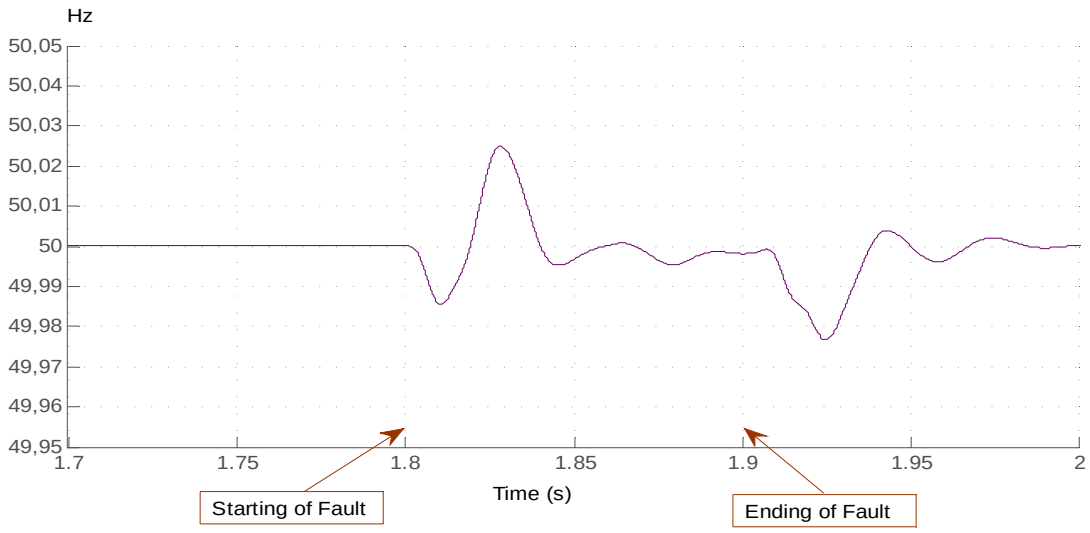


Figure 5.40. Frequency change of MV Line side during 5.3.1 case

5.3.2. Phase-C-to-Ground Fault

In this case study, the impact of phase-to-ground fault on interconnected transmission line investigated from Group B. Phase-to-ground faults occurs on Phase-C in Group B WT1 low voltage side during 1.8 s < t < 1.9 s. During the short circuit fault, low voltage sag in all phases of interconnected transmission system was observed. The voltage waveform and rms voltages of each phase seen from high voltage side are presented in Figure 5.41 and Figure 5.42 respectively. It can be seen from Figure 5.8 that, RMS value of Phase-A voltage is decreased from 89.1 kV to 88.9 kV, resulting in 0.3% sag occurs; RMS values of Phase-B and Phase-C voltages are decreased from 89.1 kV to 88.4 kV that approximately 0.8% voltage sag occurs.

Phase current waveforms and the rms currents injected from interconnected transmission system are presented in Figure 5.43 and Figure 5.44 respectively. During phase-to-ground fault occurred in WT1 in Group B, rms values of short-circuit currents are reached to 190 A at Phase-A, 162 A at Phase-B and 238 A at Phase-C respectively.

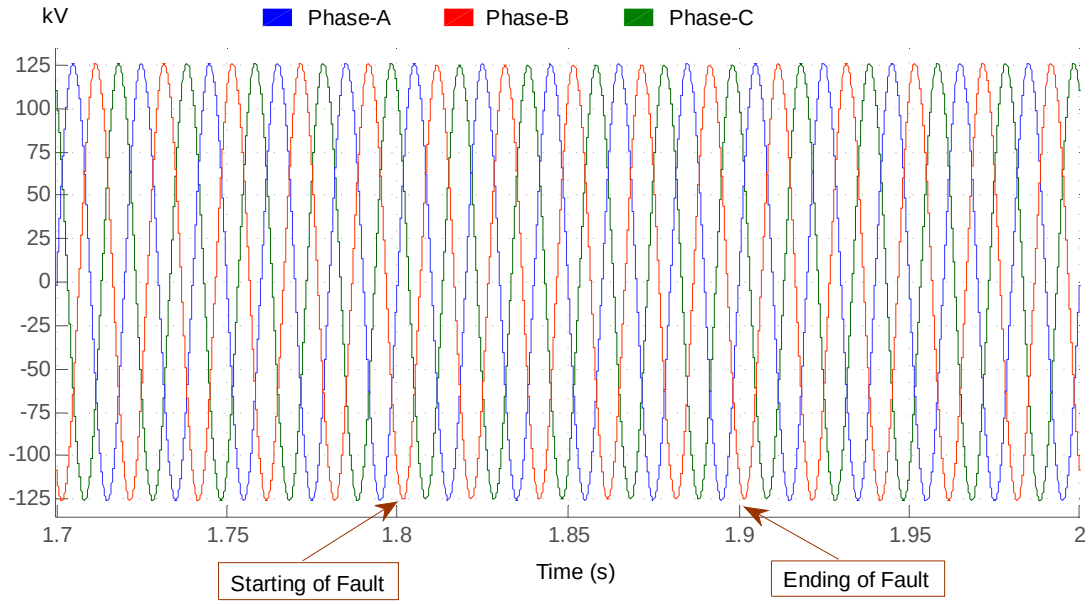


Figure 5.41. Phase voltages of High Voltage Line side during 5.3.2 case

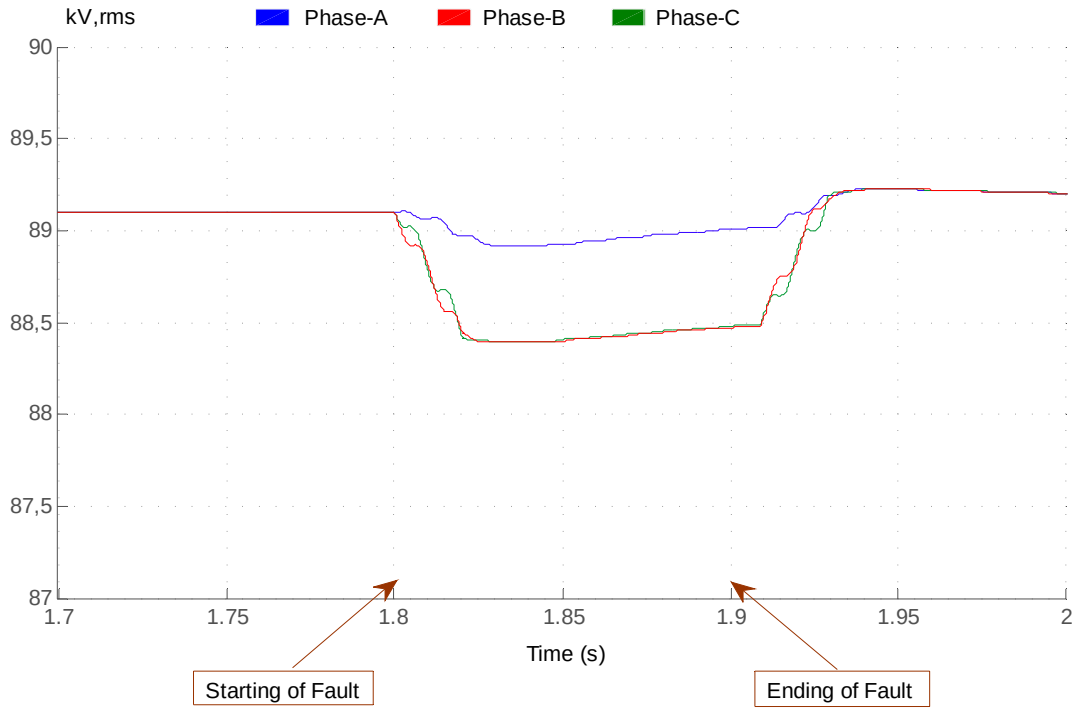


Figure 5.42. RMS voltages of High Voltage Line side of the system during 5.3.2 case

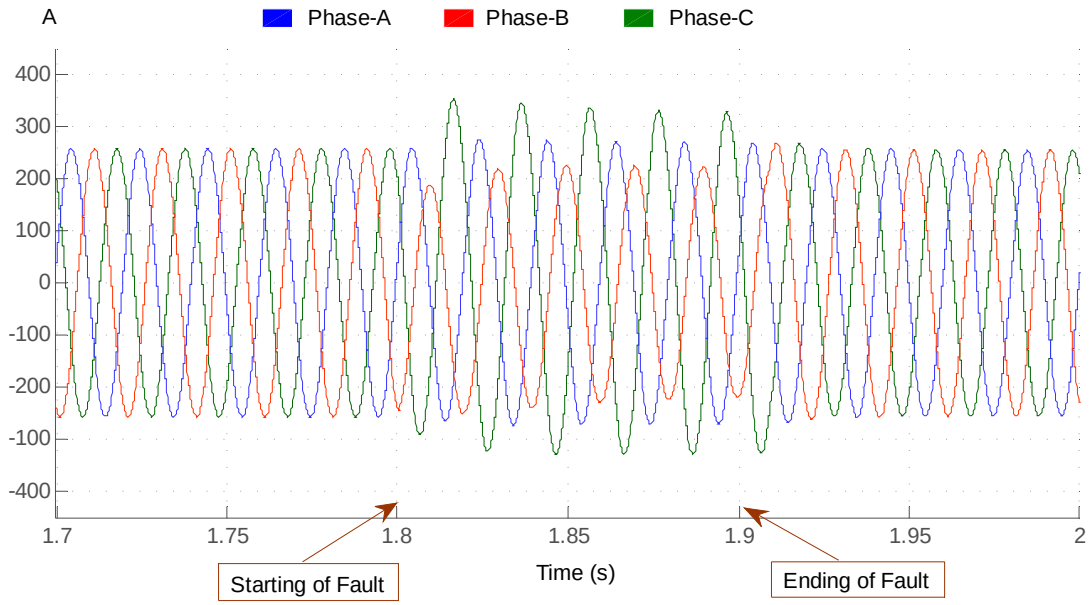


Figure 5.43. Phase currents of High Voltage Line side during 5.3.2 case

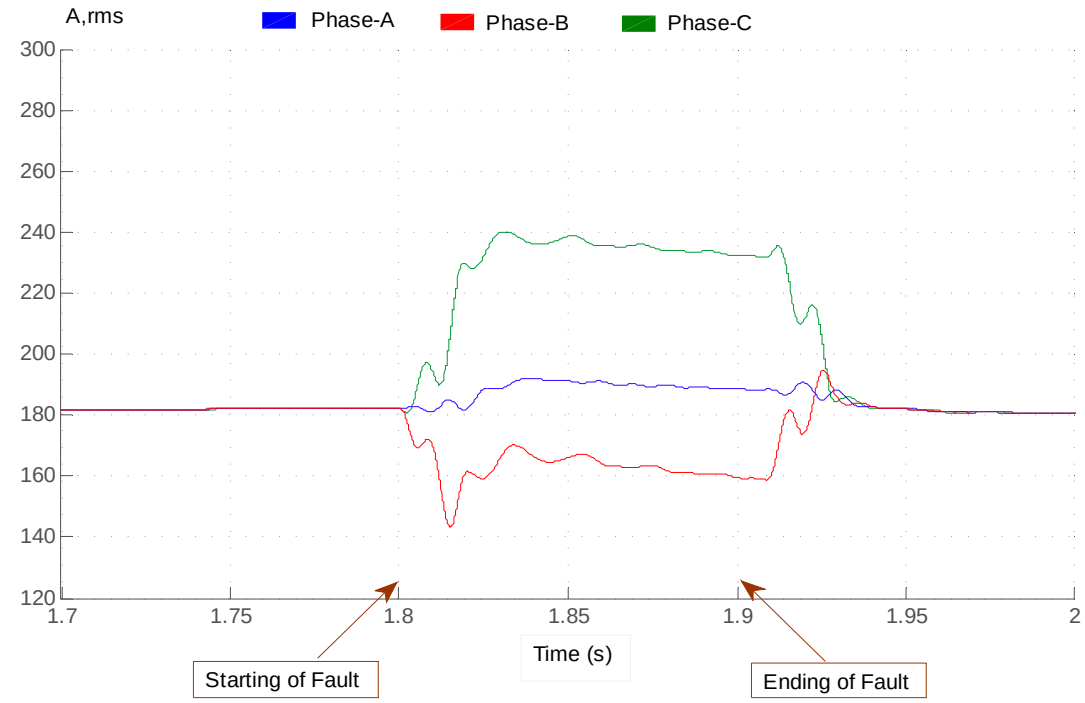


Figure 5.44. RMS currents of High Voltage Line side of the system during 5.3.2 case

Active and reactive power change is showed in Figure 5.45 and it is observed that generated active power is 45.9 MW and absorbed reactive power is 15.1 MWAR during phase-to-ground fault occurred in B group wind turbine.

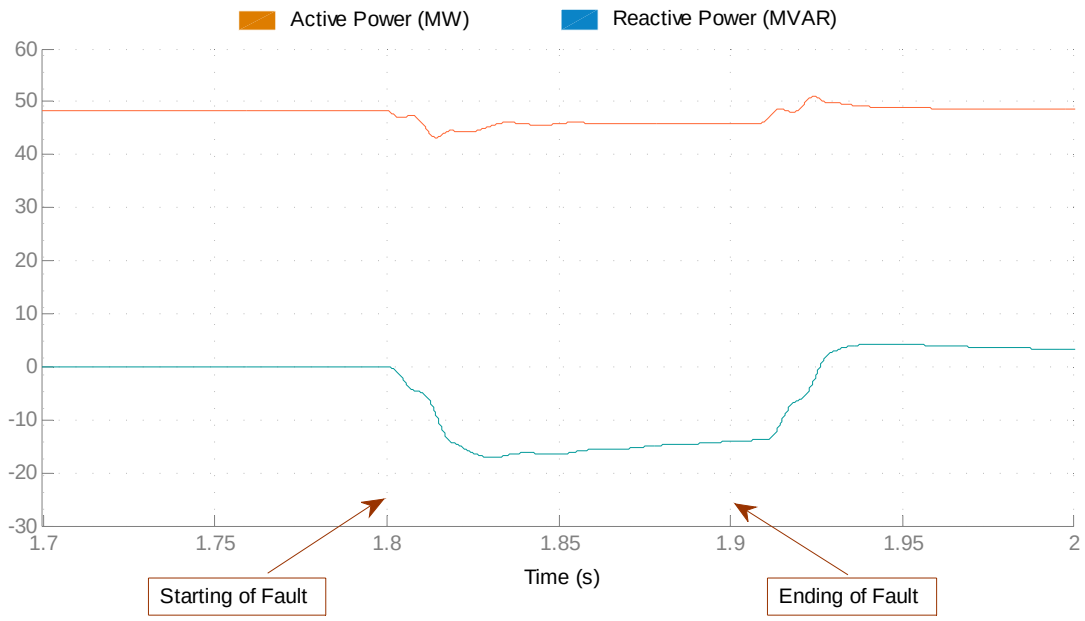


Figure 5.45. Active and reactive powers of MV Line side during 5.3.2 case

Frequency deviation is observed and shown in Figure 5.46 during phase-to-ground fault occurred in B group wind turbine.

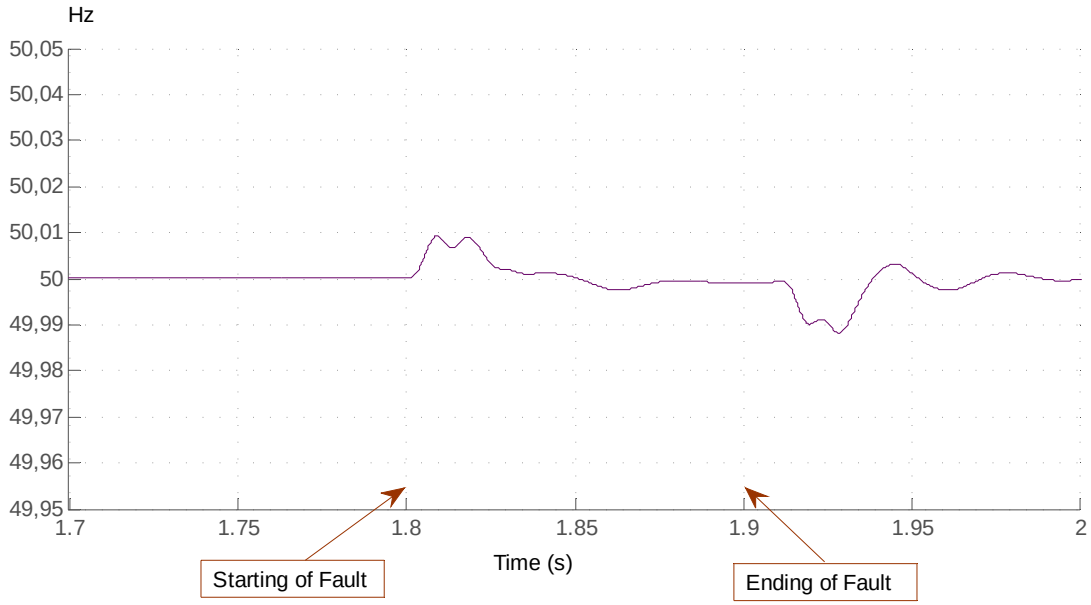


Figure 5.46. Frequency change of MV Line side during 5.3.2 case

5.3.3. Three Phase (A-B-C) Fault

In this case, three phase fault in B group wind turbine is investigated which occurs on A, B and C phases between 1.8 s and 1.9 s. This fault condition affects high voltage side of system and relatively low voltage sag was observed. Figure 5.47 and Figure 5.48 shows the voltage waveforms of each phase seen from high voltage side and the rms values of these voltages respectively. As it can be seen from this figure clearly that, RMS value of all phase voltages are decreased from 89.1 kV to 87.7 kV that approximately 1.6% voltage sag occurs in phases of A, B and C in a balanced manner.

Figure 5.49 shows that the phase current waveforms and Figure 5.50 presents the rms currents injected from interconnected transmission system. For steady state operation, the nominal rms current is 180 A. However, rms values of short-circuit currents are reached to 257 A at Phase-A, 248 A at Phase-B and 255 A at Phase-C respectively during three phase fault occurred on A group wind turbine.

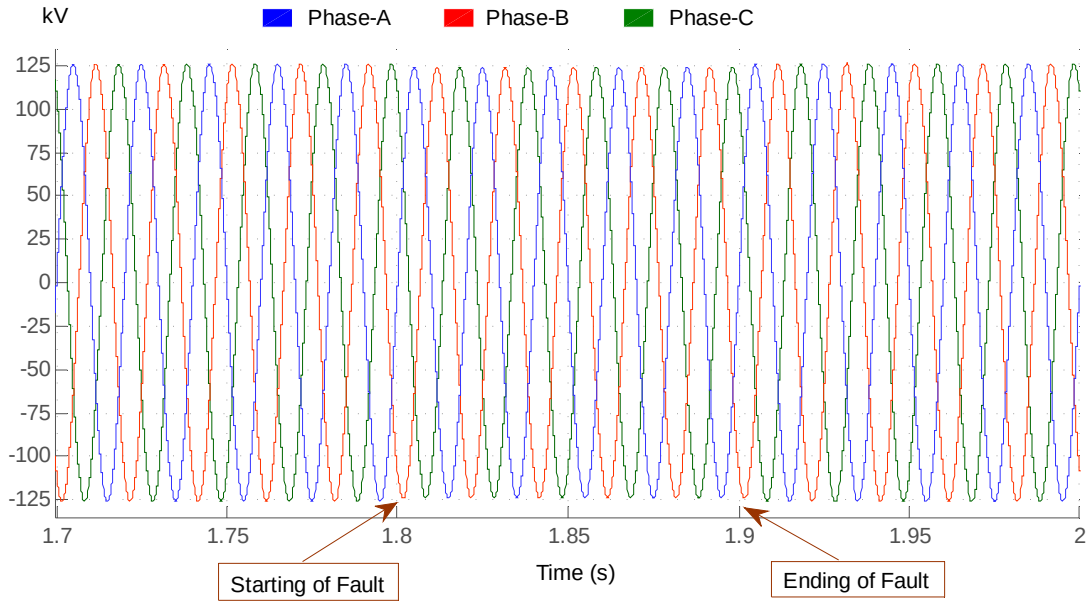


Figure 5.47. Phase voltages of High Voltage Line of the system during 5.3.3 case

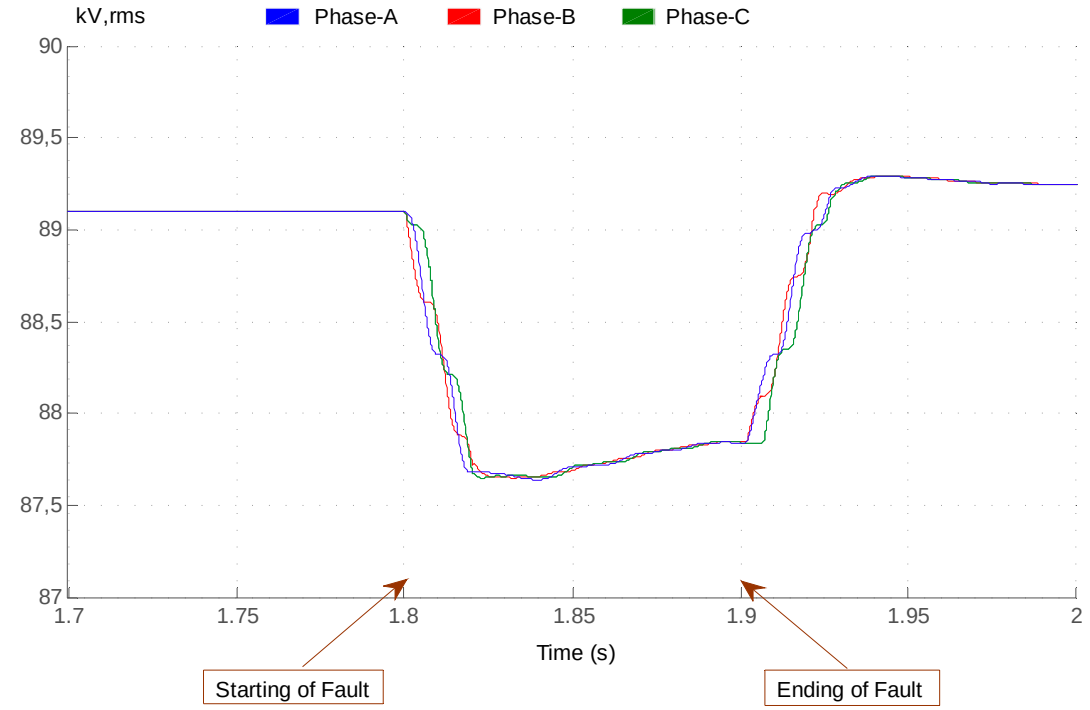


Figure 5.48. RMS voltages of High Voltage Line side of the system during 5.3.3 case

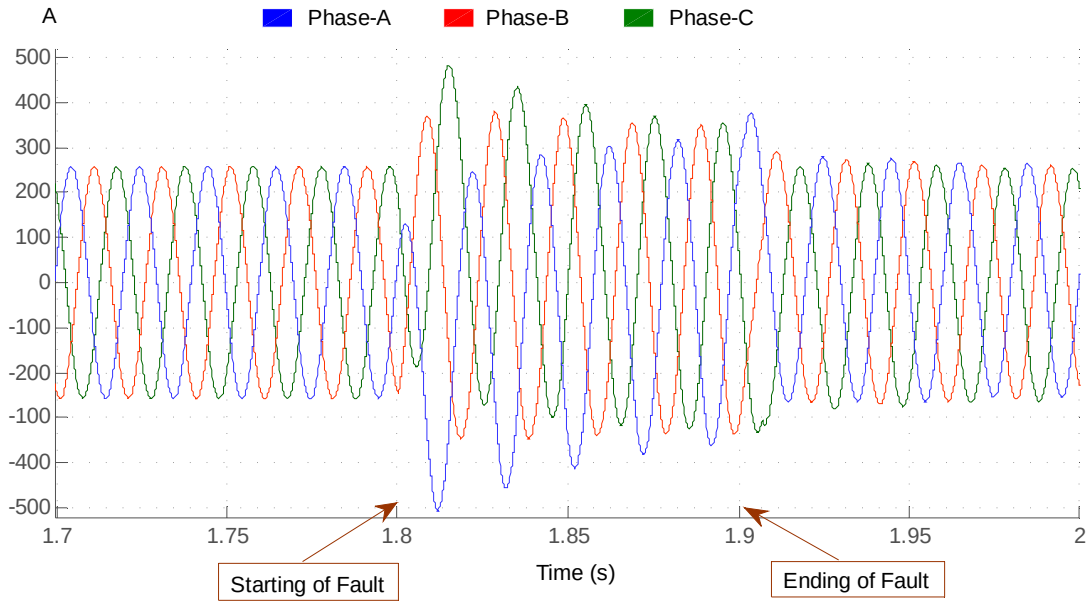


Figure 5.49. Phase currents of High Voltage Line of the system during 5.3.3 case

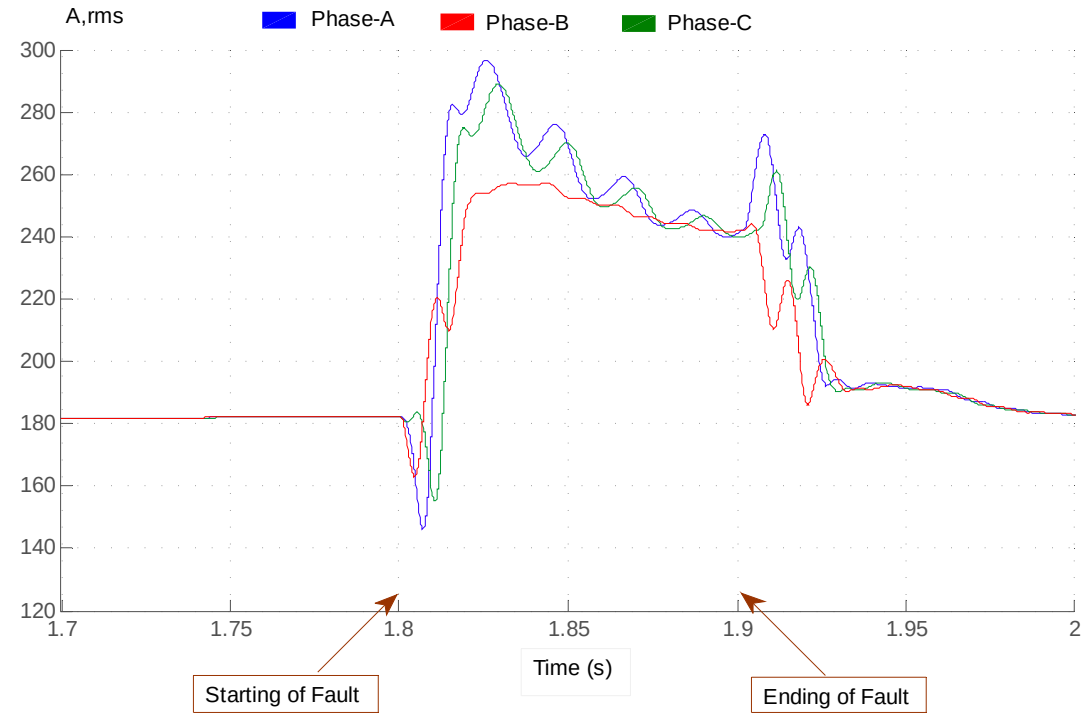


Figure 5.50. RMS currents of High Voltage Line side of the system during 5.3.3 case

Active and reactive power change observed on medium voltage line and is presented in Figure 5.51 during three phase fault at B group wind turbine. Active

power is decreased from 48 MW to 40.9 MW and 37.4 MVAR of reactive power is absorbed from interconnected transmission system during three phase fault.

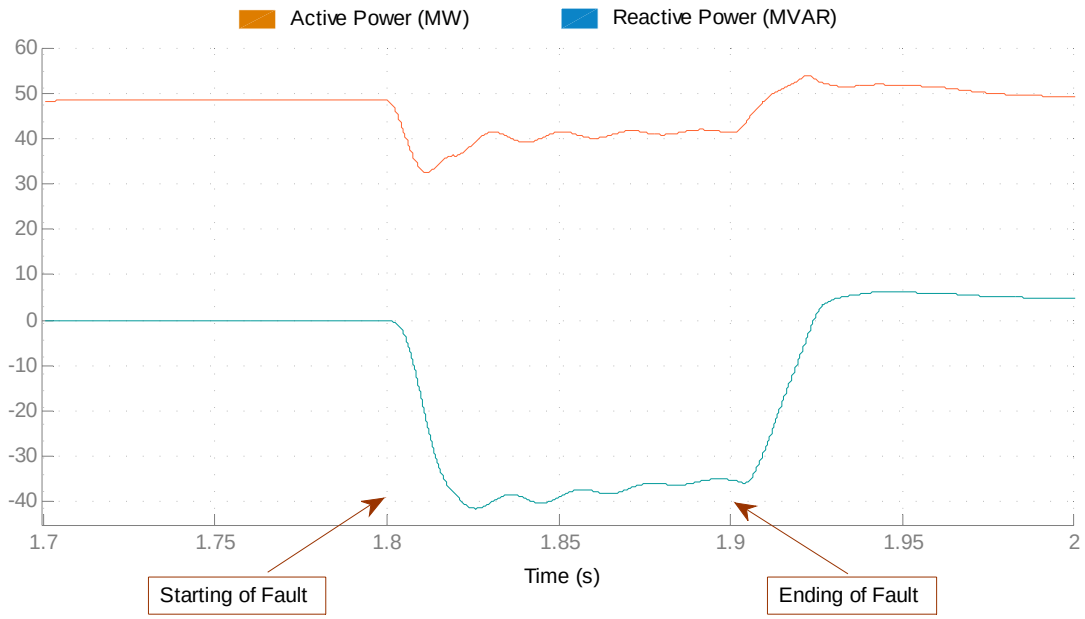


Figure 5.51. Active and reactive powers of MV Line side during 5.3.3 case

Frequency deviation is observed and presented in Figure 5.52 during three fault occurred in B group wind turbine. It is seen that frequency is changed between 49.98 Hz to 50.03 Hz.

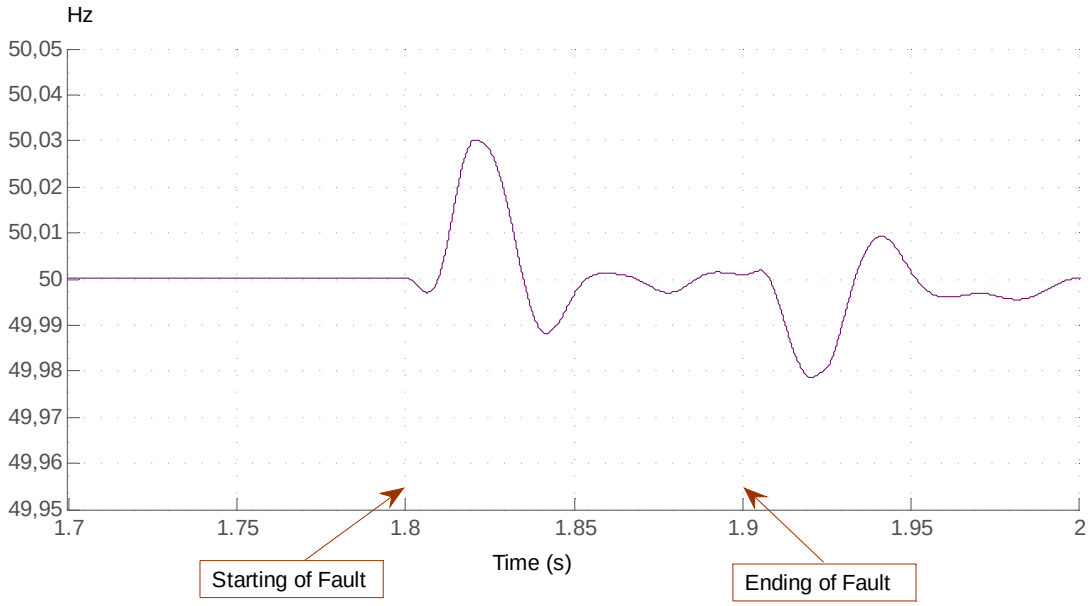


Figure 5.52. Frequency change of MV Line side during 5.3.3 case

5.4. Case 4: Faults in Medium Voltage Line

5.4.1. Phase-A-to-Phase-C Fault

In the first case, phase-to-phase fault in medium voltage line is investigated which occurs on A and C phases between 2.0 s and 2.1 s that fault time is determined as 0.1 seconds. This fault condition and its effect on high voltage side of system is investigated. During the short circuit fault occurs at medium voltage line, voltage sag was observed especially in phases of high voltage side that fault occurs on it. Figure 5.53 shows the voltage waveforms of each phase seen from high voltage side. Figure 5.54 shows the rms values of these voltages and as it can be seen from this figure clearly that, RMS value of Phase-A voltage is decreased from 89.1 kV to 82.4 kV (7.6% voltage sag), Phase-B voltage is decreased to 87.7 kV (1.6% voltage sag) and Phase-C voltage is decreased to 83 kV (6.8% voltage sag). The sag values are in acceptable band (10 %) on high voltage lines.

Phase current waveforms and rms currents injected from interconnected transmission system are presented in Figure 5.55 and Figure 5.56 respectively. For steady state operation, the nominal rms current is 180 A. RMS values of short-circuit

currents are increased to 1200 A at Phase-A, 390 A at Phase-B and 970A at Phase-C respectively during phase-to-phase fault occurred in medium voltage line.

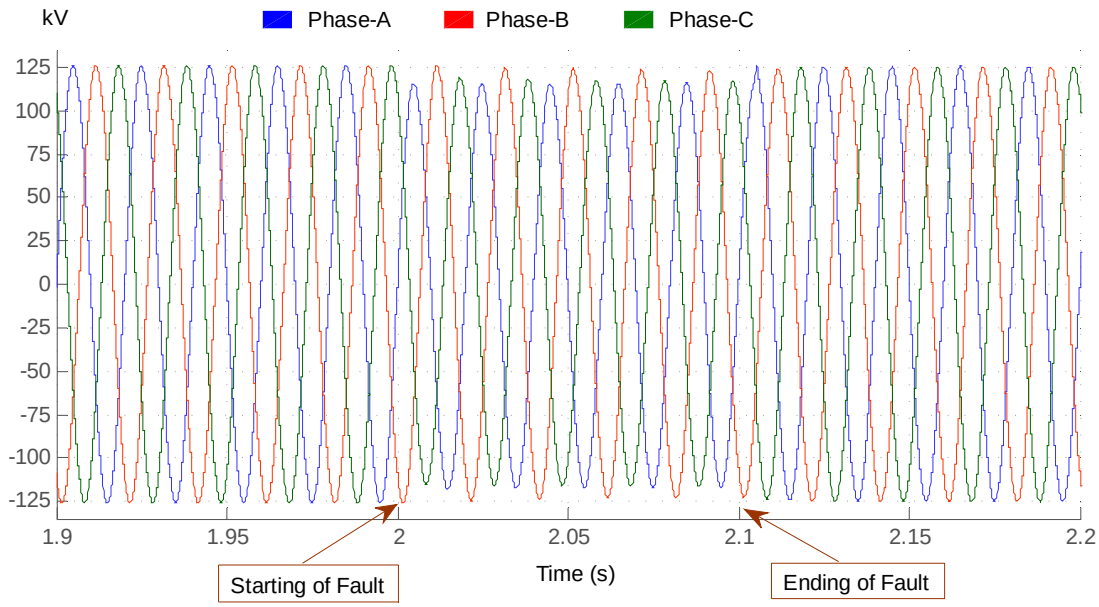


Figure 5.53. Phase voltages of High Voltage Line side during 5.4.1 case

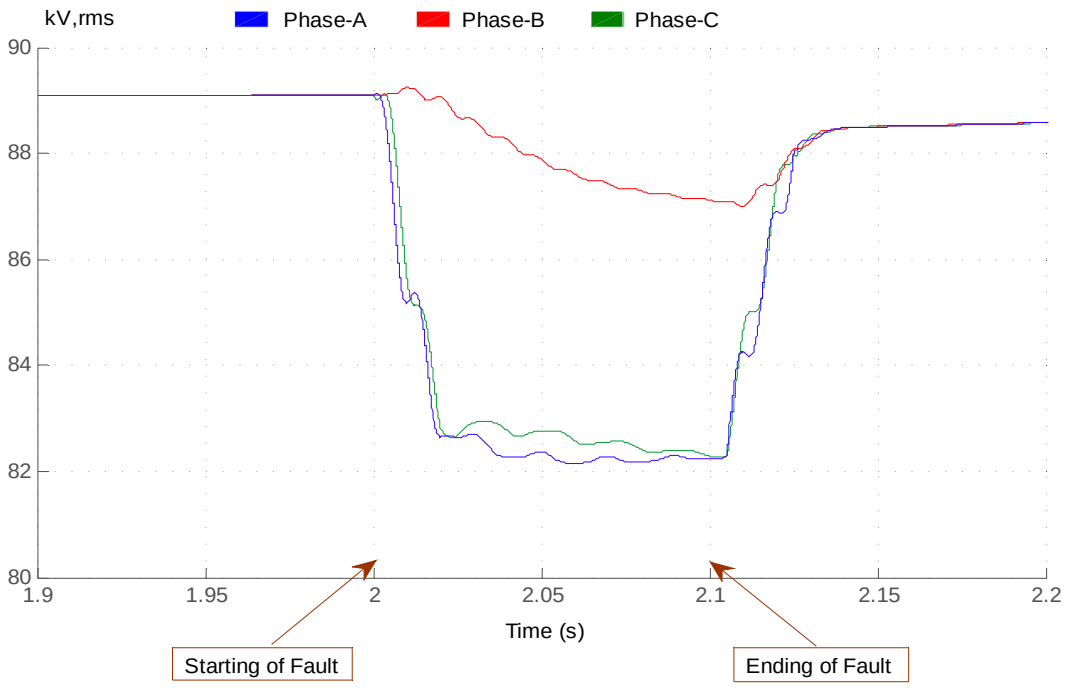


Figure 5.54. RMS voltages of High Voltage Line side of the system during 5.4.1 case

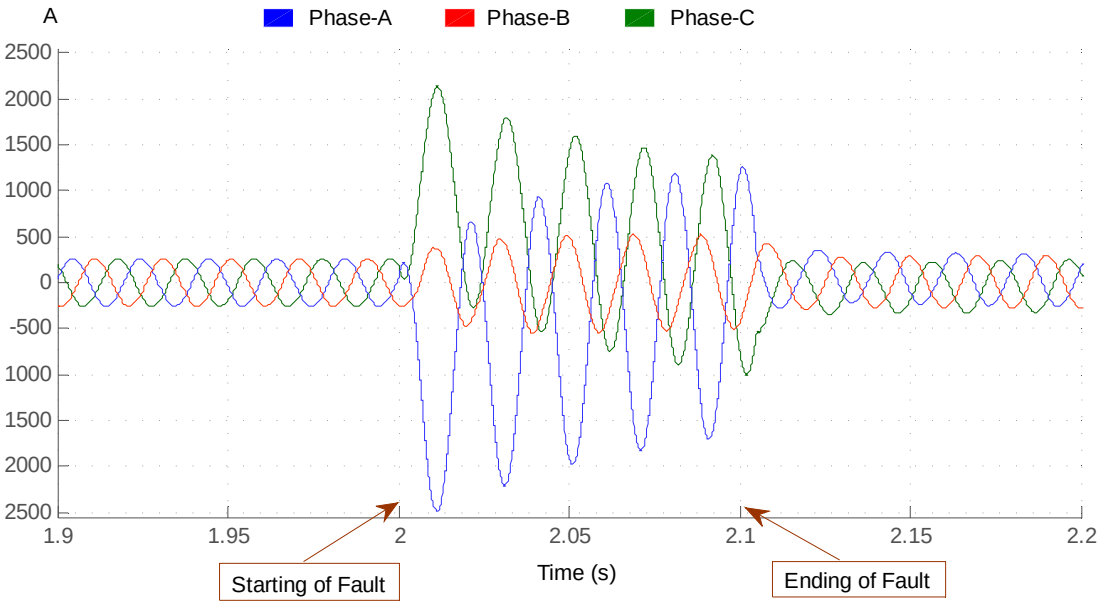


Figure 5.55. Phase currents of High Voltage Line side during 5.4.1 case

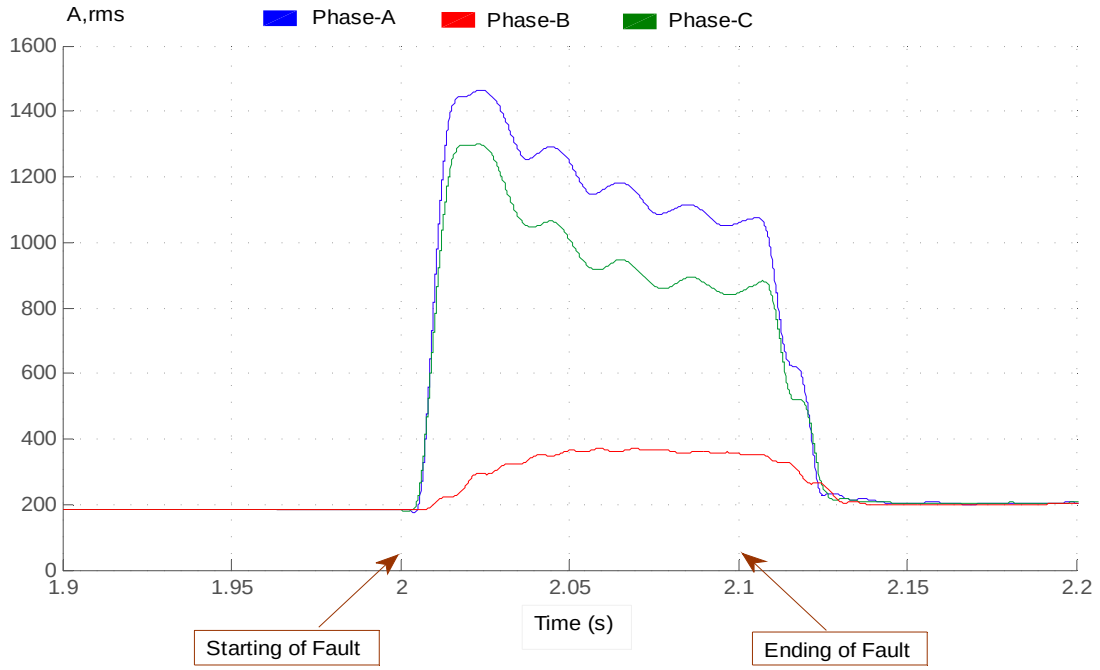


Figure 5.56. RMS currents of High Voltage Line side of the system during 5.4.1 case

Active and reactive power at the point of common coupling are measured and showed in Figure 5.57 during phase-to-phase fault occurred in medium voltage line. It is observed that generated active power is decreased from 48 MW to 30 MW and 65 MWAR reactive power is absorbed from interconnected transmission system.

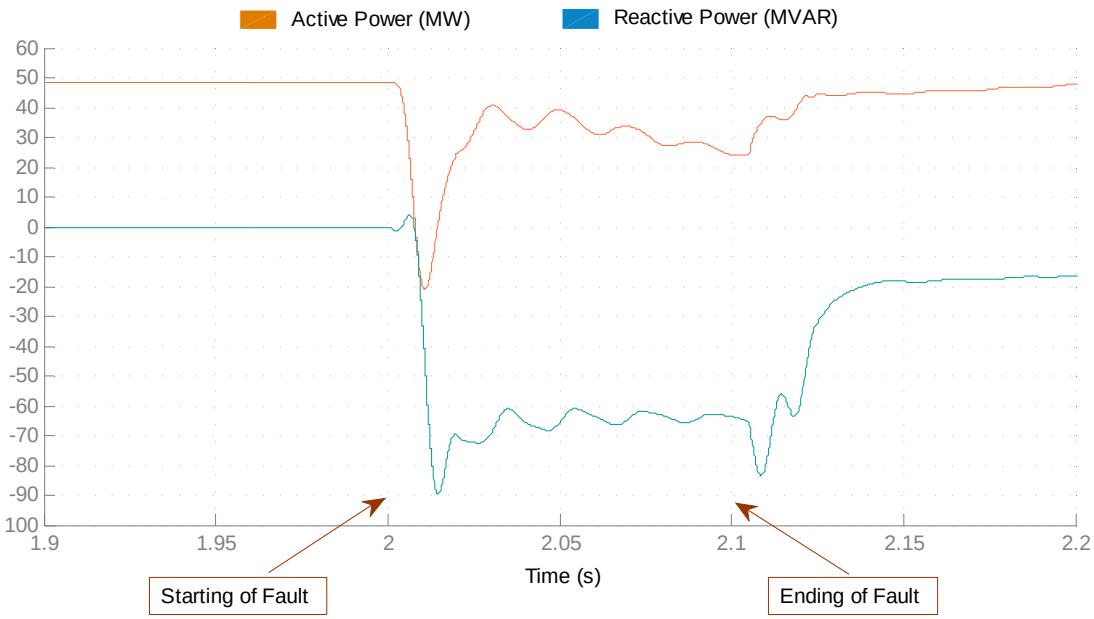


Figure 5.57. Active and reactive powers of MV Line side during 5.4.1 case

Frequency deviation is observed and presented in Figure 5.58 during phase-to-phase fault occurred in medium voltage line. It is seen that frequency is changed between 49.97 Hz to 50.07 Hz.

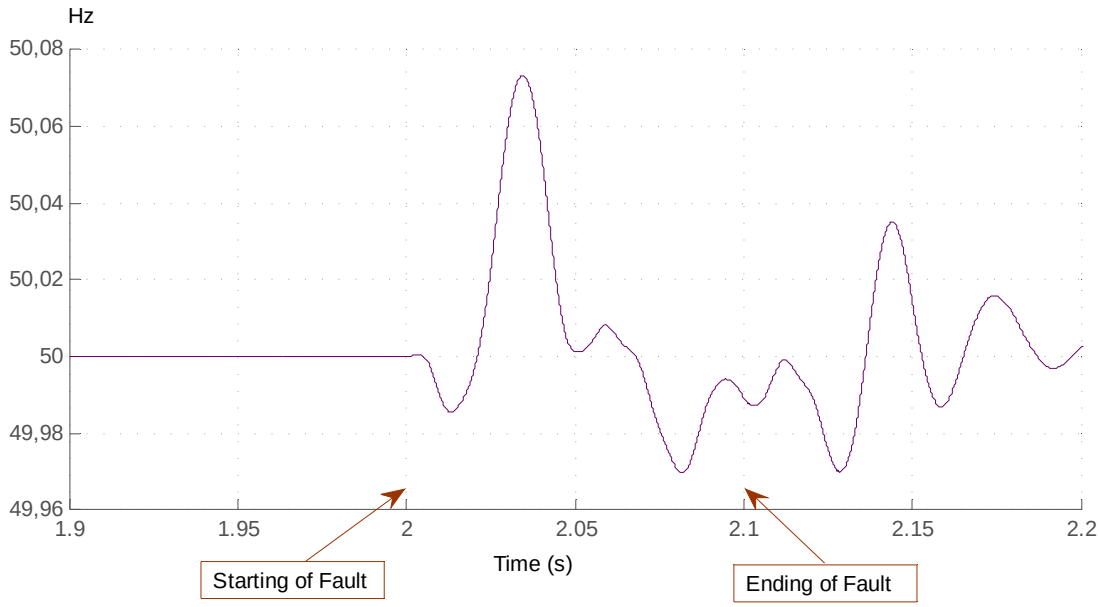


Figure 5.58. Frequency change of MV Line side during 5.4.1 case

5.4.2. Phase-B-to-Ground Fault

In this case, the impact of phase-to-ground fault that occurs on Phase-B of medium voltage line on interconnected transmission line investigated during 1.8 s < t < 1.9 s. During the short circuit fault, voltage sag in Phase-B of interconnected transmission system was observed. The voltage waveform and rms voltages of each phase seen from high voltage side are presented in Figure 5.59 and Figure 5.60 respectively. It can be seen from Figure 5.60, RMS value of Phase-A and Phase-C voltages are not changed; but RMS value of Phase-B voltage is decreased from 89.1 kV to 80.9 kV, so 9.2% voltage sag occurs only in that phase.

Phase current waveforms and rms currents injected from interconnected transmission system are presented in Figure 5.61 and Figure 5.62 respectively. The nominal rms current is 187 A for steady state operation of wind farm system. During phase-to-ground fault occurred in medium voltage line, rms value of short-circuit current in Phase-B is observed as 1100 A, while Phase-A is 330 A and Phase-C is 110 A respectively.

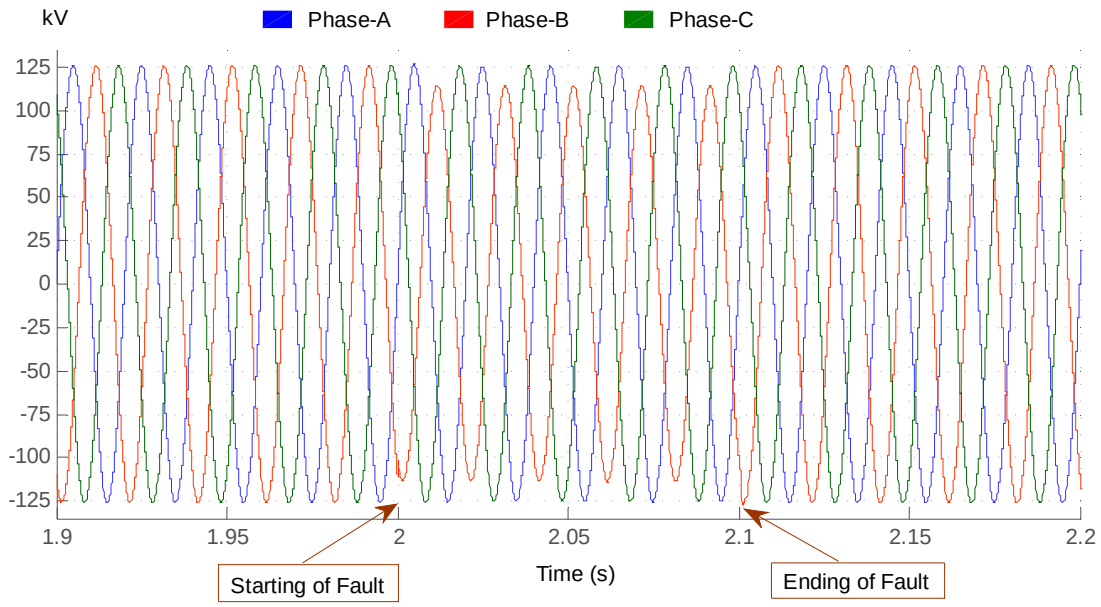


Figure 5.59. Phase voltages of High Voltage Line side during 5.4.2 case

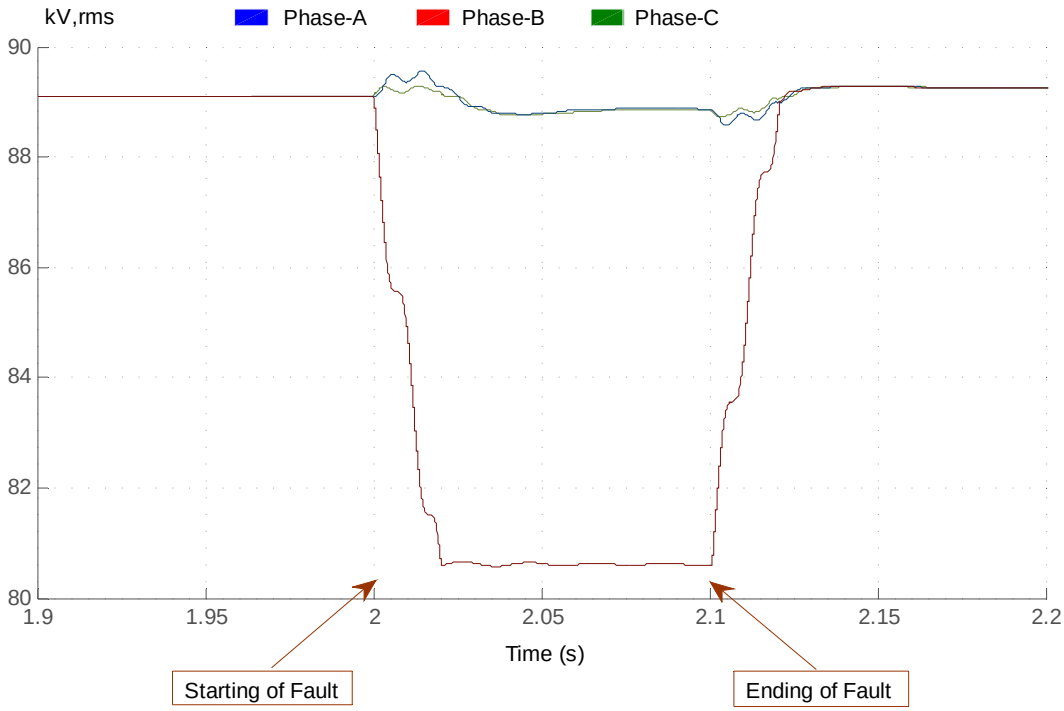


Figure 5.60. RMS voltages of High Voltage Line side of the system during 5.4.2 case

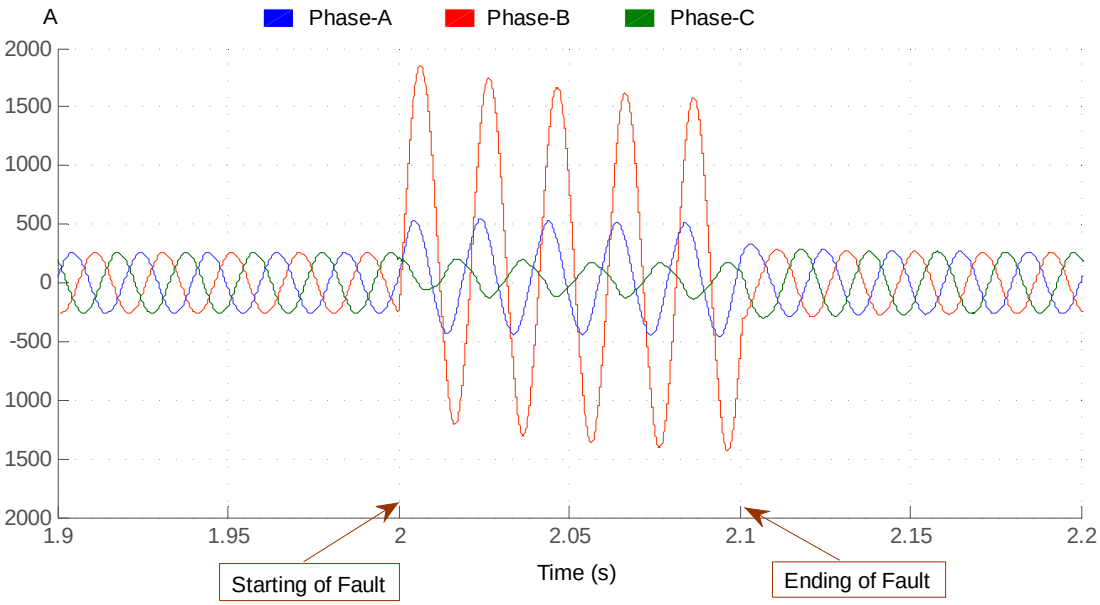


Figure 5.61. RMS voltages of High Voltage Line side of the system during 5.4.2 case

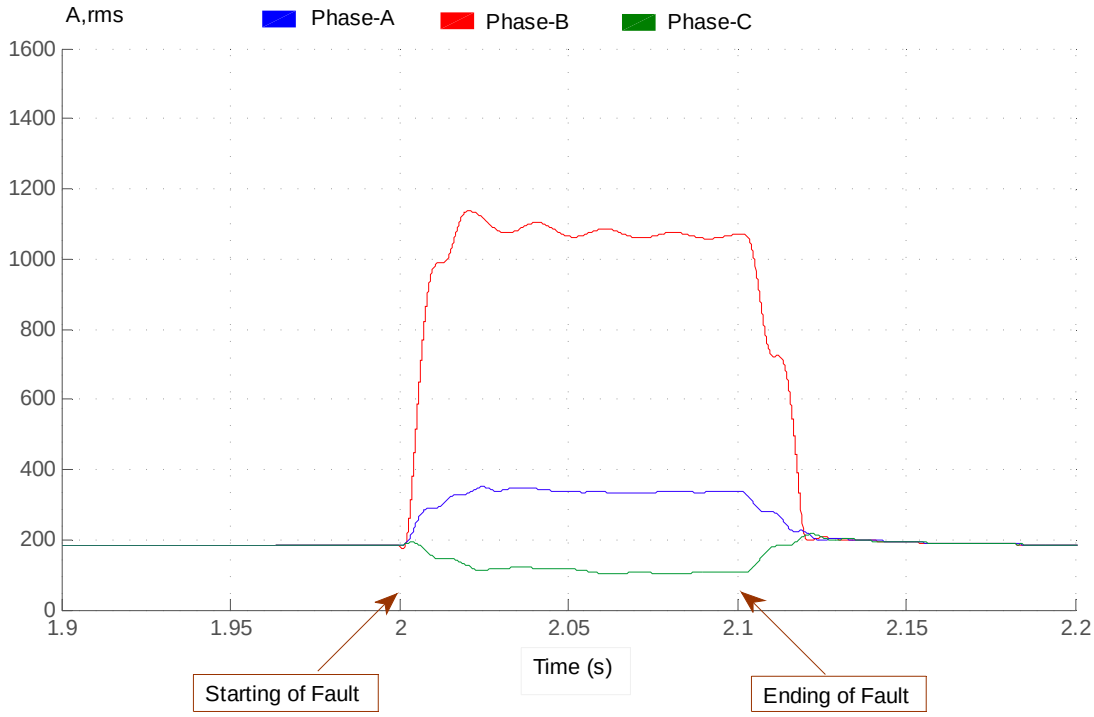


Figure 5.62. RMS currents of High Voltage Line side of the system during 5.4.2 case

Active and reactive power change is showed in Figure 5.63 that generated active power is 34 MW and absorbed reactive power is 63 MWAR.

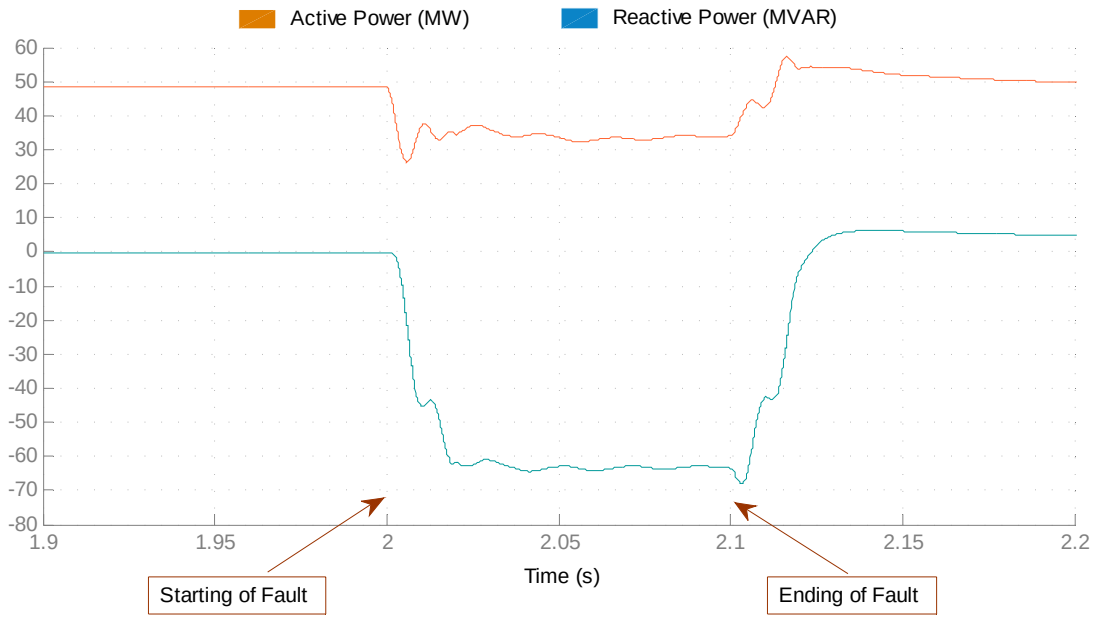


Figure 5.63 Active and reactive powers of MV Line side during 5.4.2 case

Frequency deviation is observed and shown in Figure 5.64 during phase-to-ground fault occurred in medium voltage line of the system. It is seen that frequency is changed between 49.98 Hz to 50.03 Hz.

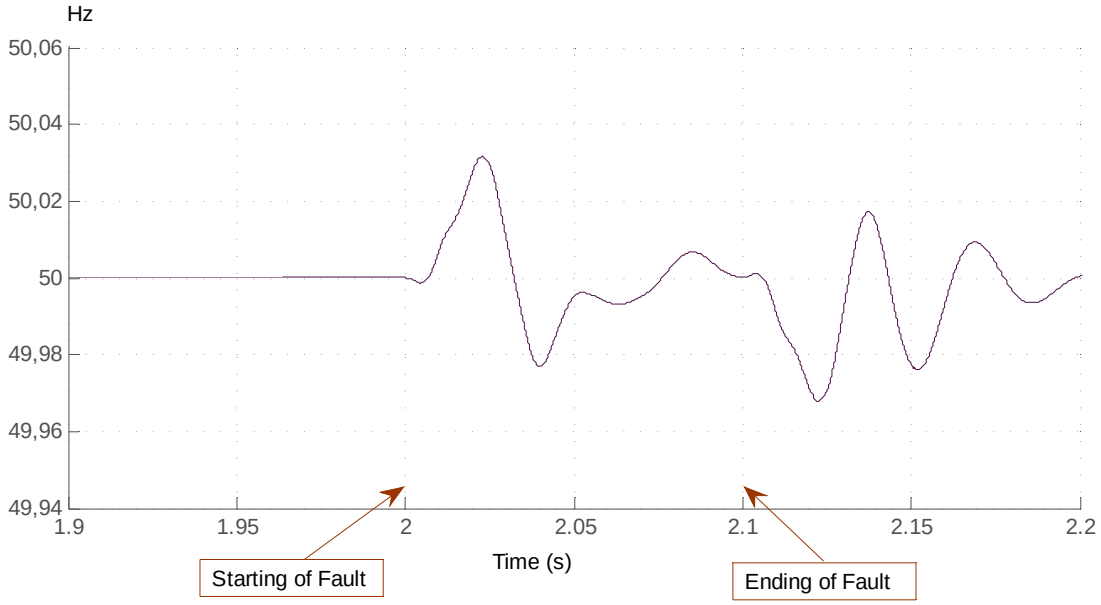


Figure 5.64. Frequency change of MV Line side during 5.4.2 case

5.4.3. Three Phase (A-B-C) Fault

In this case, three phase fault in medium voltage line is investigated which occurs on A, B and C phases between 2.0 s and 2.1 s. This fault condition affects high voltage side of system and 9.4% voltage sag was observed in all phases. Figure 5.65 and Figure 5.66 shows the voltage waveforms of each phase seen from high voltage side and the rms values of these voltages respectively. It can be seen from Figure 5.66 clearly that, RMS value of all phase voltages are decreased from 89.1 kV to 80.8 kV. Figure 5.67 shows that the phase current waveforms and Figure 5.68 presents the rms currents injected from interconnected transmission system. For steady state operation, the nominal rms current is 195 A. RMS values of short-circuit currents are reached to high values: 1210 A at Phase-A, 1080 A at Phase-B and 1170 A at Phase-C respectively during three phase fault occurred in medium voltage line.

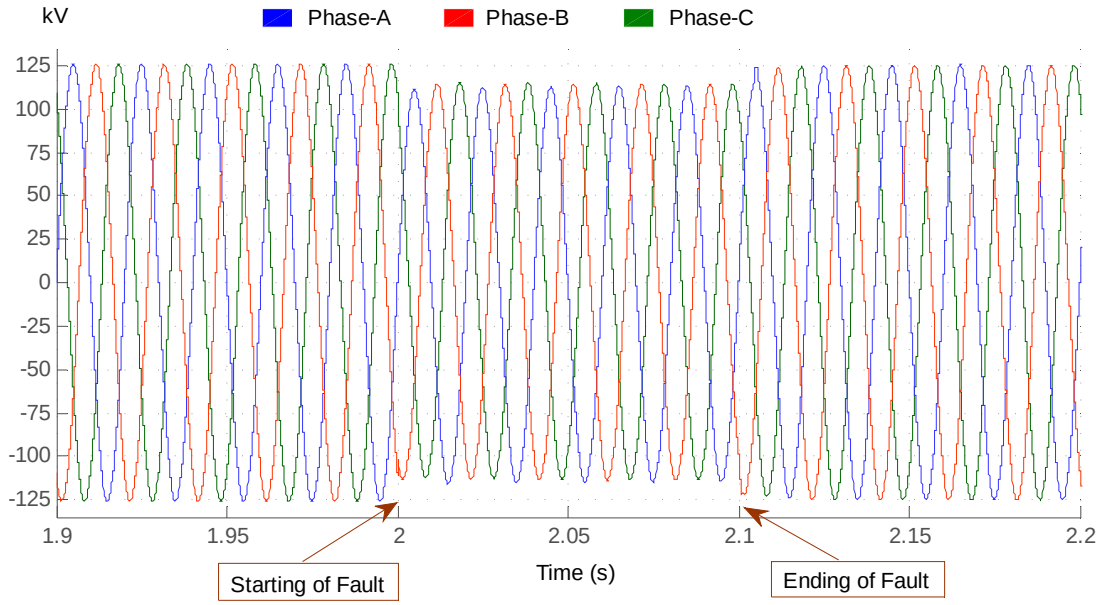


Figure 5.65. Phase voltages of High Voltage Line of the system during 5.4.3 case

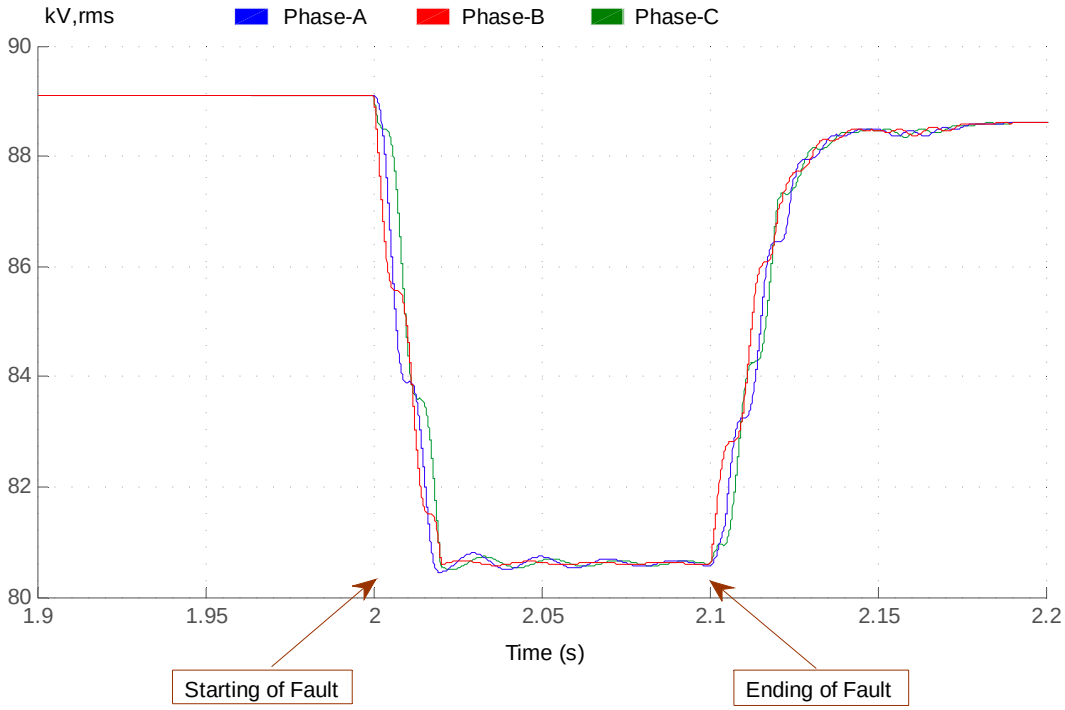


Figure 5.66. RMS voltages of High Voltage Line side of the system during 5.4.3 case

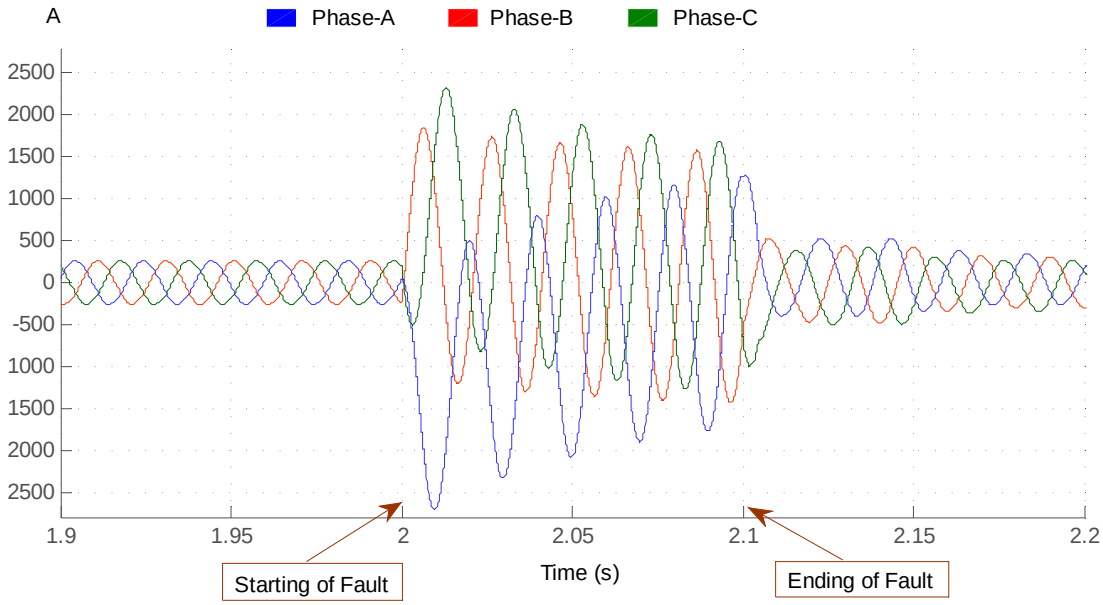


Figure 5.67. Phase currents of High Voltage Line of the system during 5.4.3 case

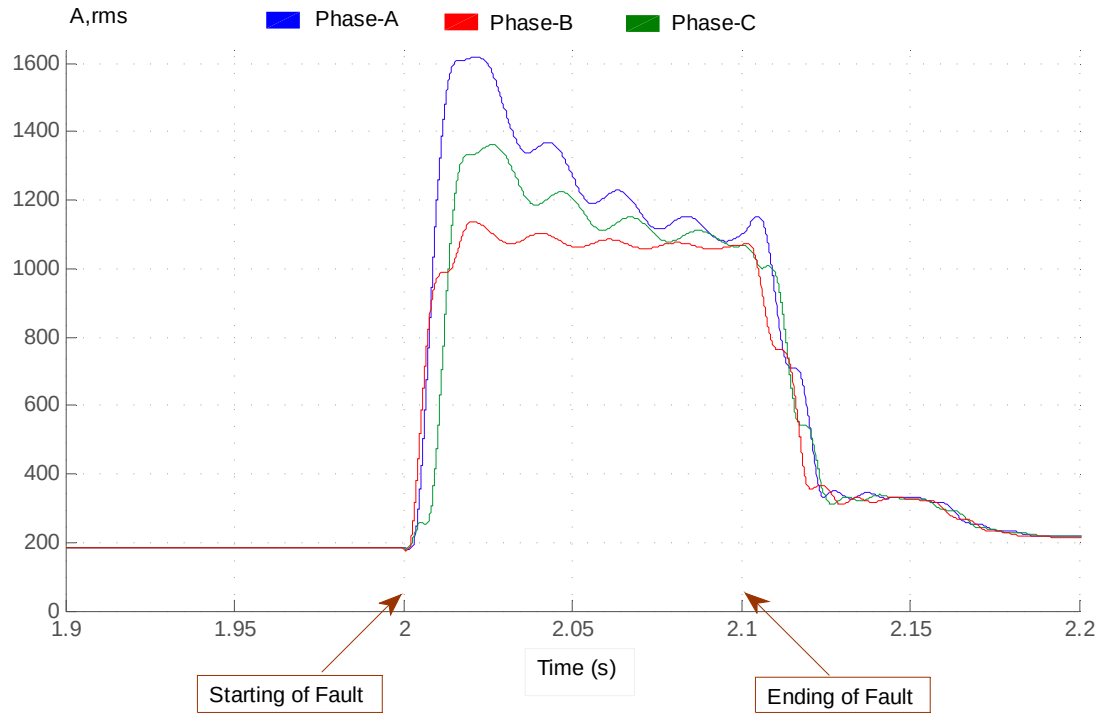


Figure 5.68. RMS currents of High Voltage Line side of the system during 5.4.3 case

Active and reactive power change observed over medium voltage line and is presented in Figure 5.69 during three phase fault in medium voltage line. It is seen that no active power is generated and no reactive power is absorbed from

interconnected transmission system during three phase fault that occurs in medium voltage line. In that case, wind farm system that is connected in medium voltage line is out of operation.

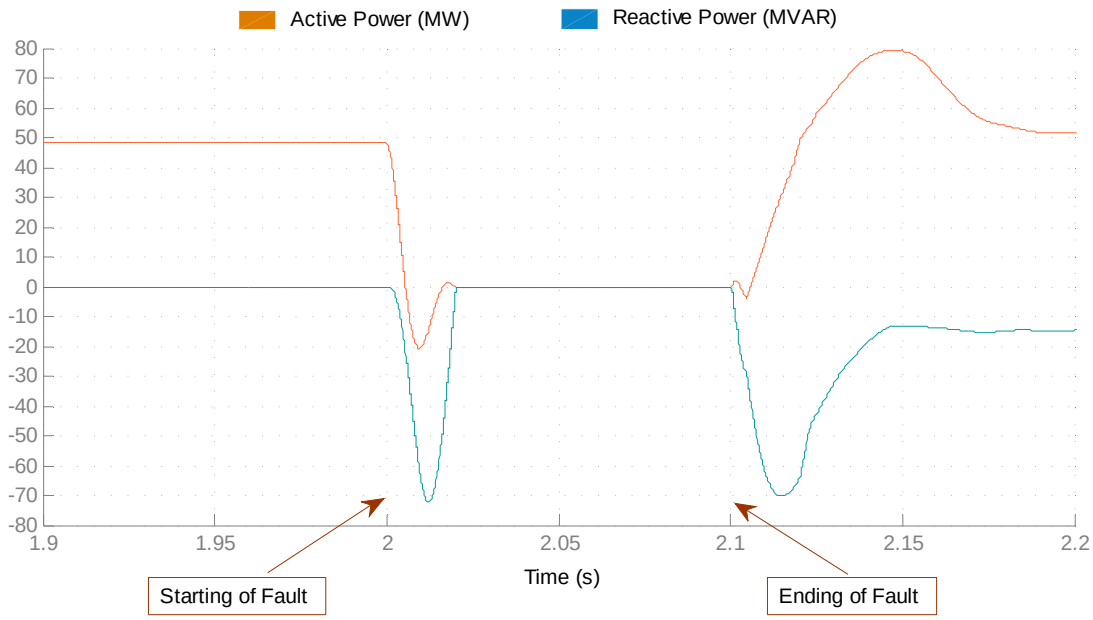


Figure 5.69. Active and reactive powers of MV Line side during 5.4.3 case

Frequency deviation is observed and presented in Figure 5.70 during three fault occurred in medium voltage line.

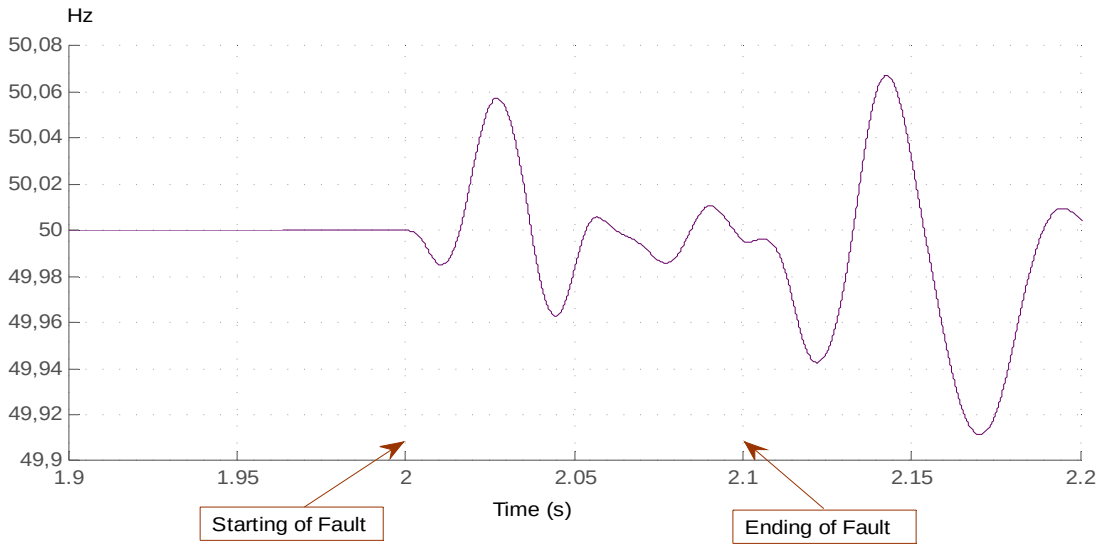


Figure 5.70. Frequency change of MV Line side during 5.4.3 case

6. CONCLUSION

In recent years, the world is increasingly going renewable in its energy use. Many countries have recognized the wind as the most important and promising renewable and sustainable source of energy that can compete effectively with fossil fuel. The installed capacity of wind generation worldwide exceeds 25 GW and wind farms totaling hundreds of MW are being considered.

In this thesis; a wind farm that is located in a region in Turkey that has totally 48 MVA powered 16 wind turbines in two groups is modeled. Because of the advantages of Doubly Fed Induction Generator (DFIG) over other generators, it is preferred and used in the simulation model. In order to understand the behavior of the wind turbine over its region, mathematical model of the wind turbine is examined. The operation of Doubly Fed Induction Generator (DFIG) and it's control system, using AC/DC/AC converter, have been discussed. Grid and rotor side controllers based on PI and dq transform are also described.

In order to evaluate the performance of the wind farm model, different case studies are investigated. In the first case study, simulation of normal operation of the wind turbines with fixed wind speed is performed as a reference point. The first case in the study shows the operation of wind turbines under variable wind speeds. Each turbine is subjected to a variable wind speed generated by autoregressive moving average model based noise generator. The power generation capabilities of wind turbines under these conditions are examined.

Short circuit fault simulations are performed at different fault locations to investigate the impact of wind farm faults on the national grid. In the case studies, three phase, phase to phase, and phase to ground short circuit faults have been examined. THD values of phase voltages are observed. There are two groups of wind turbines named as Group A and Group B in the wind farm. The second case study covers the short circuit faults occurred at a wind turbine low voltage output in Group A while the third case study covers the same case for Group B. The short circuit faults in the medium voltage level are investigated in the last case study.

From the simulation results, it has been observed that national grid stability have not been affected for most of the case studies. Simulation results also showed that the THD values are in the acceptable values of 1% to 1.5%. Three phase short circuit fault at MV level is the only fault that greatly affects the grid. In this case, the wind turbines were not able to generate power as they cannot tolerate the short circuit currents.

As a future work, the whole system can be modeled by using PSCAD/EMTDC. The system can be examined for different fault locations. Several controller can be investigated to improve the performance of the system.

REFERENCES

ACKERMANN T. S., 2000. Wind Energy Technology and Current Status: A Review. Renewable and Sustainable Energy Reviews.

AGANAH K. A., 2013. On-Grid Doubly Fed Induction Generator Wind Turbinewith Nine-Switch Converter as Grid Side Converter for Low Voltage Ride Through. Phd Thesis. Tennessee Technological University.

BAHIRAT H. J., MORK B. A., HØIDALEN H. Kr., 2012. Comparison of Wind Farm Topologies for Offshore Applications. Power and Energy Society General Meeting, 2012 IEEE.

BELMOKHTAR K., DOUMBIA M. L., AGBOSSOU K., 2011. Modelling and Power Control of Wind Turbine Driving DFIG connected to the Utility Grid, International Conference on Renewable Energies and Power Quality (ICREPQ'11), Las Palmas de Gran Canaria (Spain), 13-15 April.

BIJAYA, 2011. Modeling, Control and Analysis of a Doubly Fed Induction Generator based Wind Turbine System with Voltage Regulation. Master of Science Thesis. Tennessee Technological University.

DUTTA A., 2006. Basics of Wind Energy Technology. Energy, Asian Institute of Technology Presentation.

ENERGY INSTITUTE, http://enerjienstitusu.com/tu rkiye-kurulu-el ektrik-enerji-gucu-mw/

GANGON R., SYBİLLE G., BERNARD S., PARÉ D., Casoria S., Larose C., 2005. Modeling and Real-Time Simulation of a Doubly-Fed Induction Generator Driven by a Wind Turbine Modeling and Real-Time Simulation of a Doubly Fed Induction Generator Driven by a Wind Turbine. International Conference on Power Systems Transients (IPST'05), Montreal, Canada.

GUPTA A., SINGH S. N., KHATOD K., 2013. Modeling and Simulation of Doubly Fed Induction Generator Coupled With Wind Turbine-An Overview. Journal of Engineering, Computers & Applied Sciences (JEC&AS),Volume 2, No.8.

HYONK S.K., DYLAN D.L., 2010. Wind Energy Conversion System from Electrical Perspective - A Survey. Smart Grid and Renewable Energy, Vol. 1, No. 3, pp.119-131.

IOV F., SØRENSEN P., HANSEN A.-D., BLAABJERG F., 2005. Grid connection of active stall wind farms using a VSC based DC transmission system. Power Electronics and Applications, 2005 European Conference IEEE.

JAMIESON P., 2005. Fundamentals of Wind Turbines.

JENKINS N., WALKER J., 1997. Wind Energy Technology. Wiley, England.

JING X., 2009. Modeling and Control of a Doubly-Fed Induction Generator for Wind Turbine-Generator Systems. Master of Science Thesis. Marquette University.

KALMIKOV A. and DYKES K., 2010. Wind Power Wind Power Fundamentals. MIT Wind Energy Group & Renewable Energy Projects in Action.

KRUGER T. and ANDRESEN, B., 2001. Vestas OptiSpeed - Advanced control strategy for variable speed wind turbines. Proceedings of European Wind Energy Conference, pp. 983-86, July 2-6, Copenhagen, Denmark.

KUO B., 1995. Automatic Control Systems, Prentice Hall.

LI, S.; HASKEW, T. A.; MULJADI, E. and SERRENTINO,C., 2009. Characteristic Study of Vector Controlled Direct-Driven Permanent Magnet Synchronous Generator In Wind Power Generation. Electric Power Components and Systems, Vol. 37, No. 10, pp. 1162-1179.

MARTINEZ J., 2007. Modelling and Control of Wind Turbines. Master of Science in Process Systems Engineering, Imperial College London.

MATLAB, 2013. The MathWorks, "SimPower Systems for use with Simulink", User's Guide Version 4.

MOLINA M. G., MERCADO P. E., 2011. Modelling and Control Design of Pitch-Controlled Variable Speed Wind Turbines. Engineering » Energy Engineering » "Wind Turbines", book edited by Ibrahim Al-Bahadly, ISBN 978-953-307-221-0, Published: April 4.

MULLER, S.; DEICKE, M. & De DONCKER, R. W., 2002. Doubly Fed Induction Generator Systems for Wind Turbines. IEEE Industry Applications Magazine, Vol. 8, No. 3, pp. 26-33.

QIAO, W.; HARLEY, R. G. & VENAYAGAMOORTHY, G. K., 2007. Dynamic Modeling of Wind Farms With Fixed-Speed Wind Turbine Generators, Proceedings of IEEE PES 2007 General Meeting, June 24-8, Tampa, USA.

RAYMOND W.F., SU S.W., 2009. Wind turbines. McGraw-Hill Companies.

SINGH M., SANTOSO S., 2011. Dynamic Models for Wind Turbines and Wind Power Plants, The University of Texas at Austin.

SINGH M., SANTOSO S., 2011. Dynamic Models for Wind Turbines and Wind Power Plants, The University of Texas at Austin.

TANG Y., JU P., HE H., QIN C., WU F., 2013. Optimized Control of DFIG-Based Wind Generation Using Sensitivity Analysis and Particle Swarm Optimization. IEEE Transactions on Smart Grid, Vol.4, No.1.

VARMA A.P., CHAKRI K.B., 2012. Study of Grid Connected Induction Generator for Wind Power Applications. National Institute of Technology, Rourkela.

VILLALVA M. G., GAZOLI J. R., and FILHO E. R., "Comprehensive approach to modeling and simulation of photovoltaic arrays," IEEE Trans. Power Electron., vol. 24, no. 5, pp. 1198–1208, May 2009.

YANG B., LI W., ZHAO Y., and HE X., "Design and analysis of a gridconnected photovoltaic power system," IEEE Trans. Power Electron., vol. 25, no. 4, pp. 992–1000, Apr. 2010.

BIOGRAPHY

Servet YOLALAN was born in Aydın, Turkey in 1968. He received his B.S. degree in Electrical and Electronics Technical Faculty from Gazi University in 1990. After completion his B.S. education, he started MSc education in Electrical and Electronics Engineering Department in Çukurova University in 2009. His research areas are Wind Turbines, Renewable Energy Resources, Power Electronics and Automatic Control Systems and Energy Efficiency.